

https://dspace.org/

Three dimensional analysis of stress and strain distributions around Bord and Pillar geometries

Ndlovu, Xolisani

2007-04-10T08:07:15Z
http://hdl.handle.net/10539/2351

Downloaded from a DSpace repository. https://dspace.org/

DECLARATION

I declare that this dissertation is my own, unaided work. It is being submitted for the Degree of Master of Science in the University of the Witwatersrand, Johannesburg. It has not been submitted before for any degree or examination in any other University.

……

(Signature of candidate)

…….. day of ……..... (year) …...

at ……

ABSTRACT

Underground observations at a coal mine indicated failure of the immediate roof above the bords while pillars were observed to be intact. To determine the underlying causes of roof failures, careful observations and photographic recording of occurrences of roof failures have been made. Rock samples of the immediate shale roof were collected for laboratory testing to determine the rock strength and deformation properties. Numerical simulations were carried out to analyse stress and strain distributions and also to attempt to explain the guttering process.

Mapping of roof failures showed that these took place mainly towards the centre of the roadways. The roof failures, termed "roof guttering", were observed to occur violently and with little warning. Occurrence of roof guttering had a negative impact on production. Some panels are abandoned, production times have increased and safety of workers is compromised. The mine authorities initially thought that roof guttering was caused by shear failure of the rock mass. Roof bolts are therefore used as a means of primary support. No improvements have been observed. Increasing the size of pillars has not solved the problem either. It has only increased the amount of coal left in the pillars without any improvements in reducing roof failures.

Stress measurement results carried out in 2001 showed that high horizontal stresses exist at the mine. The immediate shale roof was observed to be weak. Laboratory testing showed that the shale rock is transversely isotropic. Numerical modelling results indicated that there are insignificant stress concentrations towards the centre of the roadway using the elastic and transversely isotropic elastic models. Stress concentrations were predicted at the roof-pillar contact area. It is therefore expected that failure should initiate and occur at the roof-pillar contact area. The Mohr-Coulomb and Mohr-Coulomb strain softening models predicted shear failure at the roof-pillar contact area. The two models over predicted the depth and under predicted the width of failures.

The extension strain criterion predicted correctly the depth and width of failures although the failures were predicted at the roof-pillar contact area while the observations indicated failure mainly towards the centre of the roads. Initiation of failure was predicted ahead of the coal face at the centre of the road position using the extension strain criterion.

Although none of the constitutive behaviours predicted correctly the observed underground failures the extension strain criterion has shown the best agreement. Guttering that occurred at the roof-pillar contact was modelled successfully using the extension strain criterion. The extension strain criterion predicted initiation of failure ahead of the coal face at the road centre position. It is possible that fracture initiation could be taking place in this location ahead of the coal face, and, on blasting the rock that has been fractured falls forming a gutter at the centre of the road.

ACKNOWLEDGEMENTS

I would like to express my sincere gratitude on the assistance and support rendered by the following persons and institutions:

(i) Professor T. R. Stacey for his supervision, guidance, encouragement and motivation throughout this research.

(ii) Dr. J. Wesseloo for guidance on the implementation of the extension strain criterion.

(iii) University of the Witwatersrand for granting me the opportunity to embark on this research.

(iv) GENMIN Laboratories for affording me the opportunity to carry out the laboratory tests.

(v) The Safety in Mines Research Advisory Committee (SIMRAC) for funding this research.

(vi) Anglo Coal for affording me the opportunity to carry out mapping of roof guttering at Nooitgedacht Section.

(vii) Messrs D. Minney and G. Makusha of Anglo Coal's Rock Engineering Department for making previous results of mapping of roof guttering available for this study.

(viii) Mr. A. Ndobe of Greenside Colliery for assisting with data collection.

(ix) Family and friends for their motivation and support.

To mama, you are the best…….and to Sharon, ngiyabonga…...

Table of contents

CONTENTS **PAGE**

DECLARATION I
ABSTRACT II
ACKNOWLEDGEMENTS IV
LIST OF FIGURES IX
LIST OF SYMBOLS XVI

CHAPTER 1 1
INTRODUCTION 1
1.1 BACKGROUND 1
1.2 DEFINITION OF THE PROBLEM 3
1.3 OBJECTIVES 5
1.4 RESEARCH METHODOLOGY 6
1.5 CONTENT OF THE DISSERTATION 6

CHAPTER 2 8
BORD AND PILLAR DESIGN IN COAL MINING 8
2.1 INTRODUCTION 8
2.2 DESIGN FOR BORD AND PILLAR MINING 9
2.3 STRESS CHANGES DUE TO CREATION OF UNDERGROUND EXCAVATIONS 13
2.4 EFFECT OF HIGH HORIZONTAL STRESSES IN BORD AND PILLAR MINES 15
2.5 GUTTERING OCCURRENCE IN SOUTH AFRICAN COLLIERIES 26
2.6 STRESS MEASUREMENTS AT NOOITGEDACHT COLLIERY 29
2.7 CONCLUSIONS 31

CHAPTER 3 32
MAPPING OF GUTTERING AT NOOITGEDACHT COLLIERY 32
3.1 INTRODUCTION 32
3.2 THE MINING METHOD AND PANEL POSITIONS 33
3.3 OBSERVATIONS OF THE OCCURRENCE OF ROOF GUTTERING 33
3.4 PROGRESSIVE FAILURE OF BRITTLE ROCK 49
3.4.1 Summary of URL studies 49
3.4.2 Observation of fracture surfaces 54
3.4.3 Possible mechanisms of development of guttering at Nooitgedacht Colliery 59
3.5 CONCLUSIONS 63

CHAPTER 4 65
LABORATORY TESTING 65
4.1 INTRODUCTION 65
4.2 ULTRASONIC TESTS 66
4.3 UNIAXIAL COMPRESSION STRENGTH TESTS 67
4.4 BRAZILIAN TENSILE STRENGTH TESTS 68
4.5 CONCLUSIONS 71

CHAPTER 5 72
NUMERICAL MODELS AND CONSTITUTIVE LAWS 72
5.1 MODELLING IN ROCK ENGINEERING 72
5.2 TYPES OF NUMERICAL MODELS 73
5.3 TWO DIMENSIONAL VERSUS THREE DIMENSIONAL MODELLING 75
5.4 CONSTITUTIVE BEHAVIOUR FOR ROCK MASS 76
5.4.1 Linear elastic 76
5.4.2 Transversely isotropic elastic 76
5.4.3 Mohr-Coulomb 76
5.4.4 Mohr-Coulomb strain softening (MCSS) 80
5.4.5 Extension strain criterion 80
5.5 CONCLUSIONS 85

CHAPTER 6 86
NUMERICAL MODELLING METHODOLOGY AND RESULTS 86
6.1 INTRODUCTION 86
6.2 NUMERICAL MODELLING PROCEDURE IN FLAC3D 86
6.2.1 Grid generation 86
6.2.2 Constitutive behaviours and material properties 88
6.2.3 Initial and boundary conditions 88
6.2.4 Solution to initial equilibrium 90
6.2.5 Loading and sequential excavation 90
6.3 MODELLING RESULTS 91
6.3.1 Results of elastic analyses 93
6.3.1.1 Results of isotropic analyses 93
6.3.1.2 Results of transversely isotropic analyses 98
6.3.2 Results of non elastic analyses 99
6.3.2.1 Results of isotropic analyses for model with an interface 100
6.3.2.2 Results of transverse isotropic analyses for model with an interface 102
6.3.2.3 Results of Mohr-Coulomb analyses 104
6.3.2.4 Results of Mohr-Coulomb strain softening analyses 110
6.3.3 Results of extension strain analyses 113
6.4 ANALYSES OF RESULTS AND COMPARISON TO MINE OBSERVATIONS 122
6.5 CONCLUSION 126

CHAPTER 7 128
CONCLUSIONS 128
REFERENCES 132
APPENDIX A1: LABORATORY TEST RESULTS 145
APPENDIX A2: MATERIAL PROPERTIES 150

LIST OF FIGURES

Caption **Page**

Figure 1.1: Fatality rates per million hours worked for South African mines 1994 to 2004 (MHSC 2004/2005 Annual Report) 5
Figure 2.1: Section through a roadway showing stress redistribution when an opening is created underground..... 14
Figure 2.2: Crushing of the roof (after Parker, 1973) 16
Figure 2.3: Thrusting of the roof (after Parker, 1973) 17
Figure 2.4: Offsets in empty roof bolt holes (Parker, 1973) 17
Figure 2.5: Guttering roof failure sequence (After Hill, 1986)..... 20
Figure 2.6: Schematic diagram of angle bolting (Hill, 1986) 21
Figure 2.7: Schematic diagram of truss bolting (Hill, 1986) 21
Figure 2.8: Schematic plan diagram showing the stress shadow created by mining a roadway some distance ahead of other roadways 22
Figure 2.9: Cross-sectional view of rib-slotting method (Adapted from Kripakov, 1982)..... 23
Figure 2.10: Probable stress redistribution patterns around oval-shaped roof falls, concentrating stress above and along the axial ends and reducing stress (stress shadow) adjacent to the long axis of the roof fall (Iannacchione et al 2001)..... 25
Figure 2.11: Guttering occurrence in a South African colliery..... 27
Figure 3.1: Generalised geological log for Nooitgedacht Colliery..... 32
Figure 3.2: Photograph showing typical depth of gutter (about 0.3 m) 34
Figure 3.3: Photograph showing typical depth of gutter (about 0.5 m) 35
Figure 3.4: Photograph showing typical depth of gutter (about 0.5 m) and width of gutter (about 1.2 m) 35
Figure 3.5: Photograph showing a fractured roof which on scaling results in a gutter 36
Figure 3.6: ‘Upturned’ boat-shaped nature of guttering occurrence..... 36
Figure 3.7: Photograph showing thin slabs associated with roof guttering 37

Figure 3.8: Photograph showing stress induced fracturing associated with roof guttering. The roof gutter occurred towards a pillar edge 37
Figure 3.9: Interlocking nature of surfaces in guttering roof 38
Figure 3.10: Photograph showing stress induced fracturing ahead of a gutter. The roof gutter occurred towards the centre of a roadway 38
Figure 3.11: Schematic diagram showing boat-shaped nature of guttering and fracture surface ahead of guttering 39
Figure 3.12: A roof bolt exposed due to guttering is replaced by another one 40
Figure 3.13: Plan view showing occurrence of guttering between roof bolts. The diagram also shows the guttering occurring between pillars that is stopped by the pillars from developing further longitudinally 40
Figure 3.14: Occurrence of roof guttering along roof bolts 41
Figure 3.15: Occurrence of guttering in part of a section. Dotted lines represent the gutters. The numbers 6, 7, and 8 denote split number while 1L, 2L etc denote roadways 42
Figure 3.16: Plan view showing occurrence of guttering in part of two panels. Lines indicate guttering while shaded areas indicate slabbing 43
Figure 3.17(a): Occurrence of guttering on a mine-wide scale 44
Figure 3.17(b): Guttering in seven selected panels 45
Figure 3.18: Disced core from one of the guttering sites 46
Figure 3.19: Photograph showing roof slabbing initiated by roof guttering 47
Figure 3.20: Roof guttering occurring in the solid roof just above a delaminated roof 48
Figure 3.21: Fall of muddy roof 48
Figure 3.22: Occurrence of guttering in combination with slabbing was common in muddy roof 49
Figure 3.23: The three parameters determined from laboratory compression test: crack initiation (σ_{ci}); initiation of sliding (σ_{cd}), and peak strength (σ_f). $\Delta V/V$ is the volumetric strain (Martin, 1997) 51

Figure 3.24: Illustration of the major processes involved in the initiation, development, and stabilisation of the V-shaped notch (Martin, 1997) 53
Figure 3.25a: Photograph of an extension fracture surface..... 56
Figure 3.25b: Photograph of an extension fracture surface 56
Figure 3.25c: Photograph of an extension fracture surface..... 57
Figure 3.25d: Photograph of an extension fracture surface 57
Figure 3.26a: Photograph of a shear fracture surface 58
Figure 3.26b: Photograph of a shear fracture surface 58
Figure 3.27a: Schematic diagram of a roadway cross-section showing possible fracturing just before occurrence of guttering..... 60
Figure 3.27b: Schematic diagram of a roadway cross-section showing the fallen rock and the "V-shaped" nature of guttered roof..... 61
Figure 4.1(a): Loading along the bedding in Brazilian test 69
Figure 4.1(b): Loading perpendicular to the bedding in Brazilian test..... 69
Figure 4.1(c): Loading perpendicular to the bedding in UCS tests..... 70
Figure 4.1(d): Loading along the bedding in UCS tests 70
Figure 5.1: Holling's (1978) classification of modelling. Most rock engineering problems fall into region 4, whereas region 3 is better suited to routine quantitative modelling (after Starfield and Bleloch, 1986) 73
Figure 5.2: Mohr-Coulomb criterion in terms of (a) principal stresses (b) normal and shear stresses 78
Figure 5.3a: Mohr circle that lies below the failure envelope and represents a stable stress state 78
Figure 5.3b: Mohr circle that is tangent to the failure envelope and represents the state of stress at the instant of failure..... 79
Figure 5.3c: Mohr circle that intersects the failure envelope and represents an unstable stress state 79
Figure 6.1: Plan view of bord and pillar geometry showing the quarter symmetry model..... 88
Figure 6.2: Quarter geometry model grid in three dimensions 89

Figure 6.3: Plan view of model geometry with a coal heading (Line M-M/Section M-M can be moved to different locations behind and ahead of the coal face) 90
Figure 6.4: Plan view showing the bord and pillar geometry and Lines A and B across the pillar, along which history points are located. For contour plots A becomes Section A. 91
Figure 6.5: Section showing the bord and pillar geometry and Lines C, D, E and F above the roof, along which history points are located 92
Figure 6.6: Contour plot of vertical stress distribution for the isotropic model (along Section A, Figure 6.4) 93
Figure 6.7: Contour plot of major horizontal stress distribution (along Section A, Figure 6.4) 94
Figure 6.8: Contour plot of minor horizontal stress distribution along Section A 95
Figure 6.9: Distribution of stresses (along Line A, Figure 6.4) 96
Figure 6.10: Distribution of major horizontal stresses (along Line M-M in Figure 6.3) at various positions behind, at and ahead of coal face . 97
Figure 6.11: Principal stress tensors for the isotropic model (along Section A, Figure 6.4) 97
Figure 6.12: Distribution of vertical stresses at the horizontal pillar mid-plane for the isotropic model (along Line G-H Figure 6.5)..... 98
Figure 6.13: Distribution of stresses for the transversely isotropic model (along Line A in Figure 6.4) 99
Figure 6.14: Contour plot of vertical stress distribution along Section A for the elastic model with an interface 100
Figure 6.15: Contour plot of major horizontal stress distribution along Section A for the elastic model with an interface 101
Figure 6.16: Distribution of stresses (along Line A, Figure 6.4) 101
Figure 6.17: Distribution of vertical stress in the pillar horizontal mid-plane for the isotropic model with an interface (along Line A)..... 102
Figure 6.18: Vertical stress distribution (along Section A, Figure 6.4) 103
Figure 6.19: Major horizontal stress distribution (along Section A, Figure 6.4) 104

Figure 6.20: Plot of major principal stress distribution along Section A..... 105
Figure 6.21: Plot of vertical stress distribution along Section A 105
Figure 6.22: Stress distribution above bord and pillar geometry 106
Figure 6.23: Induced vertical displacements (along Line B, Figure 6.4)..... 107
Figure 6.24: Failure state in the immediate roof (along Section A, Figure 6.4) . 107
Figure 6.25: Plan view showing failure zones at the roof level for model with a coal heading..... 108
Figure 6.26: Failure zones 0.2 m behind the coal face (along Section M-M)..... 109
Figure 6.27: Failure zones 1 m behind the coal face (along Section M-M)..... 109
Figure 6.28: Failure zones 6 m behind the coal face (along Section M-M, Figure 6.3)..... 110
Figure 6.29: Failure state above immediate roof for strain softening model (along Section A, Figure 6.4)..... 111
Figure 6.30: Failure zones 1 m behind the coal face (along Section M-M)..... 111
Figure 6.31: Plan view showing failure state at the roof level for Model 1 geometry with an interface 112
Figure 6.32: Extension strain distribution (along Section A, Figure 6.4)..... 114
Figure 6.33: Plan view of extension strain distribution at roof level..... 114
Figure 6.34: Plan view of extension strain distribution at 1 m above roof level 115
Figure 6.35: Plan view of extension strain distribution at roof level (based on Model 2 geometry) 116
Figure 6.36: Extension strain distribution at 3 m behind the coal face (along Section M-M, Figure 6.3) 117
Figure 6.37: Extension strain distribution at 1.4 m ahead of the coal face (along Section M-M, Figure 6.3) 118
Figure 6.38: Extension strain distribution (along Section A, Figure 6.4)..... 119
Figure 6.39: Plan view showing extension strain distribution at 1 m above the roof level position 119
Figure 6.40: Plan view of extension strain distribution at roof level..... 120
Figure 6.41: Plan view of extension strain distribution at 0.5 m above the roof level position 121

Figure 6.42: Distribution of extension strain (along Section A, Figure 6.4) 122
Figure A1.1: Typical stress – strain graph for a cylindrical sample for loading normal to bedding 147
Figure A1.2: Typical stress – strain graph for a cylindrical sample for loading along bedding 147

LIST OF TABLES

Table 2.1: Principal stresses and their orientations 29
Table 2.2: Horizontal and vertical stress components at other Anglo Coal mines (Munsamy, 2003) 30
Table 3.1: Guttering areas compared to non-guttering areas 46
Table 4.1: Results of laboratory tests 70
Table 6.1: Comparison of results for the different constitutive behaviours 123
Table A1.1: Dynamic Young's modulus for loading along bedding for cylindrical samples 145
Table A1.2: Dynamic Young's modulus for loading normal to bedding for cylindrical samples 145
Table A1.3: UCS, Young's modulus and Poisson's ratio values (static) for cylindrical samples for loading normal to bedding 146
Table A1.4: UCS, Young's modulus and Poisson's ratio values (static) for cylindrical samples for loading along bedding 146
Table A1.5: Tensile strength for loading along bedding 148
Table A1.6: Tensile strength for loading normal to bedding 149
Table A1.7: Calculated critical extension strain for loading parallel to bedding 149
Table A2.1: Bulk and shear moduli values used in the elastic analysis 151
Table A2.2: Young's modulus and Poisson's ratio values used in the calculations 151
Table A2.3: Mohr-Coulomb material properties 152
Table A2.4: Strain softening material properties for the shale layer 153

LIST OF SYMBOLS

AECL	Atomic Energy Canada Limited
C	Cohesion
CSIRO	Commonwealth Scientific and Industrial Research Organisation
D	Diameter of a test specimen
E	Static Young's modulus
E_{dyn}	Dynamic Young's modulus
FLAC	Fast Lagrangian Analysis of Continua
FLAC3D	Fast Lagrangian Analysis of Continua in Three Dimensions
G	Shear modulus
K	Bulk modulus
MCSS	Mohr-Coulomb strain softening
P	Load at failure
SIMRAC	Safety in Mines Research Advisory Committee
t	Thickness of a test specimen
UCS	Uniaxial compressive strength
URL	Underground Research Laboratory
V_p	Velocity of compression waves
V_s	Velocity of shear waves
$\Delta V/V$	Volumetric strain
e_3	Strain in the direction of the minimum principal stress
e_c	Critical extension strain
τ	Shear stress
ϕ	Angle of internal friction
ρ	Density
ν	Poisson's ratio
σ_1	Major principal stress
σ_2	Intermediate principal stress
σ_3	Minor principal stress
σ_n	Effective normal stress

σ_t	Tensile strength
σ_x	In situ horizontal stress
σ_y	In situ horizontal stress
σ_z	Vertical stress due to gravity

CHAPTER 1

Introduction

1.1 Background

Mining of coal contributes significantly to the economy of South Africa. The main domestic uses of coal are for electricity generation, production of oil fuels and petro-chemicals, in the metallurgical industry and the cement industry (Chamber of Mines of South Africa, 2005). Over 80 per cent of South Africa's coal is mined in Mpumalanga province. The country's total saleable production was 238 Mt in 2004 (World Coal Institute, 2006). Coal production is mainly by bord and pillar mining, which accounts for about half of the total production and 90 per cent of the total underground production. Longwall mining and rib-pillar extraction are the other mining methods used for extraction of underground coal. Underground operations account for 60 per cent of total coal production. The remaining 40 per cent is recovered by open cast operations (Chamber of Mines of South Africa, 2005).

Bord and pillar mining, which currently permits less than 65 per cent of coal extraction, involves mining of bords and leaving coal pillars to support the overburden strata. The pillars are expected to remain stable while mining is in progress. The key to safe implementation of the method is good design of the bord and pillar geometry. A good pillar design is one properly sized for both safety and efficiency (Pariseau and Eitani, 1981). In order to create a safe working environment pillars should be able to support the overburden strata while the roof and floor should not fail into the roadway. Safe roadways are needed to provide for safe access of personnel, transportation of coal and underground supplies, and for ventilation purposes.

Design of coal pillars in South Africa intensified after the Coalbrook Colliery disaster in January 1960 where 437 miners lost their lives. The tragedy occurred as a result of failure of more than 7000 coal pillars, 4400 of them within 5 minutes (York et al, 2000). After the Coalbrook Colliery disaster, design for bord and pillar mining has been done using Salamon and Munro's pillar strength formula. Salamon and Munro's pillar strength formula uses a safety factor to relate strength of coal pillars with load acting on the pillars. It is an empirical, geometrically based formula which was determined statistically from an analysis of underground pillars and found to be a function of three parameters. These are the inherent strength of the coal material, the width and the height of the pillar (Salamon and Munro's, 1967).

The load acting on the pillars is calculated using the Tributary Area Theory where each pillar is assumed to bear the load of the overburden material immediately above it. The Tributary Area Theory is applicable for regular mining layouts where the width of the panel is greater than the mining depth. The main limitation of the tributary load is that it is restricted to the normal pre-mining stress applied to the vertical axis of the pillars. It assumes that other stress components of the mining stress field, e.g., high horizontal stresses, have no effect on the pillar performance. The load acting on the pillars is a function of the mining depth, pillar width and bord width.

Salamon and Munro's strength formula is basically used to determine any one of the design parameters i.e., pillar width, bord width and pillar height given the other parameters. A safety factor, defined as the strength of pillar divided by pillar stress, of 1.6 is usually recommended. One weakness of Salamon and Munro's strength formula is that it does not provide the physical insight to stresses acting in the pillar, roof and floor and surrounding rock mass. ***In addition, the formula disregards the fact that roof and floor rocks may themselves be in a state of failure at the time of, or even before, pillar failure (Mohan et al, 2001).***

Several minor collapses have occurred with pillars designed to Salamon and Munro's strength formula, especially in the Vaal Basin coalfields (Madden, 1989). By using techniques similar to those used by Salamon and Munro's, Van der Merwe (1993) found that the Vaal basin, and in particular Sigma Colliery, has weaker coal than the rest of South Africa.

Nowadays, the ability to include detailed geological data in numerical models and the availability of powerful computer packages has seen an increase in the use of numerical models for simulation of stress and strain distributions around underground openings (Starfield and Cundall, 1988). Numerical models provide physical insight to stresses acting in the pillar, roof, floor, and surrounding rock mass and the induced displacements thereof.

1.2 Definition of the problem

A problem associated with bord and pillar mining of coal is roof instability. One such cause of roof instability is roof guttering. Occurrence of roof guttering takes place when fractured roof rock falls down leaving a groove along a roadway. Roof guttering in coal mines has proved to be a safety and production constraint. It is believed that the occurrence of roof guttering at Nooitgedacht Colliery is a result of higher than normal horizontal stresses (Munsamy and Minney, 2004). The occurrence of guttering results in roof instability directly, as well as indirectly from the interaction of the guttering with natural planes of weaknesses in the immediate roof rock. The occurrence of guttering impacts negatively on the cost of production, since more man-hours are dedicated to making the work place safe by barring down and installing an intensive roof bolt support system. The roof bolt support system is, however, not very effective as guttering takes place in supported rock in some instances. Increasing the size of pillars did not solve the problem either. It has only increased the amount of coal left in the pillars without any improvements in reducing roof failures. Guttering exposes miners to the hazard of rock falls. An important factor, which cannot be quantified, is the

psychological effect of potentially unstable roof conditions on the workforce (Nicholls, 1978).

Frith *et al* (2002) noted that in most situations guttering is a result of high horizontal stresses. Van der Merwe and Madden (2002) acknowledged that the occurrence of guttering in South African coal mines is stress-related. However, Van der Merwe and Peng (2000) had argued that the role of horizontal stress is being exaggerated in roof instability of South African coal mines. As such, over-emphasis of horizontal stress effects could result in ineffective remedial action being taken on the mines.

Another cause of instability, besides roof guttering, is rockbursts. Ortlepp (1997) noted that rockbursts, in the sense normally conveyed by the term, do not occur in coal mines in South Africa. However, he described a rockburst which occurred in a shallow coal mine at a depth of 25m.

Rock falls and rockbursts cause accidents to underground personnel, and cause damage to machinery and mine workings. In some instances endangered workings can be abandoned, leading to loss of valuable mineral reserves (Pothini and von Schonfeldt, 1978). The cost of labour, materials, equipment and lost production is often significant.

Rockfalls are the single largest contributor to safety related fatalities in the South African mining industry (MHSC 2004/2005 Annual Report). Rockfalls have accounted for about half of the accidents that cause injuries and fatalities to personnel in the coal mining industry (Van der Merwe, 1998). Figure 1.1 shows fatality rates for different mining sectors during the period 1994 to 2004.

To eliminate, control, or minimise the risk of rockfalls, rockbursts, pillar failure, and roof and floor failure as a result of the instability associated with bord and pillar mining, knowledge of stress and strain distribution around a bord and pillar geometry is essential. In other words it is necessary to understand the distribution

of stress and strain around bord and pillar geometries for a good and sound design, and implementation, of bord and pillar mining.

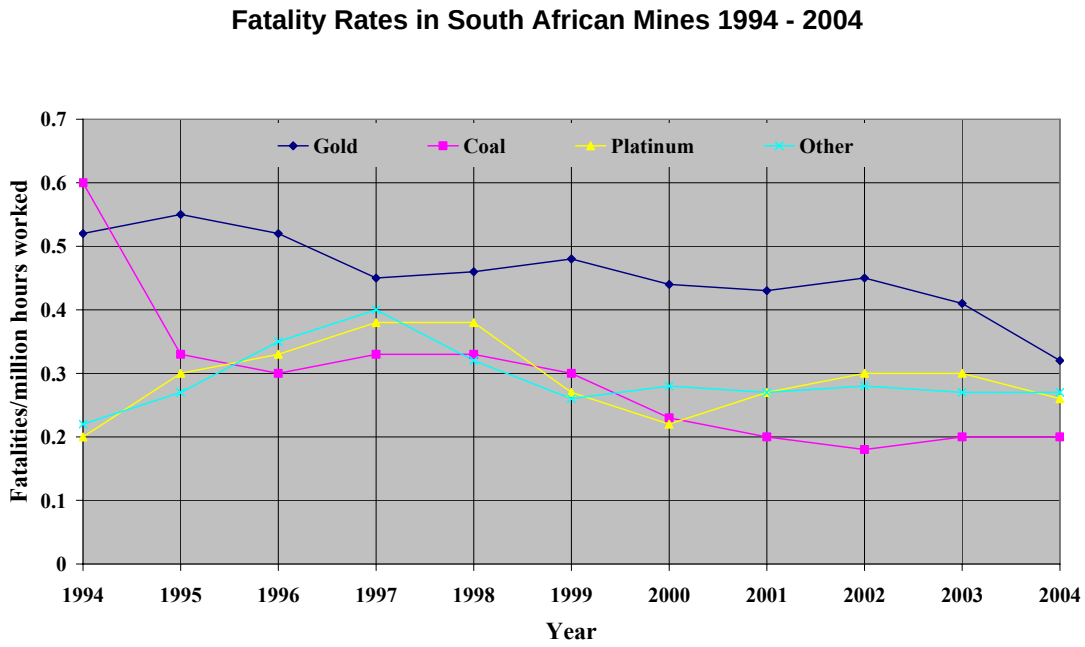

Figure 1.1: Fatality rates per million hours worked for South African mines 1994 to 2004 (MHSC 2004/2005 Annual Report)

1.3 Objectives

The objective of this research is to improve the understanding of the three dimensional distribution of stresses and strains around bord and pillar workings. The primary project output is the prediction of potential behaviour of bord roof strata and coal pillars as a result of high horizontal stresses that exist at a local coal mine. This should impart enhanced understanding of stress induced instability in bord and pillar geometries observed at a local coal mine. The development of guttering and other instabilities in the roof of coal mine workings is to be investigated. Rock failure mechanisms involved in guttering process will be investigated. Once rock mass behaviour around a bord and pillar geometry is understood it may be possible to contain failure by optimisation of excavation shape and positioning or through the design and installation of an effective and

efficient support system. The consequence is safety improvement implications which should result in maximum extraction of the mineral reserves in a safe manner.

1.4 Research Methodology

Occurrences of roof guttering have recently been observed at a local coal mine in Mpumalanga province. Mapping of occurrences of roof guttering and data collection were carried out at the mine. The following is a summary of the tasks that were carried out:

(i) Mapping of guttering areas on a macro and micro scale;
(ii) Collection of information on roof instability and on previous mapping of roof guttering;
(iii) Possible mechanisms involved in the failure of intact rock through guttering were investigated;
(iv) Collection of rock samples of immediate roof for laboratory testing;
(v) Laboratory testing to determine different rock material properties e.g. Modulus of Elasticity, Poisson's ratio, density, uniaxial compressive strength and tensile strength. The material properties were required as input parameters to the numerical modelling software;
(vi) Use of numerical modelling software for analyses of stresses and deformations around bord and pillar geometries, and simulation of occurrences of guttering as observed at the mine.

1.5 Content of the dissertation

The following chapter details the background discussion of bord and pillar mining as applied to coal mining from the 1960s to its current application. The problems associated with high horizontal stresses are discussed together with possible methods of amelioration. The subject of roof guttering in South African collieries as discussed by a variety of researchers is included in this chapter. Results of

mapping of roof guttering at Nooitgedacht Colliery are given in Chapter 3. Photographs of guttering roof are included here to aid in the descriptions. Results of the study of the progressive failure of rock at the Atomic Energy Canada Limited's (AECL's) Underground Research Laboratory (URL) are discussed. A comparison of these results is then made with results of observations of roof guttering at Nooitgedacht Colliery. Results of laboratory work are discussed in Chapter 4. Numerical and constitutive laws used in this dissertation are discussed in Chapter 5. Results of numerical modelling are discussed in Chapter 6. The findings of the research and conclusions are given in Chapter 7. Two appendices complete this dissertation. Appendix A1 gives the laboratory test results and Appendix A2 gives the material properties used for numerical modelling.

CHAPTER 2

Bord and pillar design in coal mining

2.1 Introduction

Pillar design in bord and pillar workings involves determining the dimensions of pillars necessary to support the overburden material. As summarised in Chapter 1, the strength of pillars and the load acting on the pillars are the two important parameters in the design of coal mine pillars. The strength of a coal pillar is affected by the strength of the coal material which forms the pillar. The strength characteristics of coal mine pillars have received considerable research over the past 40 years. The subject is well discussed in the literature by Salamon and Munro's (1967), Bieniawski (1968), Cook et al (1971), Oravecz (1973), Bieniawski and van Heerden (1975), Hustrulid (1976), Hill (1989), Madden (1990), Mark and Iannacchione (1992), van der Merwe (1993, 1995), Madden et al (1995), Gale (1996), Esterhuizen (1998) and York et al (2000).

Pillar strength relationships have been derived from four main sources (Gale 1999):

(i) laboratory strength measurements on coal block specimens of different sizes and in-situ strength measurements;
(ii) empirical relationships from observations of collapsed and intact pillars;
(iii) theoretical fit of statistical data and observations;
(iv) theoretical extrapolation of the vertical stress build up from the ribside towards the pillar centre to define the load capacity of a pillar

The strength relationships derived provide a wide range of potential strength for the same pillar geometry. In practice, different formulae are modified to suit the

geological environment of a specific coal seam. Section 2.2 reviews the literature on the history of bord and pillar design from the 1960s to present day South Africa.

2.2 Design for bord and pillar mining

Salamon and Munro's (1967) used statistical methods to determine a pillar strength formula from back analysis of 27 collapsed and 98 intact cases. Salamon and Munro's formula assumed that the coal was the weakest element with strong surrounding roof and floor. Their power formula has been used in the South African coal industry at the expense of the linear formula of Bieniawski (1968) that was determined from in situ tests of large coal specimens although the differences between the two formulae were not significant.

Great achievements have been made in understanding the behaviour of coal pillars although problems still exist. Design of coal pillars has generally been achieved by use of empirical and analytical methods. Empirical methods:

(i) Have been proven to be reliable as they are developed from field observations;
(ii) Are easy to implement as they require few input parameters, such as safety factor, pillar height, pillar width and depth of workings in the case of Salamon and Munro's formula;
(iii) Can be customised for a particular operation by adjusting the necessary constants in the formulae, e.g., van der Merwe (1993) found that the strength of coal pillars for the Vaal Basin was 4.5 MPa compared to 7.2 MPa generally used by South African collieries.

Limitations of the empirical methods are:

(i) The data range from which the formulae are derived limits the application of the method to conditions whose data ranges are close to the original database;
(ii) Empirical methods incorporate the properties of the surrounding rock mass in the constants. For this reason the constants of the formula cannot tolerate large variations in rock mass quality;
(iii) Empirical methods lack the explanations of the loading mechanisms i.e., they do not provide physical insights to the actual state of stress within a pillar.

Extensive laboratory investigations were carried out between 1963 and 1969 to determine the strength of coal from the Witbank Coalfield. The results showed a reduction in strength with increasing specimen size. During the period 1966 to 1974 extensive in situ testing of pillar strength was conducted. A critical sample size of 1.5 m was determined, beyond which there was no decrease in strength (Bieniawski and van Heerden, 1975). Cook et al's (1971) in situ tests showed that the centre portion of a pillar was capable of withstanding high stresses beyond the strength of the pillar. Field measurements, analytical solutions and use of the electrical resistance analogue were used by Oravecz (1973) to investigate the load on coal pillars. He concluded that at low levels of stress as well as small displacements, the theory of elasticity applied to coal strata.

In 1982 Salamon derived a pillar strength formula that took cognisance of the increasing ability of a pillar to carry higher loads with an increasing width to height ratio (Madden et al, 1998). The formula caters for mining conditions which are outside the empirical range of the original design formula i.e., very shallow depths and greater depths. At shallow depths pillars designed using Salamon and Munro's strength formula are small and prone to failure while at greater depths, the pillars are very large implying low extraction ratios. Wide pillars are much stronger than calculated from the original Salamon and Munro's formula since the

formula does not take into account the strength increase caused by lateral constraint of the pillars. The use of the squat pillar design formula resulted in increased extraction of coal at greater depths and enhanced stability in shallow workings.

Madden (1990) investigated the effect of blast damage on the stability of pillars. He showed that the fractured side of a pillar was a result of the weakening effect of blasting. He noted that Salamon and Munro's coal pillar design formula implicitly considered the weakening effect of blasting on the strength of a coal pillar. The study showed that the "continuous miner formed pillars" do not have a blast damaged zone hence they could be designed to a smaller width than those designed for drill and blast mining. This could result in an increased extraction of coal.

Esterhuizen (1998) investigated the effect of structural discontinuities on coal pillar strength. Discontinuities are not explicitly taken into account in the empirical methods of pillar design. For this reason, pillars formed in coal with a high intensity of discontinuities may be under designed, while pillars in undisturbed coal may be over designed. Laboratory strength tests showed a reduction in strength of coal samples with increase in volume. This was attributed to the increased intensity of discontinuities in large samples among other factors. Numerical models were also used to assess the effect of discontinuities on pillar strength. Results showed that the effect of discontinuities became less pronounced as the width to height ratio increased. From the field data on discontinuities and pillar dimensions, Esterhuizen (1998) developed a set of equations to quantify the effect of discontinuities on the strength of coal pillars.

van der Merwe (2003) detailed the study of time related decay of bord and pillar workings. He analysed the database of failed coal pillars in South Africa with regard to the time of failure. The aim was to develop a method for the prediction of time that it took pillars to fail after their formation. Based on observations and experience it was postulated that coal pillars failed by progressive weakening

starting from the edges and progressing into the pillar. The predictions of time to failure of pillars correlated well with field observations. Frequencies of future pillar failures may now be predicted.

The empirical design methods used in South Africa utilize the ultimate strength design approach. The assumption of this method is that once the ultimate strength of a pillar is exceeded the pillar will have zero strength and failure will occur, which may not be necessarily true in reality. The following trends are considered in the determination of the ultimate strength of a pillar (Badr, 2004):

(i) as size of a pillar increases its uniaxial compressive strength decreases;
(ii) as width to height ratio increases the pillar strength also increases;
(iii) laboratory UCS has a correlation to the ultimate strength of a pillar

The other design approach is the progressive failure approach which assumes a non-uniform stress distribution within the pillar. Failure of a pillar begins at a point that has reached its ultimate strength and gradually progresses until ultimate failure of the whole pillar. Numerical models can adopt both the ultimate strength and the progressive failure approaches.

Salamon and Munro's (1967) design formula implicitly takes into account different factors that affect pillar strength (York et al, 2000). These factors include in situ rock mass strength, pillar dimensions, effect of jointing, loading system, contact conditions, stability of the floor and roof and creep and other time effects. York et al (2000) investigated the influence of these factors on pillar strength. They came up with a formula that explicitly quantifies most of these factors. The formula takes care of interaction between the behaviour of the pillar, the roof, the floor and the loading system. The design depends on the weakest element or the dominant factor. This is an improvement to Salamon and Munro's (1967) formula which assumed that the coal was the weakest element where failure took place while the roof and floor were strong. The advantage of York et al's (2000) design approach is the ability to design on a site or region specific basis, both for

increased and decreased strength, as required in specific circumstances. The new methodology allows for parameters to be changed while the Salamon and Munro formula is fixed. The following section provides an insight into stress redistributions that take place when an underground opening is excavated in a rock mass. Knowledge of stress redistribution is necessary for an effective design methodology.

2.3 Stress changes due to creation of underground excavations

Prior to the excavation of an underground opening, the rock mass has been shown to be in equilibrium under the action of virgin stresses. When an excavation is created, stresses on the surface of the excavation change and equilibrium is destroyed. In the vicinity of the opening stress redistribution takes place and equilibrium is re-established. This results in horizontal stress concentrations in the roof of an opening while vertical stresses are concentrated at the sides of the opening as shown in Figure 2.1. Part of the rock mass is displaced. Work done during the displacement of the rock mass is usually stored in the surrounding rock mass as strain energy. Part of this strain energy may be dissipated in fracturing of part of the rock mass surrounding the opening (Budavari, 1983).

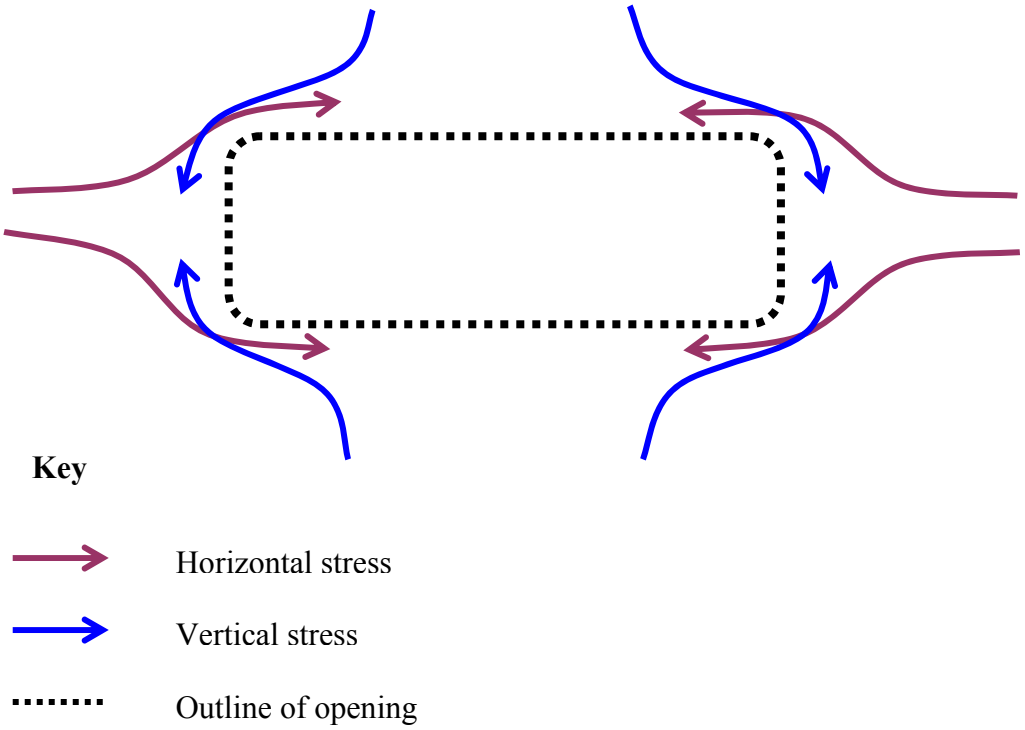

Figure 2.1: Section through a roadway showing stress redistribution when an opening is created underground

The role of high horizontal stresses has not been fully explained in the design of the coal pillar–roof–floor system. Salamon and Munro's design method assumes that the coal pillar is the weakest element of the system. Design is based on determining the pillar size with enough strength to avoid failure of the pillars as a result of overburden loading. Effect of horizontal stress is not considered in Salamon and Munro's design formula. Section 2.4 reviews the available literature on the role of high horizontal stresses in coal pillar–roof–floor systems.

2.4 Effect of high horizontal stresses in bord and pillar mines

Most coal fields worldwide have been shown to experience abnormally high horizontal stresses which cannot be explained by the Poisson effect (i.e. due to confinement stresses generated when rock under vertical compression attempts to expand laterally). Theories for the origin of these high horizontal stresses which have been put forward include the following (van der Merwe and Madden, 2002):

(i) Horizontal stresses generated by plate tectonics – stresses are generated when continental plates push against each other. This theory is not widely accepted in South Africa since coal mining regions are remote from any known plate contact points;

(ii) Locked in horizontal stresses – due to the erosion of about 1 000 m of lava which once covered the earth, vertical stresses have been relaxed while horizontal stresses have remained 'locked in';

(iii) Horizontal stresses generated during dyke intrusions – dyke intrusions generated the high horizontal stresses during the process of forcing the rock mass apart to create routes for themselves. However, this theory does not explain the occurrence of high horizontal stresses in areas which are free from dykes, an example being Nooitgedacht Colliery;

(iv) Horizontal stresses generated as a result of cooling down of the earth – it is possible that the earth is still shrinking as the molten mass deeper down gradually cools down. The solid crust is being contracted and squeezed in the process.

The effect of excessive horizontal stresses on the behaviour of the coal pillar-roof-floor system has not been fully understood. Phillips (1947) and Roley (1948) agreed that abnormally high horizontal stresses caused roof guttering. The high horizontal stresses were cited as the cause of shear failures that were observed in the roof rock at the rib line. Thomas (1950) observed that the immediate roof rock should be more competent compared to the overlying roof rock for guttering to take place at the edges of the roadways, otherwise failure takes place at the centre

of roadways. He identified rock type as a cause for localised occurrences of guttering. He proposed, from underground observations, that two conditions were necessary to produce guttering. These are:

(i) a relatively strong immediate roof that may be thinly laminated with strong cementation between laminations;
(ii) a series of weaker strata that tend to sag and slowly load the immediate roof below them.

Mining in a stress field where the horizontal stress is greater than the vertical stress was also documented by Parker (1973). Earlier "strange" observations of roof failure (i.e., crushing of roof and thrusting as shown in Figure 2.2 and 2.3, respectively) were explained to be a result of the high horizontal stresses.

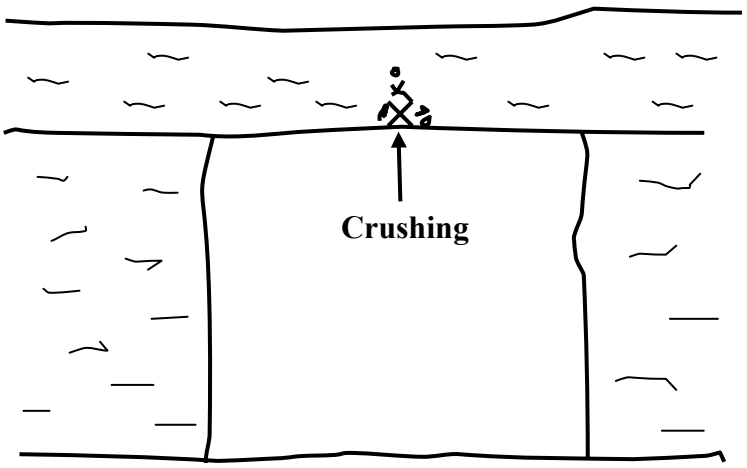

Figure 2.2: Crushing of the roof (after Parker, 1973)

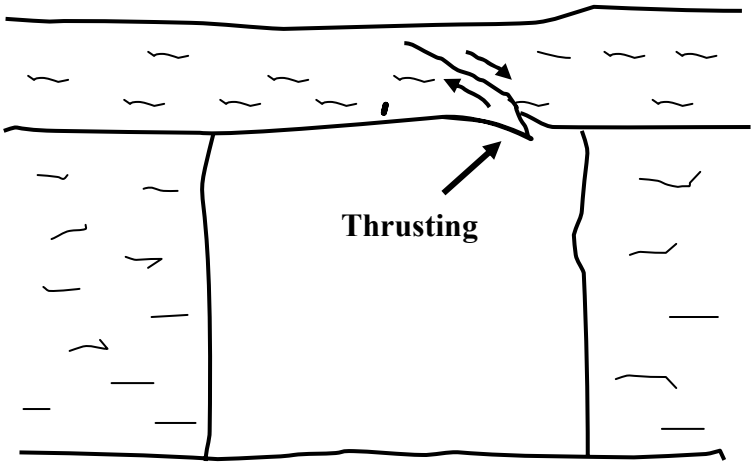

Figure 2.3: Thrusting of the roof (after Parker, 1973)

Strange offsets in empty roof bolt holes, as illustrated in Figure 2.4, were also explained to be a result of high horizontal stresses. Parts of the roof sheared past each other. Thin layers of roof rock under high horizontal stress crumpled and broke. Sometimes a moderately thick layer buckled downward, and when roof bolts were installed and tightened to push the layer back up again, it broke and fell apart. A slightly thicker layer usually buckled upward, and then crushed along the centre line, where deflection and compression were greatest. From these observations, Parker (1973) concluded that the roof was likely to be failing in compression or in shear.

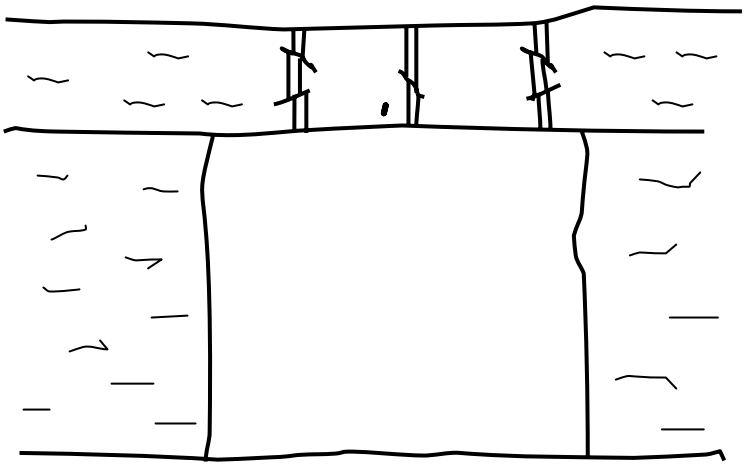

Figure 2.4: Offsets in empty roof bolt holes (Parker, 1973)

The influence of high horizontal stresses and roof rock competency on the occurrence of roof guttering was also assessed by Wang *et al* (1974) using two dimensional finite element analyses. Their results mirrored observations that had been made in the field. Aggson (1978, 1979a, 1979b) and Agapito *et al* (1980) also concluded from numerical modelling and in-mine verification that roof guttering was a result of high horizontal stresses. Two dimensional finite element models representative of the mine sites were analysed and a close correlation was found between in-mine observations of guttering and the failure modelled by the computer. They concluded that the most probable roof failure was shear failure near the pillar edge. The inclination of the failure surface and the height of the probable roof fall were deemed to be a function of the relative magnitudes of the horizontal stresses and the shear strengths of the members in the stratified roof. Kripakov (1982) conducted a similar study using in-mine in situ stress measurements and two dimensional finite element analyses. His modelling results were closely related to field observations. Iannacchione *et al* (1984) and Hill and Bauer (1984) showed that minor geologic structures (for example, clastic dykes and bedding planes) contributed to the instability of roof rock, resulting in the initiation of guttering.

Peng (1986) described the formation of guttering in the roof rock. According to him, guttering begins with a fracture that initiates and propagates upward from one or both upper corners of an entry. When the fracture extends to a height above the roof bolt anchorage and/or breaks along weak bedding planes, a roof fall occurs. According to Peng (1986) occurrence of guttering may be confined to the upper left or upper right corner of an entry. It may change, however, from one corner to the other in the same entry. Sometimes it occurs at the upper corner on one side of an entry accompanied by a floor crack on the lower corner on the other side of the entry. Peng (1986) also concluded that guttering was probably caused by shear stresses at the entry corners being larger than the shear strength of the rock. These high shear stresses are believed to be due to large overburden weight and/or excessive horizontal stresses. Other factors e.g., local geology and relative

stiffness of the floor, coal pillars, and immediate roof conditions also contributed to guttering.

Hill (1986) shared the same views with Peng (1986). Hill defined guttering as a failure process that initially begins as a fracture in the roof rock parallel to, and located at, the roof rib intersection. The fracture propagates upward into the roof and initial failure is confined to the roof-rib intersection. The roof guttering failure sequence according to Hill is illustrated in Figure 2.5 (Hill, 1986). The first stage involves fracture propagation in a nearly vertical direction from the roof-rib intersection as shown in Figure 2.5a. The second stage involves fracture propagation along a weak zone at or above the roof bolt anchorage horizon and is illustrated in Figure 2.5b. Tension cracks develop due to bending of the beam. The tension cracks grow and finally a roof fall occurs (Figure 2.5c). Hill (1986) noted that although theoretical explanations of the causes of roof guttering existed they lacked comprehensive in-mine verification through instrumentation and mapping.

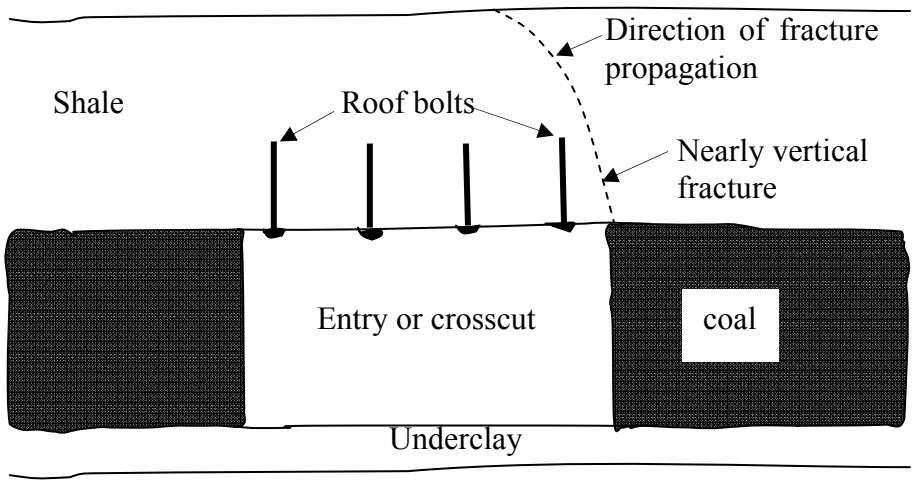

(a) Initial fracture propagation

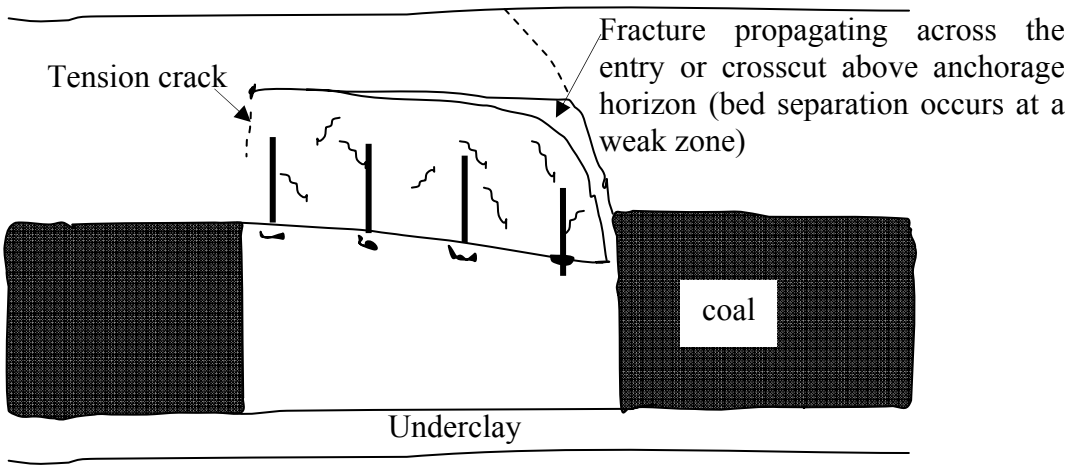

(b) Propagation of fracture along weak zone (bed separation)

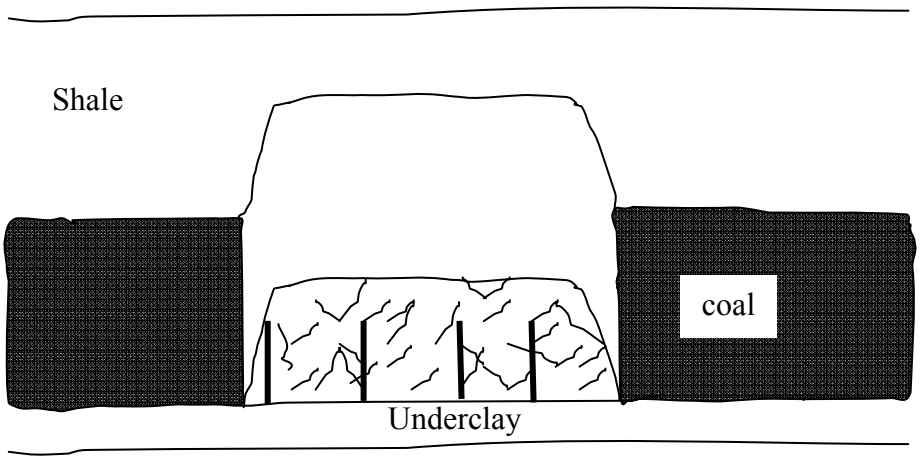

(c) Massive roof collapse

Figure 2.5: Guttering roof failure sequence (After Hill, 1986)

Hill (1986) investigated the factors that influenced the propagation of roof guttering. He found that two critical factors were the stress environment and rock type. A noticeable and most often cited sign of regionally high horizontal stresses in coal mines is that roof guttering occurs in one particular orientation. In addition to artificial support, Hill (1986) discussed mine design changes for controlling or avoiding roof guttering. Artificial support included angle bolting as shown in Figure 2.6 and truss bolting as shown in Figure 2.7.

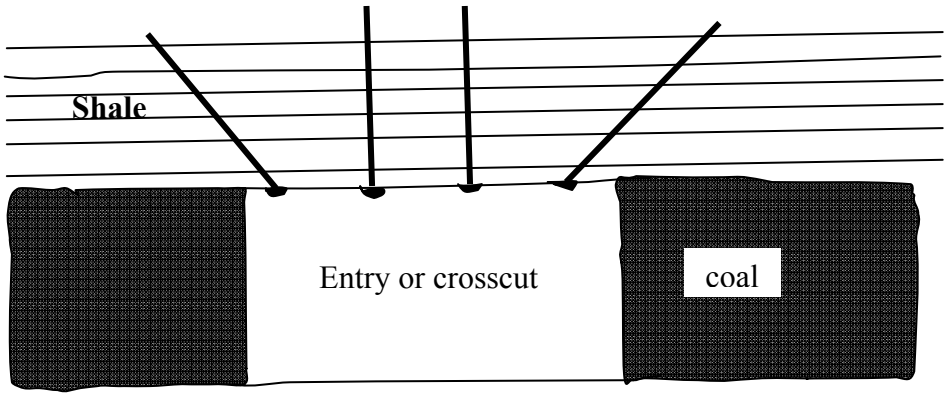

Figure 2.6: Schematic diagram of angle bolting (Hill, 1986)

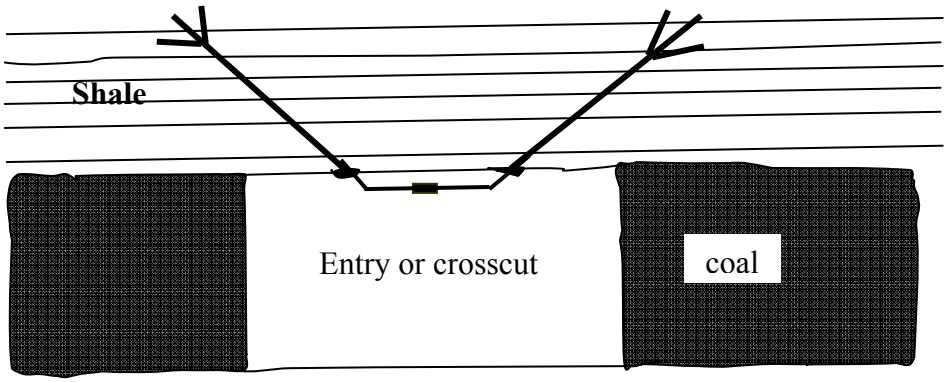

Figure 2.7: Schematic diagram of truss bolting (Hill, 1986)

Mine design changes included “sacrifice” entries, pillar softening, yield pillars, roof slotting, pillar staggering, reduction in the width of openings, and entry re-orientation. A “sacrifice” entry, shown in Figure 2.8, is a roadway developed ahead of and parallel to future adjacent roadways. Failure is allowed to initiate in “sacrifice” entries thereby relieving in situ stresses to manageable levels in adjacent entries.

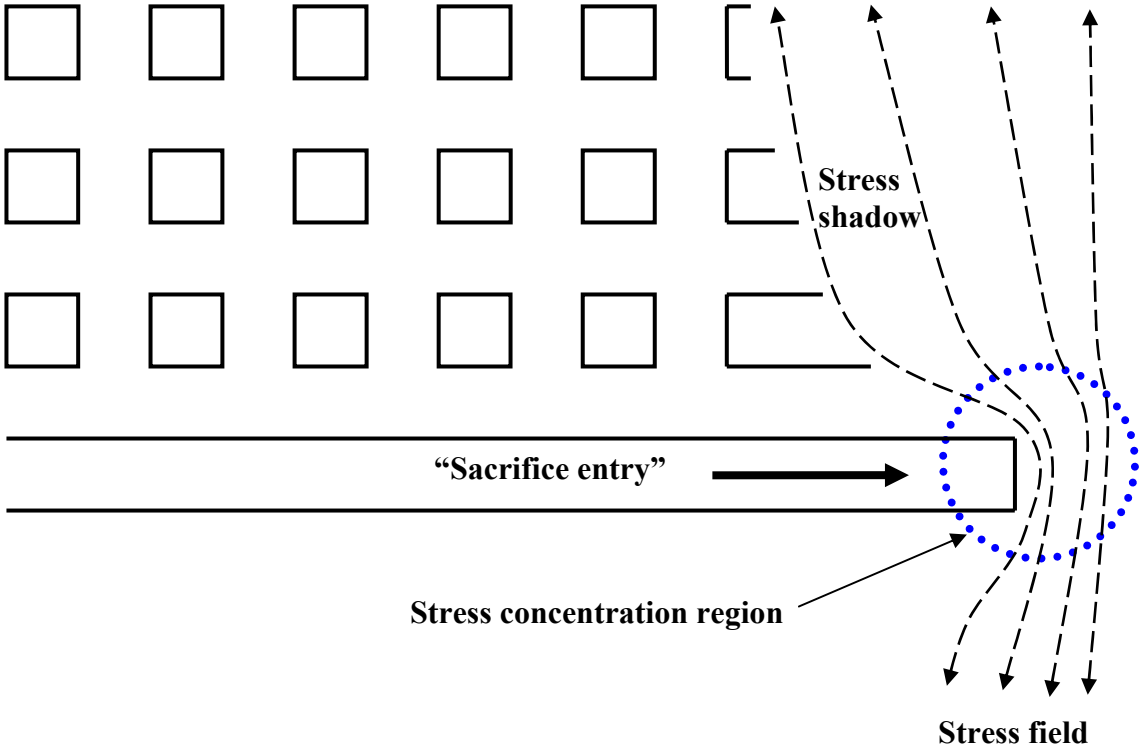

Figure 2.8: Schematic plan diagram showing the stress shadow created by mining a roadway some distance ahead of other roadways

Pillar softening is a concept based on coal pillar elasticity versus roof rock elasticity and the effect of this ratio on the magnitude of stresses in the corners of the entry. Stress concentrations in the corners of an entry are re-distributed when the elasticity of the pillars is reduced. This is done by pillar slotting – drilling holes into pillars at the roof-coal interface as shown in Figure 2.9.

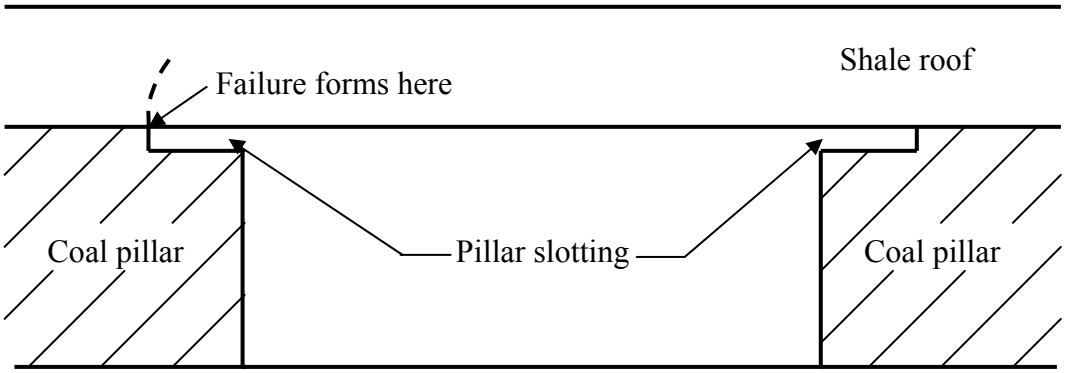

Figure 2.9: Cross-sectional view of rib-slotting method (Adapted from Kripakov, 1982)

Yield pillars also reduce the elasticity of coal pillars. The concept is that pillars are small enough so they intentionally yield and transfer the majority of roof loads to the abutments. The result is reduction of overall roof and floor stresses. Research on the application of the yield pillar concept is currently receiving much attention. It promises to be a solution to relieving high stress levels at greater depths.

Entry re-orientation is used where roof guttering is caused by a strongly biaxial horizontal stress field. If a biaxial stress field exists, entries oriented perpendicular to the maximum principal horizontal stresses are under the greatest influence of the stress. By orienting mine headings so that both entries are perpendicular to the same least stress value, the influence of biaxial stress field can be offset.

Mark et al (1997) noted that two factors that determined the degree to which horizontal stresses affected ground control were:

(i) Roof type: weak roof was more likely to suffer damage than strong roof, and laminations reduced a roof's ability to resist horizontal stress;

(ii) Entry orientation: entries that are aligned with the maximum horizontal stress suffered less damage on development than those perpendicular to it.

Iannacchione et al (1998) acknowledged that high horizontal stresses usually caused sudden roof failures. They mentioned that under high horizontal stresses roof beams have been observed to fail in shear as well as in tension. Barron and Baydusa (1999) acknowledged that proposed theories on the causes of guttering have been confusing; with some implying that a horizontal compressive stress in excess of vertical stress was the prime cause. Others stated that high horizontal stress, "strong" rock versus "weak" rock, and competent versus incompetent adjacent pillars all contributed to guttering. Barron and Baydusa (1999) developed a theory for gutter roof failure and showed that the key parameters influencing the likelihood of roof guttering were:

(i) rock strength;
(ii) vertical stress (depth), and;
(iii) horizontal to vertical stress ratio

From underground observations at one mine, Dolinar et al (2001) noted that high horizontal stresses caused long running roof falls which resulted in hazardous conditions for the miners and premature abandonment of panels. The stress damage was in the form of gutters. The majority of the roof falls occurred from a few days to several weeks after an opening was mined.

Iannacchione et al (2001) noted that mining perpendicular to the orientation of the maximum horizontal stress can concentrate that stress in the immediate roof rock. When stress levels exceeded the strength of the roof rock, beams within the roof usually buckled and failed in shear. They mentioned that the shear planes can coalesce and form a semi-linear trend tens to hundreds of metres in length across a mining section. Major shear zones usually resulted in large roof falls that were often oval in shape with the long axis perpendicular to the orientation of the maximum horizontal stress as shown in Figure 2.10. They observed that typical falls showed stress concentrations along the axial ends of the oval. Also common was for the oval shaped type of fall to grow both vertically and horizontally over

the course of days, weeks, and even years, depending on conditions. Another recognised characteristic of a roof fall caused by high horizontal stress was the zone of reduced stress adjacent to the long axis of an oval shaped roof fall.

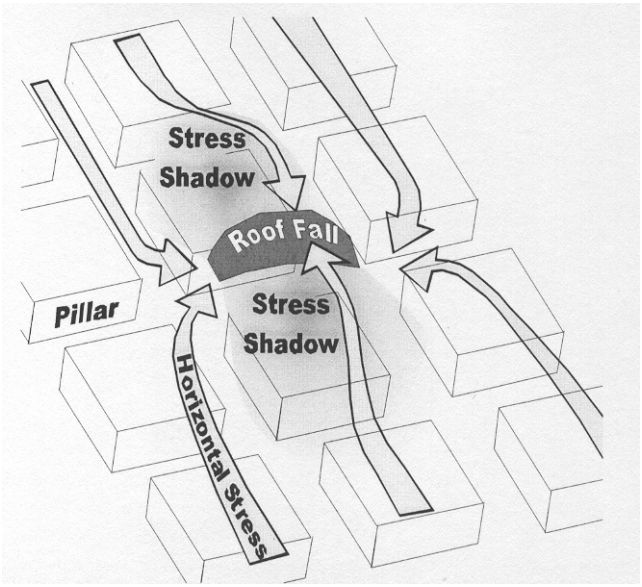

Figure 2.10: Probable stress redistribution patterns around oval-shaped roof falls, concentrating stress above and along the axial ends and reducing stress (stress shadow) adjacent to the long axis of the roof fall (Iannacchione et al 2001)

Agapito and Gilbride (2002) acknowledged that high horizontal stresses have been associated with difficult ground conditions. High horizontal stresses were recognised as a cause of sudden failures, including violent bursts, at shallow depth. Evidence of stability problems due to high horizontal stresses have been obtained from sudden fracturing and rock bursting at shallow depths where vertical stresses were low. Agapito and Gilbride listed three major symptoms of high horizontal stresses as:

(i) compressional roof failure (guttering);
(ii) roof falls in predominant directions, and;
(iii) more ground problems in headgates as compared to tailgates

Esterhuizen and Iannacchione (2004) summarised typical failure under high horizontal stresses as progressive shearing and buckling of individual rock layers in the roof. They noted that the failures were often preceded by excessive deflection of the roof beams. Collapse of the roof beams was progressive in the vertical direction, with individual beds typically failing from the bottom up. They also noted that failure progressed over days, weeks or months until a stable rock layer was reached. Once a portion of the roof had failed, the failed zone tended to propagate laterally, in a direction perpendicular to the major horizontal stress. Guttering has been observed in a South African colliery. The literature survey shows that studies to explain the mechanisms of formation of roof guttering in South African collieries have been very limited. Section 2.5 reviews some of the papers that have been written on the subject of guttering in South African collieries.

2.5 Guttering occurrence in South African collieries

Occurrence of guttering in South African collieries has been mentioned in various publications (Altounyan and Taljaard, 2000; van der Merwe, 2000; van der Merwe and Madden, 2002; Frith *et al*, 2002; Munsamy, 2003 and Munsamy and Minney, 2004). These researchers tended to describe the guttering phenomenon in the same way as described in papers reviewed in the previous section for UK mines. Figure 2.11 shows a guttering occurrence observed in one of the South African collieries.



Figure 2.11: Guttering occurrence in a South African colliery

Altounyan and Taljaard (2000) mentioned that the significance of horizontal stress stemmed from the concentration of this stress component in the roof and floor of mine openings as illustrated earlier in Figure 2.1. In their opinion, shear failure occurred if the compressional forces exceeded the rock strength - once failure initiated, redistribution of load caused progressive propagation of fractures higher into the roof. Roof falls then occurred if the fractures developed sufficiently or intersected planes of weakness. According to Altounyan and Taljaard, inspection of existing roof failures at a mine in the Witbank area confirmed the characteristic signs of shear failure.

van der Merwe (2000) argued that the role of horizontal stresses in South African coal mines was being over-emphasised. This, according to him, could lead to incorrect remedial action being taken. He showed, with the aid of examples, three situations from practice where horizontal stresses were erroneously blamed for roof collapses in the form of guttering. He mentioned that guttering can be present without high horizontal stresses, depending on the nature of the roof material. van der Merwe (2000) noted that it was misleading to consider horizontal stress as the only cause of guttering. He mentioned that the stress condition in the roof of a roadway was a combination of a number of factors.

van der Merwe and Madden (2002) acknowledged that the occurrence of guttering in South African collieries was stress-related. Like most of the previously mentioned researchers, they characterised the type of failure as shear. Their argument was based on the fact that when there is stress redistribution around an underground opening, stress is concentrated in the corners where the tangential stress is a maximum and the normal stress is zero. As a result the shear stress is also a maximum and its magnitude is equal to half of the tangential stress. As rock is more than twice as strong in compression as in shear van der Merwe and Madden (2002) expected that the most likely mode of failure was shear, which they termed guttering. They backed their discussion with calculations and showed that horizontal stresses in excess of 100 MPa, much greater than the strength of sedimentary rocks, can be generated during stress redistribution around an underground opening.

Observations of occurrences of roof guttering were also reported by Frith *et al* (2002) who indicated that in most situations guttering was a result of high horizontal stresses. They carried out a survey of horizontal stresses in the Witbank and Highveld Coalfields from available measurements and mapping. They concluded that high horizontal stresses were evident in both coalfields. The effects of the high horizontal stresses were identified in the immediate skin of the roof as localised buckling and guttering.

From feasibility studies and underground observations, Munsamy (2003) reported that adverse roof conditions experienced at a mine in Witbank were detected during the feasibility stage of the mine. He concluded that the poor roof conditions were the result of abnormally high horizontal stresses coupled with a weak mudstone roof. He observed that the mudstone roof often failed prior to the installation of permanent support. In some cases the mudstone roof failed in supported ground. He noted that failure initiated as gutters in the roof. He also observed that the gutters had no preferred orientation. The gutters often occurred randomly moving from pillar edges to centre of the roadways.

Munsamy and Minney (2004) also considered that guttering is an indication of high horizontal stress to strength ratio and concluded that the mode of failure was shear. They based this on the assumption that the noises heard prior to roof falls was from shearing of the rock during failure. However, it should be noted that "noise" can also be associated with extension fracture.

Researchers seemed agreeable to the fact that a high horizontal stress was a major contributing factor to roof guttering. Earlier work by Walker and Altounyan (2001) had confirmed the existence of high horizontal stresses at Nooitgedacht Colliery. Stress measurement results are discussed in the following section.

2.6 Stress measurements at Nooitgedacht Colliery

Nooitgedacht Colliery believes that fracturing of the immediate roof material is a result of the existence of higher than normal horizontal stresses coupled with a weak mudstone roof layer (Munsamy and Minney, 2004). In situ stress measurements were carried out at Nooitgedacht Colliery (Walker and Altounyan, 2001) to determine the stress magnitudes at the site. The measurements were undertaken in order to quantify the stress regime in the roof of the No. 5 seam at Nooitgedacht section 50/51. The overcoring technique using the CSIRO Hollow Inclusion stress cell was employed. Using this instrument the full three dimensional state of stress can be determined from one overcoring test. The results were processed using an elastic, isotropic solution technique and are shown in Table 2.1.

Table 2.1: Principal stresses and their orientations

Test Site	Major			Intermediate			Minor		
	Value (MPa)	Bearing (°)	Dip (°)	Value (MPa)	Bearing (°)	Dip (°)	Value (MPa)	Bearing (°)	Dip (°)
Shaft	10.96	20	13	8.28	118	30	4.54	270	56
50/51	7.49	105	2	5.45	196	36	1.56	13	54

The measurements indicated the existence of high stresses in a near-horizontal direction. The major principal stress in Section 50/51 of the mine was almost horizontal, with a magnitude of 7.5 MPa, and orientated approximately East–West. It can be concluded that the maximum and minimum horizontal stress components were significantly higher than the vertical stress component. Munsamy and Minney (2004) noted that the results at the shaft site could be representing elevated stresses induced by mining as the vertical stress measured was about seven times greater than the calculated value. Although the measured value for Section 50/51 was more than the calculated value, this measurement was deemed more realistic. Stress measurements were also undertaken at other Anglo Coal mines. These are shown in table 2.2.

Table 2.2: Horizontal and vertical stress components at other Anglo Coal mines (Munsamy, 2003)

Colliery Name	Max Horizontal Stress		Min horizontal stress		Vertical stress	
	Value (MPa)	Bearing (°)	Value (MPa)	Bearing (°)	Value (MPa)	Bearing (°)
Goedehoop	13.3	328	1.7	237	1.2	065
	5.0	340	1.0	223	1.0	083
	5.1	334	0.9	232	1.0	079
Bank	6.4	010	2.3	104	1.7	258
	3.3	354	0.7	217	2.3	086
	0.8	328	0.2	326	1.0	058
Kriel	4.1	000	3.8	010	3.0	115

All except one of the sites had maximum horizontal stresses that are higher than the vertical stresses. The minimum horizontal stresses were also measured to be greater than the vertical stresses at some sites. These measurements indicate that a generally high horizontal stress regime exists at Nooitgedacht Colliery.

2.7 Conclusions

It is clear that the type of guttering discussed by most researchers initiated at the roof-pillar contact and was confined to the roof-pillar contact. This type of guttering may be associated with high stress concentration in the corners of an excavation as discussed by van der Merwe and Madden (2002). As will be described later in this dissertation, since guttering occurrences observed at Nooitgedacht Colliery commonly initiated towards the centre of bords, and generally away from the roof-pillar contact, the relevance of the high corner stresses is questionable. Shear failure might not be the cause of guttering in this case. Again, it was observed that guttering involved failure of intact rock as opposed to the guttering described by Hill (1986) and Peng (1986) where guttering was initiated by a fracture at the roof-pillar contact. The following chapter describes extensive guttering occurrences observed at Nooitgedacht Colliery.

CHAPTER 3

Mapping of guttering at Nooitgedacht Colliery

3.1 Introduction

Nooitgedacht Colliery is located in the province of Mpumalanga. The coal seam is flat lying with an average dip of less than one degree. The average depth of 5-seam is about 52 m. The coal seam averages 1.8 m in thickness. It is generally undisturbed. In some areas an intensely sheared and broken thin parting is developed towards the base of the seam and forms a false floor to the seam. Below the parting is a thin coal band, averaging 0.05 m. Micaceous mudstone or shale is developed just above the coal seam forming the immediate mining roof.

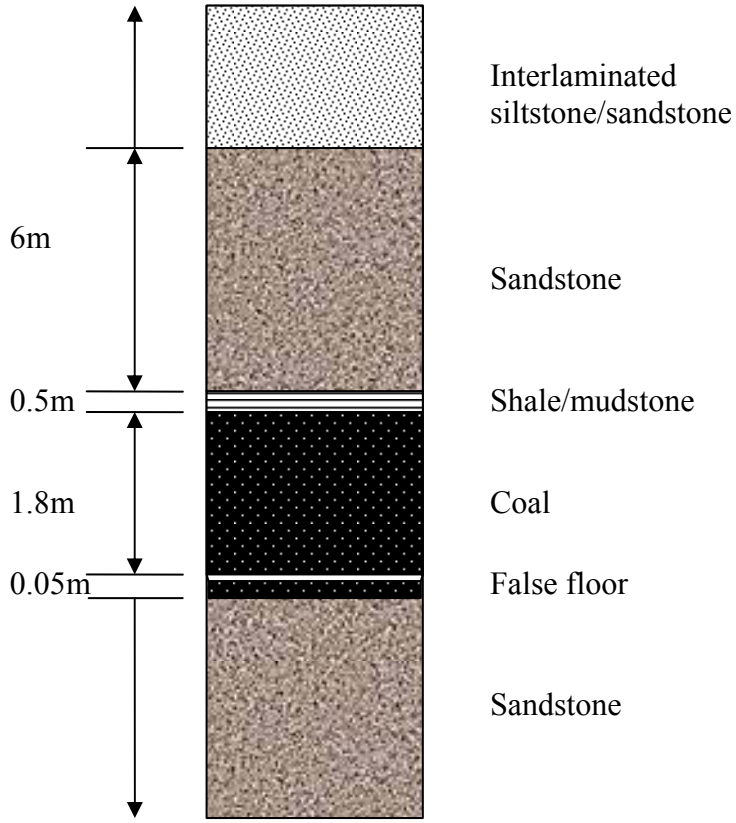

Figure 3.1: Generalised geological log for Nooitgedacht Colliery

The thickness of the shale/mudstone roof layer varies from 0 – 2 m and averages 0.52 m. A competent sandstone layer overlies the immediate roof over the entire reserve area, ranging from 0.3 m to over 12 m in thickness. Figure 3.1 shows a generalised geological log for the mine.

3.2 The mining method and panel positions

Room and pillar mining with conventional drilling and blasting is employed at the mine. Pillar widths are 8.7 m while bord widths are 6.5 m, and the mining height averages 2.0 m. The panel pillars are designed with a safety factor of 2.0. Each panel consists of thirteen roadways. The faces are advanced to keep the mining front straight mainly for ventilation purposes. The mining sequence involves ventilating the area, cutting of a horizontal slot, drilling, charging and blasting, loading and hauling, and roof support installation. Blasting of individual faces takes place separately during a shift. At the time of mapping, three contiguous panels were being mined. The panels were parallel to each other and advancing in a south-ward direction. Panel 1 had advanced about 860 m while panels 2 and 3 had advanced 690 m and 130 m respectively.

The immediate roof conditions at the mine were observed to be poor. It is thought that high horizontal stresses coupled with a weak mudstone roof are responsible for the observed roof failures. Extensive roof falls were observed in all three working sections as detailed in the next section. Photographs are included to supplement the descriptions.

3.3 Observations of the occurrence of roof guttering

Occurrence of roof guttering was mapped at the mine with the aim of determining their:

(i) size (i.e., length, width and depth);
(ii) surface features;

(iii) geometrical locations;
(iv) intensity;
(v) orientation;
(vi) initiation in relation to position of active coal face;
(vii) initiation in relation to time after mining of a particular coal face;
(viii) progression in relation to time and sequence of mining, and;
(ix) effect on coal pillars.

Inspection of areas unaffected by guttering was carried out for comparison purposes. The occurrence of guttering was mapped in all three panels of the mine. Previous mapping of guttering by the mine geologist was also used in this study.

Guttering was observed to involve the crushing and often violent fall of ground from the roof. Gutters ranged from about 2 m by 0.5 m by 0.1 m to 70 m by 3.5 m by 0.5 m in size. Figures 3.2 and 3.3 illustrate the typical depths of gutters. Figure 3.4 illustrates both the depth and width of a gutter. A few occurrences of guttering covered the whole length of a split, i.e. from one end of the panel to the other. During the process of guttering, noises and "explosions" were heard. The noises and explosions have been explained to be a result of the sudden release of strain energy during the failure process (Martin et al, 1997).



Figure 3.2: Photograph showing typical depth of gutter (about 0.3 m)

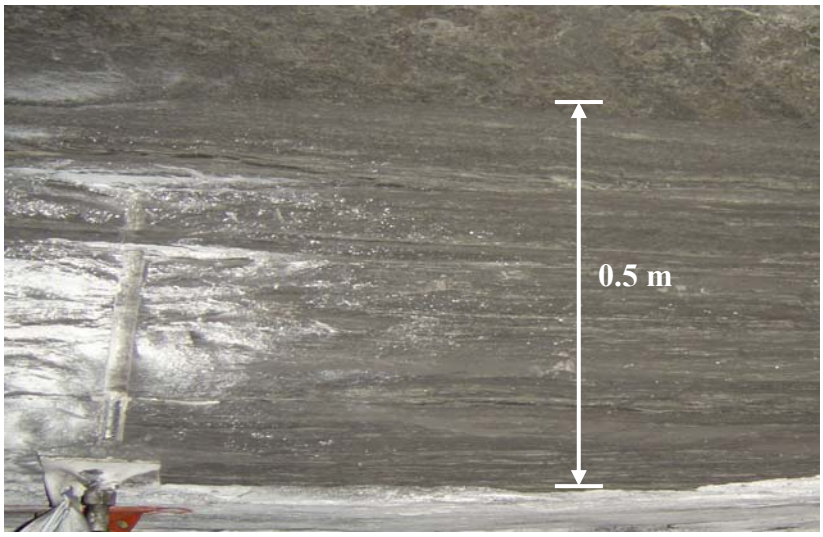

Figure 3.3: Photograph showing typical depth of gutter (about 0.5 m)



Figure 3.4: Photograph showing typical depth of gutter (about 0.5 m) and width of gutter (about 1.2 m)

Guttering also occurred during scaling of the roof. Initially a heavily fractured roof ranging from 0.2 m to 0.6 m in width and extending to about 5 m in length would be observed as shown in Figure 3.5. On scaling down the roof to make the work place safe a gutter is created following the length of the crushed roof. The gutter can extend further than the crushed length of roof. In other words, scaling

of the fractured roof can initiate guttering in the roof that is previously observed to be strong and intact.



Figure 3.5: Photograph showing a fractured roof which on scaling results in a gutter

Interesting surface features were observed along a guttering roof. These included 'upturned' boat-shaped nature of a gutter, interlocking fracture surfaces towards the centre of a gutter, thin fractured slabs from centre of gutter going outwards and a heavily fractured surface ahead of a gutter. Figure 3.6 illustrates the 'upturned' boat-shaped nature of a gutter, the fractured surface and the tip of a gutter. Results of mapping of guttering indicated that a majority of the gutters had this shape. The difference was in their size and orientation.



Figure 3.6: 'Upturned' boat-shaped nature of guttering occurrence

Figure 3.7 illustrates the occurrence of thin fractured slabs emanating from the centre of the gutter going outwards. The thin slabs are more visible at the lower left hand side of the photograph.

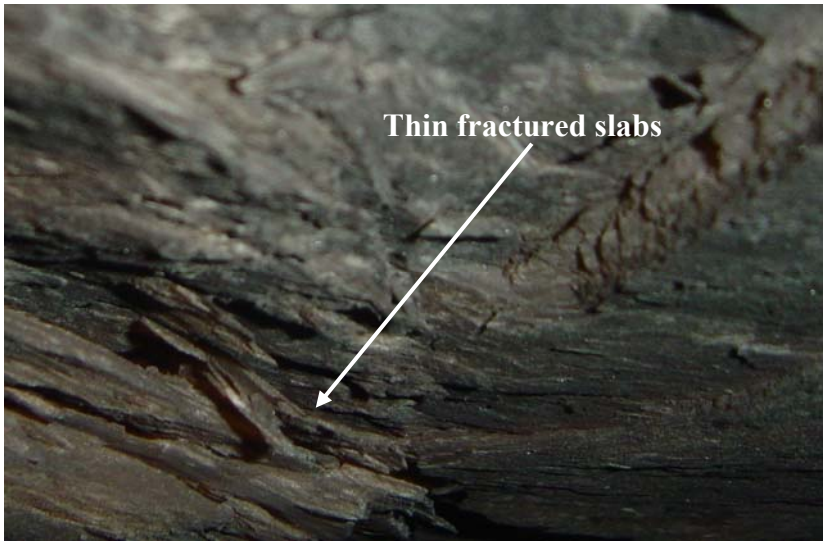

Figure 3.7: Photograph showing thin slabs associated with roof guttering

Figure 3.8 illustrates the fracture surface that occurs towards the centre of a roof gutter. On scaling the fractured surface, the roof gutter grows in depth and a new fracture surface may form. If scaling is not done the fractured surface may eventually fall down violently and without warning.

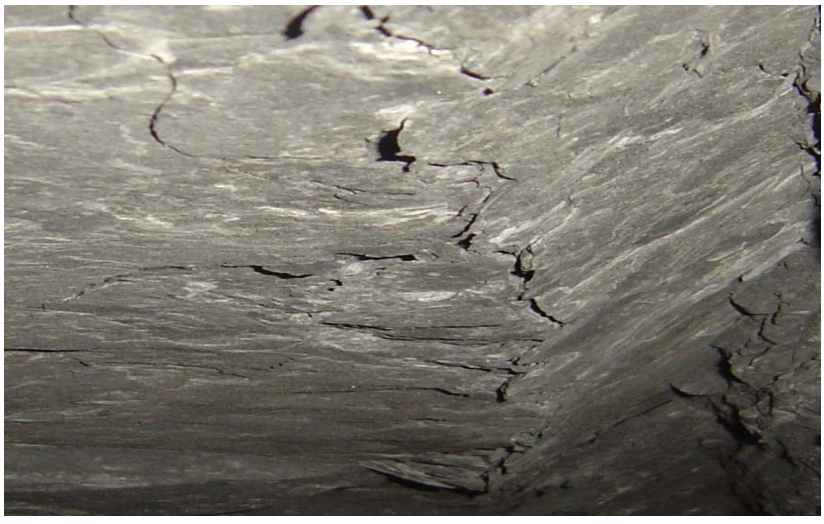

Figure 3.8: Photograph showing stress induced fracturing associated with roof guttering. The roof gutter occurred towards a pillar edge

Figure 3.9 shows the interlocking nature of fracture surfaces in guttering roof towards the centre of the gutter.



Figure 3.9: Interlocking nature of surfaces in guttering roof

Figure 3.10 illustrates the fractured surface ahead of a gutter. On scaling down the fracture surface ahead of the gutter, roof falls occurred which led to the gutter developing further longitudinally, laterally and in depth. After a few hours or days another fracture surface may develop ahead of the gutter. The process repeats itself until the gutter stabilises.

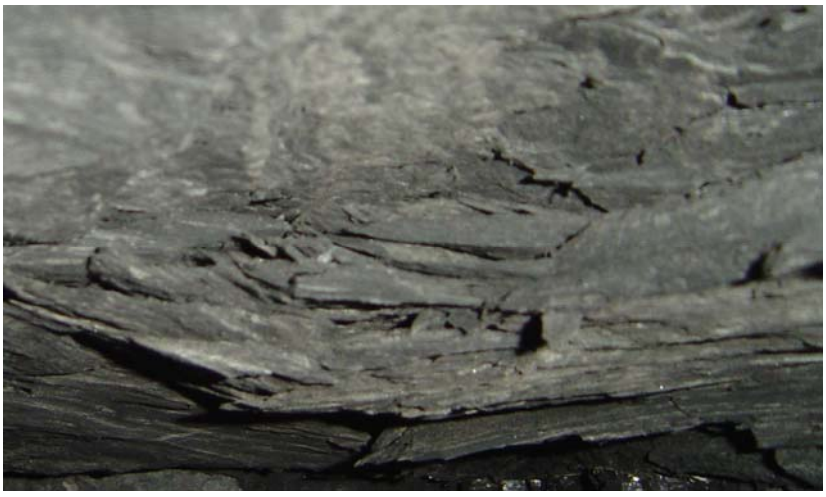

Figure 3.10: Photograph showing stress induced fracturing ahead of a gutter. The roof gutter occurred towards the centre of a roadway

Figure 3.11 below is a schematic diagram illustrating the guttering, showing the plan view looking at the roof.

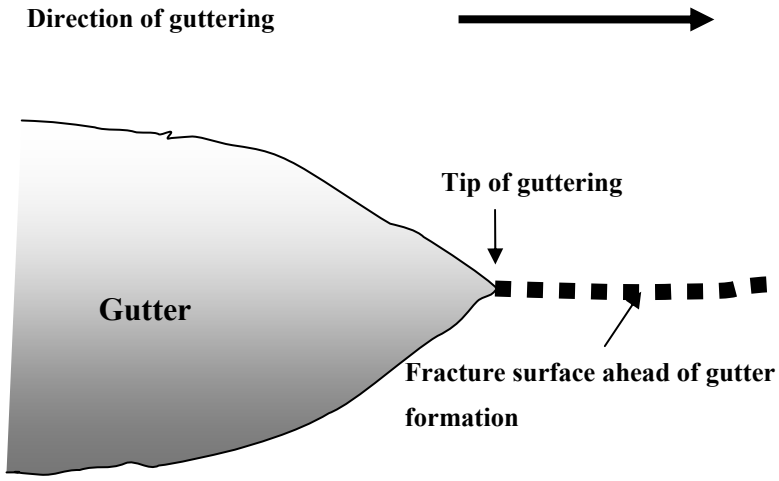

Figure 3.11: Schematic diagram showing boat-shaped nature of guttering and fracture surface ahead of guttering

In some areas, guttering was observed to develop between roof bolts and between pillars in a direction towards the pillars (Figure 3.13). Roof bolts might be playing a role in arresting lateral development of roof guttering. Additional roof bolts were installed in areas where original roof bolts had been exposed by guttering as shown in Figure 3.12 below. This is also illustrated in the schematic diagram of Figure 3.13. In Figure 3.12 roof bolt number 1 has been exposed due to guttering and roof bolt number 2 was installed as a replacement.



Figure 3.12: A roof bolt exposed due to guttering is replaced by another one

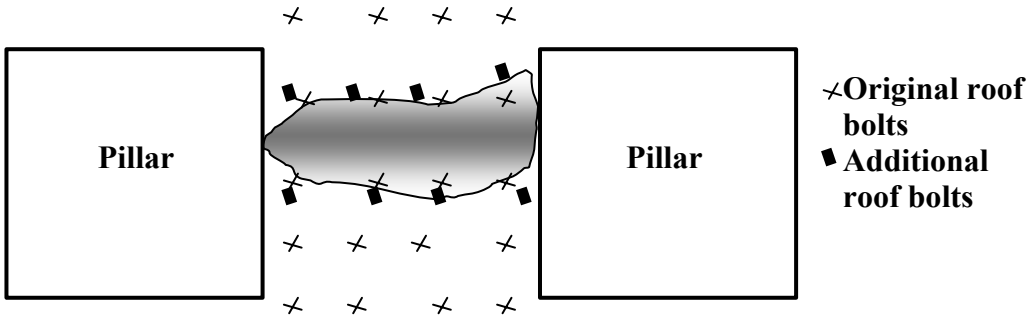

Figure 3.13: Plan view showing occurrence of guttering between roof bolts. The diagram also shows the guttering occurring between pillars that is stopped by the pillars from developing further longitudinally

Occurrences of guttering were also observed to occur along a line of roof bolts as shown in Figure 3.14. In such instances roof bolts were ineffective in preventing occurrences of guttering. Additional roof bolts were installed in such instances. Pillars prevented guttering from developing further longitudinally.

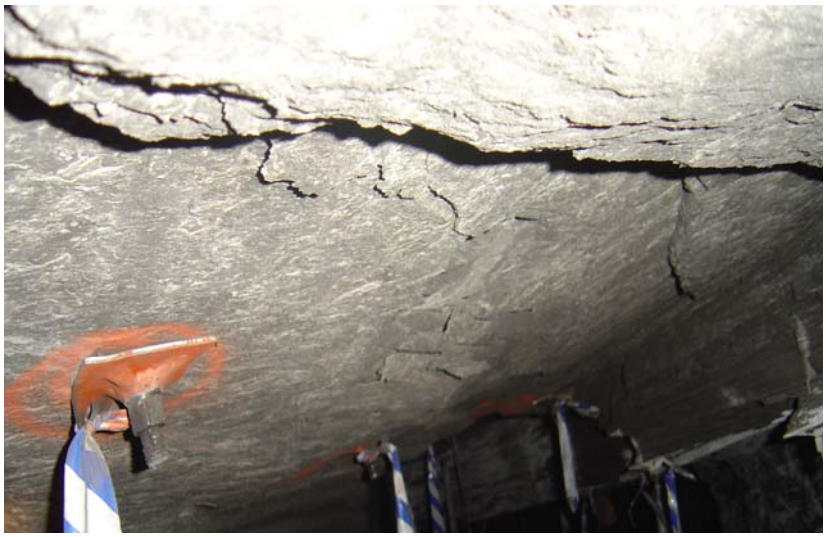

Figure 3.14: Occurrence of roof guttering along roof bolts

Guttering was observed to occur most commonly towards the centre of the roadways (about 80%), as can be seen in Figure 3.15, which shows the occurrence of guttering as mapped in one section of the mine. This was also observed by mine employees, who mentioned that they felt safer walking along the pillar sides than in the centre of roadways. However, guttering also occurred randomly, as shown in Figure 3.15, moving from centre of roadways to pillar edges and back to centre of roadways. Guttering occurred predominantly in two perpendicular directions.

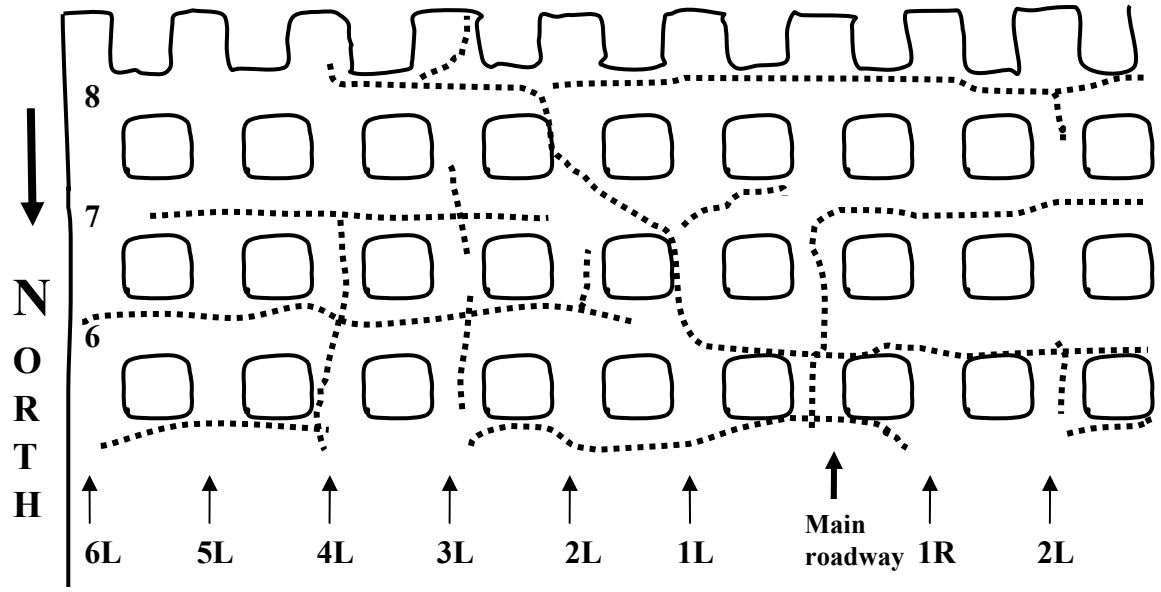

Figure 3.15: Occurrence of guttering in part of a section. Dotted lines represent the gutters. The numbers 6, 7, and 8 denote split number while 1L, 2L etc denote roadways

It was observed, from the previous mapping of guttering, that occurrence of guttering was not evenly distributed within a panel. Some sections of a panel experienced a high intensity of guttering while others had no guttering at all. This is shown in Figure 3.16. Guttering was observed to occur both along and across the roadways in all sections. In most areas guttering was longer in one particular direction compared to the other.

Analysis of the orientations of occurrence of guttering in the two main directions, East–West and North–South, is shown in the histograms in Figure 3.17. These data were obtained from mine plans with previous mapping of guttering occurrence. In a few areas guttering was observed to run in three directions. The three directions were orientated at approximately 120° to each other.

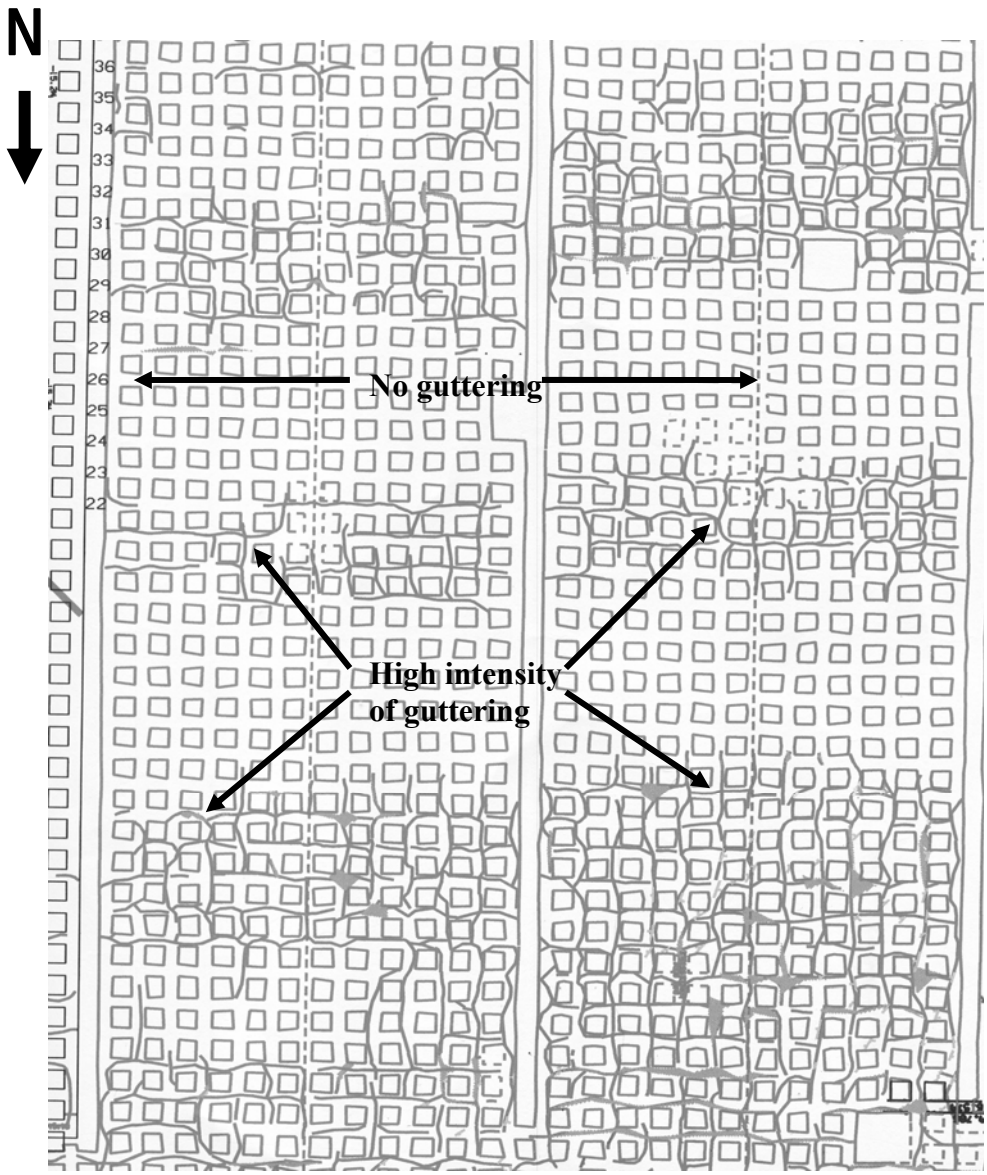

Figure 3.16: Plan view showing occurrence of guttering in part of two panels. Lines indicate guttering while shaded areas indicate slabbing

Occurrence of guttering on a mine-wide scale is almost equally distributed in the two main directions as shown in Figure 3.17a. Figure 3.17b shows guttering in seven selected panels (note that panels 1, 2 and 3 are the panels where mining was taking place at the time of mapping and their positions at that time are as previously described in Section 3.2. The rest of the panels are mined out). The histogram shows that occurrence of guttering in the two directions for each panel varies. The variation is more pronounced in panel four, which was mined in an E-W direction. The rest of the panels were mined in a N-S direction.

In some areas, initiation of guttering took place within a few seconds of blasting while in others it occurred a few days after mining of a particular face. It was also observed that the extent of guttering progressed with time. In most instances it took several roof falls over several days for the gutter to stabilise. Guttering progression was most evident from the mining faces to about three splits back. Stresses could possibly have re-equilibrated in the back area after the guttering process as evidenced by lack of active guttering in this area. Pillars were observed to be intact showing no signs of slabbing. Roof guttering and roof slabbing appeared to have no adverse effects on pillar stability.

The furthest of the active panels was observed to have a higher intensity of guttering compared with the other two panels. The panel might be having a destressing effect on the other panels. The other panels were then mined in a de-stressed rock mass.

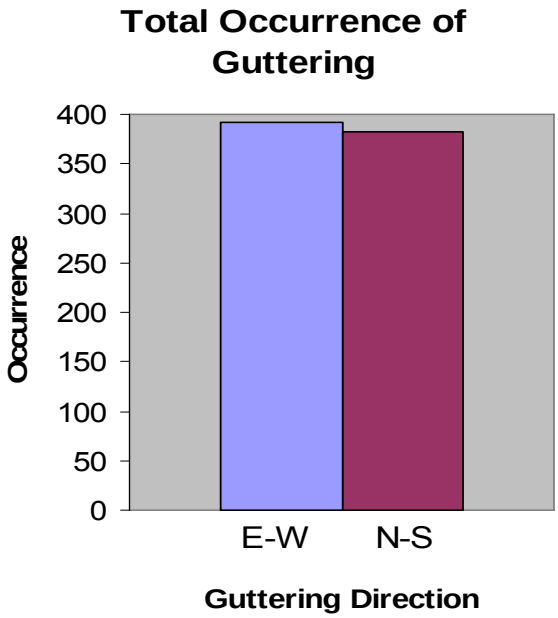

Figure 3.17 (a): Occurrence of guttering on a mine-wide scale

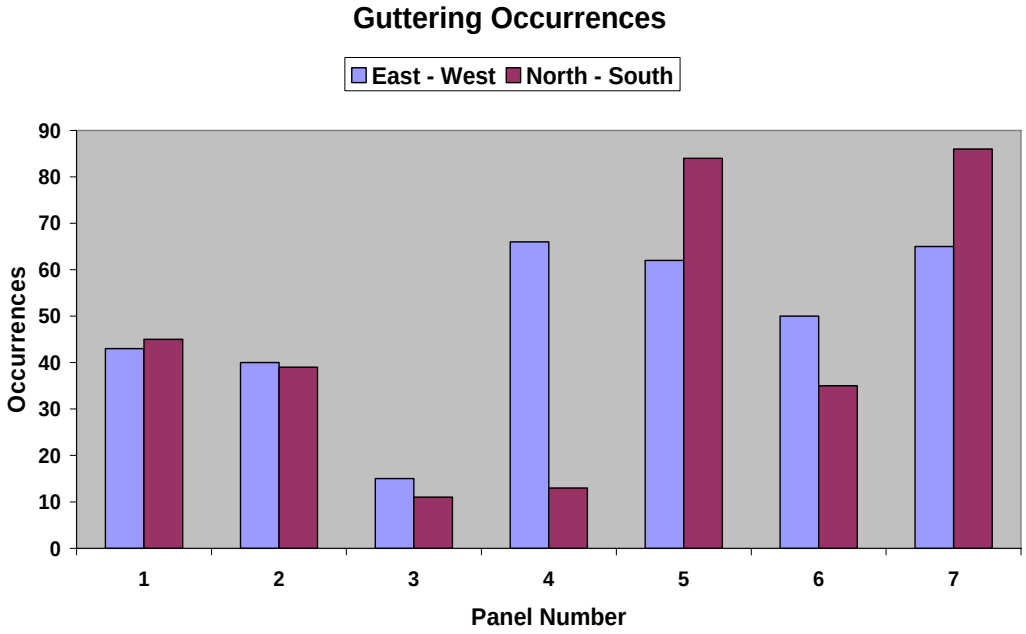

Figure 3.17(b): Guttering in seven selected panels

Most sections that did not experience guttering were observed to have siltstone or sandstone as the immediate roof rock. Guttering areas were observed to have mudstone or shale as the immediate roof rock. These observations were gathered from a core drilling program. Cores obtained from guttering sections showed core-discing as shown in Figure 3.18 for about 0.3 m of the immediate roof. Core discing is indicative of high stresses normal to the core axis direction (Stacey, 1982). However, core discing can also be attributed to bad drilling practices. The recovery of cores was generally poor compared to that from non-guttering sections. Observations made in exploration holes encountered during the course of mining showed small lateral displacements of thin layers into the holes.



Figure 3.18: Disced core from one of the guttering sites

Table 3.1 is a summary of the observations in guttering and non-guttering areas.

Table 3.1: Guttering areas compared to non-guttering areas

	Guttering roof	**Non-guttering roof**
Immediate roof rock	Generally mudstone or shale	Generally siltstone or sandstone
Drill core observation	Core discing	No core discing
Observation of encountered exploration holes	Off- sets	No off-sets

Directly associated with roof guttering is slabbing caused by the interaction of the guttering with natural planes of weaknesses in the immediate roof rock. A photograph of slabbing is shown in Figure 3.19. Slabbing is the separation of roof beds and their subsequent fall as a result of gravitational loading. The mechanism of slabbing appears to be the following:

(i) fractured roof rock material falls due to guttering;

(ii) the gutter formed exposes the bedding planes of the immediate roof rock to air and moisture;

(iii) bedding plane contacts are weakened by air and moisture;

(iv) bedding planes gradually delaminate, and;

(v) slabs fall down due to gravity loading



Figure 3.19: Photograph showing roof slabbing initiated by roof guttering

The delamination process is a gradual process that can take from a few hours after blasting to several months. Slabbing was minimised by extensive barring down of the roof rock and use of roof bolts to suspend the weak beds from the more competent sandstone bed above. In some sections, roof slabs were barred down for the entire roadway while in other sections the bedding contacts were strong, making barring down difficult. However, with time there seemed to be progressive delamination of these previously stronger roof beds. Barring down then became difficult as the area would have been supported with roof bolts and, in some places, wire mesh. Bed separation and roof delamination were also observed at the location of freshly blasted coal faces. This could imply that delamination occurred soon after mining of the horizontal slot, or was a result of blasting. When roof slabs were barred down a good looking sound roof remained. In some areas guttering then developed in the solid roof as shown in Figure 3.20.

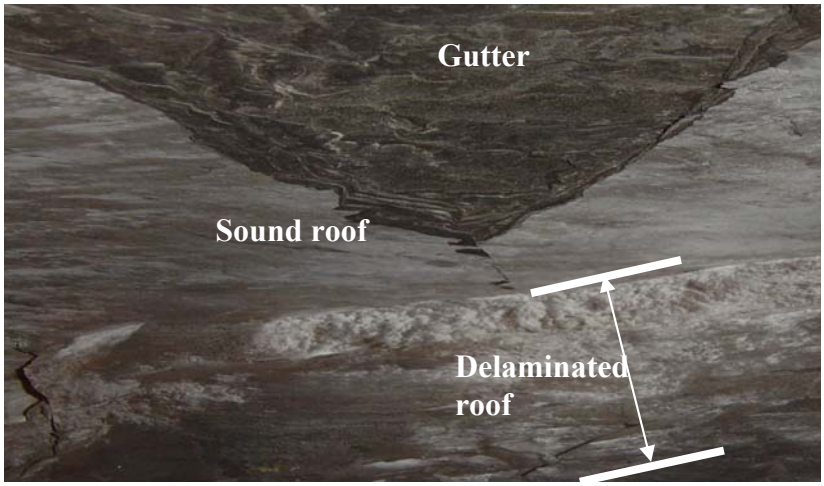

Figure 3.20: Roof guttering occurring in the solid roof just above a delaminated roof

In some areas the mudstone roof was observed to be muddy and oval shaped formations were observed after the fall of muddy material as shown in Figures 3.21 and 3.22.



Figure 3.21: Fall of muddy roof

Most occurrences of slabbing were concentrated where a high intensity of guttering occurred (See Figure 3.16). However, a few sections were observed to experience an extremely high intensity of slabbing where no guttering occurred.



Figure 3.22: Occurrence of guttering in combination with slabbing was common in muddy roof

The following section discusses progressive failure of brittle rock, fracture observations carried out on samples obtained from Nooitgedacht Colliery, and possible mechanisms of roof guttering at Nooitgedacht Colliery.

3.4 Progressive failure of brittle rock

Roof guttering has been observed to involve progressive failure of brittle rock. Progressive brittle failure of rock has been extensively studied and reported recently by Martin (1990, 1997), Martin et al (1997, 1998), Hajiabdolmajid et al (2000, 2002a, 2002b, 2003), Martino and Chandler (2004), Read (2004) and Chandler (2004).

3.4.1 Summary of URL studies

Martin (1990, 1997) described the fracturing around the Atomic Energy Canada Limited's (AECL's) Underground Research Laboratory (URL) shaft and investigated the brittle failure process from laboratory tests and underground observations. He observed the frequent spalling of the shaft walls and pop-ups of

the shaft bottom. Failure of rock involved onion-skin-like slabs which resulted in a V-shaped notch (also referred to as a breakout or dog ear). Geological mapping revealed a zone of micro-cracking in two opposite sides of the shaft. The micro-cracks were observed to be parallel to the maximum horizontal stress. The origin of the micro-cracks was not clear but Martin (1990) noted that the lack of any visible evidence of shear suggested an extensional type of failure. He suggested that the formation of the micro-cracks was the first stage in the failure process and that in highly stressed areas the micro-cracks propagated and discontinuities were formed, resulting in V-shaped notches.

Martin (1997) noted that practical experience indicated that the spalling occurred in the region of maximum compressive tangential stress around the boundary of the opening. From laboratory cylindrical compression tests it has been shown that the brittle failure process of rock is dominated by the growth of small cracks in the direction of maximum applied load. The stress-strain curves for such a test display three key stress levels as shown in Figure 3.23:

(i) stress associated with the initiation (σ_{ci}) of crack growth;
(ii) stress associated with permanent axial deformations (σ_{cd}), and;
(iii) the peak stress (σ_f)

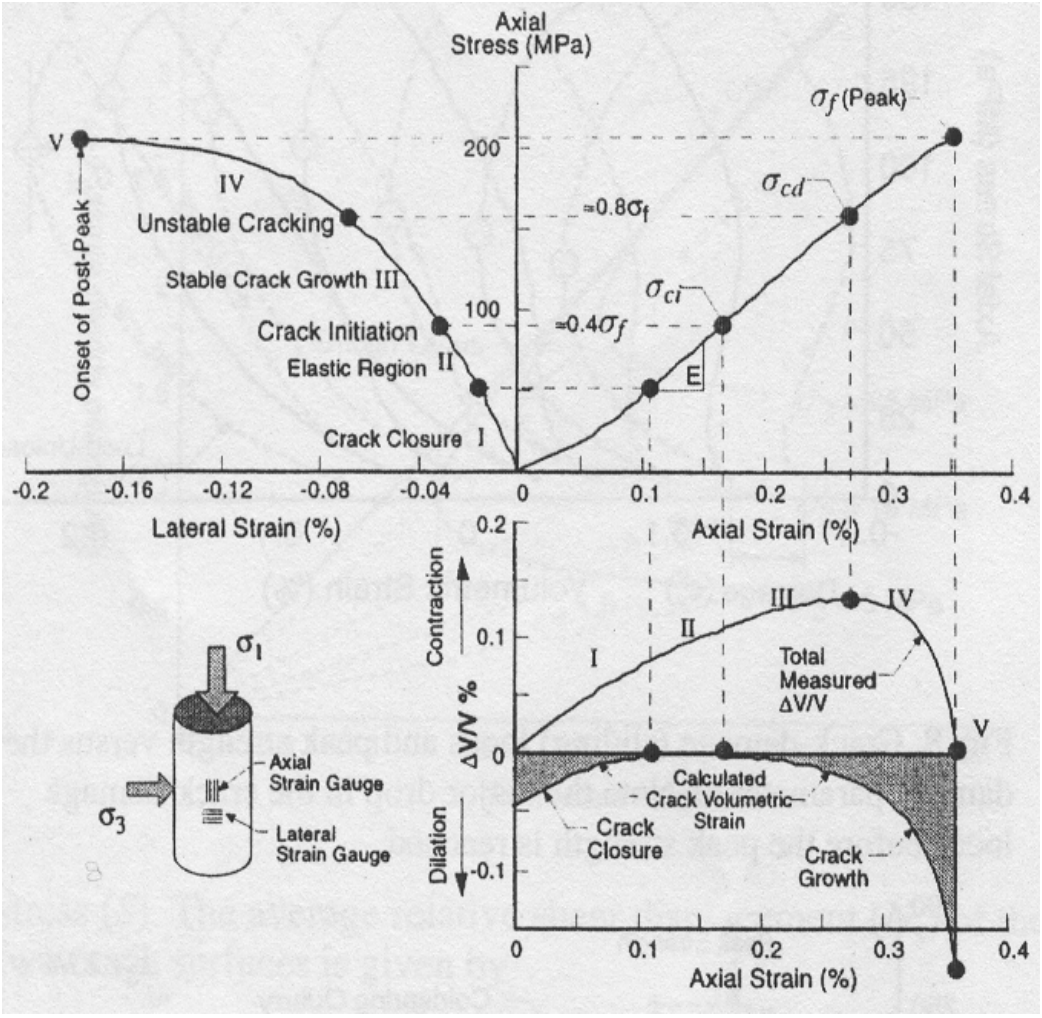

Figure 3.23: The three parameters determined from laboratory compression test: crack initiation (σ_{ci}); initiation of sliding (σ_{cd}), and peak strength (σ_f). $\Delta V/V$ is the volumetric strain (Martin, 1997)

The failure process of brittle rock is often violent as a result of the sudden release of strain energy (Martin, 1997; Martin et al, 1997). Martin (1997) noted that, for the V-notch formation, once plane strain conditions were achieved, the new tunnel geometry was stable. He summarised the observations made during the V-notch formation, Figure 3.24, as follows:

(i) damage initiation, i.e., micro-cracking of the rock ahead of the tunnel face;

(ii) visible crushing in a very narrow process zone on the tunnel periphery;

(iii) formation, in an unstable manner, of larger slabs on the flanks of the notch as the process zone develops, and;

(iv) stabilisation of the process zone when the notch geometry provides sufficient confinement to stabilise the process zone at the notch tip

Martin et al (1997) showed that the process zone was probably the single most important feature controlling the progressive nature of the failure process. It controlled when the failure initiated i.e., when the tangential stress was sufficient locally to cause crushing of this zone. Also, when the process zone was confined, slabbing in notch was observed to stop. Observations also showed that removal of crushed rock in the process zone caused a new slab to form on the flank of the notch.

Martin (1997) also noted that stress concentrations in excess of the crack-initiation stress, occurring at any period in the rock's loading history, resulted in a localised increase of damage to the rock and a corresponding loss of cohesion. The degree of damage was highest at the surface of the opening where confinement was zero and the deviatoric stress concentrations were greatest, and that this damage decreased with increasing distance into the rock.

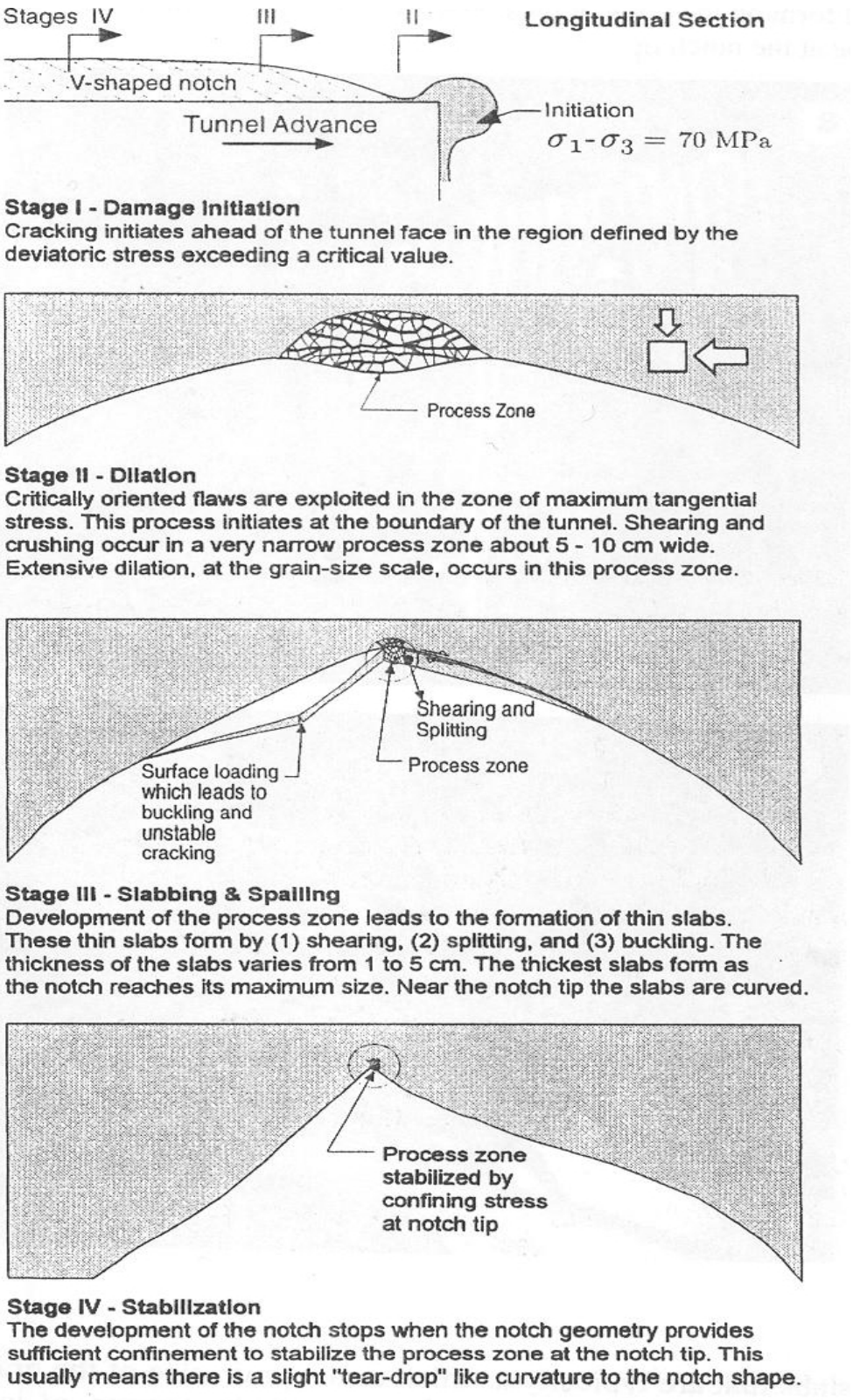

Figure 3.24: Illustration of the major processes involved in the initiation, development, and stabilisation of the V-shaped notch (Martin, 1997)

Martino and Chandler (2004) described irreversible damage that occurred in rock due to an underground opening. They noted that the damage was due to factors like:

(i) energy imparted to the rock from the excavation method;
(ii) redistribution of in situ stresses around the opening, and;
(iii) subsequent excavation that influenced the growth of damage

Martino and Chandler (2004), Read (2004) and Chandler (2004) were in agreement with Martin (1990, 1997) that in a compressive stress region, rock slabbing initiated in the region of the maximum compressive stress concentration and propagated away from such region.

3.4.2 Observation of fracture surfaces in Nooitgedacht Colliery

A fracture is a general term for any type of brittle failure. Fractures have been basically classified into two groups, which are:

(i) Natural fractures
(ii) Induced fractures

Examples of natural fractures include joints and faults. The rock mass at Nooitgedacht Colliery was observed to be almost free of natural fractures. Induced fractures in underground excavations are generally a result of high stresses. Occurrence of guttering is believed to be a result of induced fracturing. Two different stress conditions cause induced fracturing in rock. These are:

(i) tensile stresses which induce extension fractures
(ii) shear stresses which induce shear fractures

Stacey (1981) has also shown that extension fractures can form under a compressive stress environment. This is discussed later in this dissertation.

Extension fractures are opening mode type of fractures. It is well known that extension fractures represent one end of a continuous spectrum of brittle fractures while shear fractures represent the other end. Extension fractures form under a tensile stress condition, display an opening-mode displacement normal to the fracture surface, and propagate in an orientation normal to the minimum principal compressive stress direction. Longitudinal splitting during laboratory uniaxial compression is also assumed to be an extension type of fracture (Ramsey and Chester, 2004). Extension could also probably be on initiation. Subsequent movement or deformation could lead to shear or apparent shear deformation. (Stacey, 2006)

It has been observed that the surface of shear fractures is characterised by white dust caused by the relative movement of the shearing surfaces. Even though the surface is not necessarily plane, the surface variation is very regular and smooth. On the other hand, the surface of the extension fracture is much more irregular and rough. There is normally no relative movement and the original fracture surface is retained. Extension fractures display discrete and highly reflective intra-granular cleavages. If the above mentioned properties of extension fractures are observed in a fracture surface then failure is assumed to be of extension type. Furthermore, lack of visible shear surfaces is usually used to conclude that the mode of failure is extension.

Observation of fracture surfaces was carried out with the aid of a microscope. Thin slabs obtained from different areas in the guttering roof were used. Fractures were observed at both the surface and the edge of the slabs. One hundred photo images were captured during this analysis. A few of these photographs are illustrated in this dissertation. The photographs shown in Figures 3.25(a) to 3.25(d) show fracture surfaces, which the author believes to be of extension type. There are no visible shear properties.

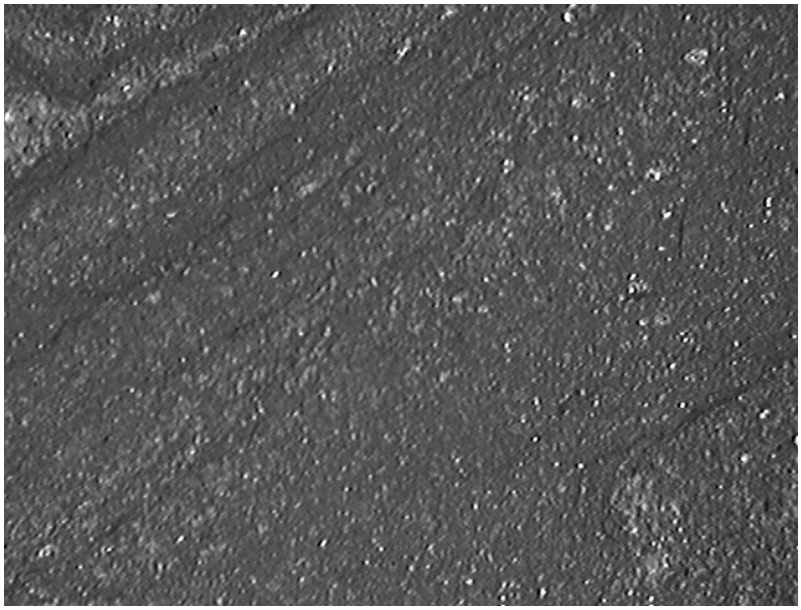

Figure 3.25a: Photograph of an extension fracture surface

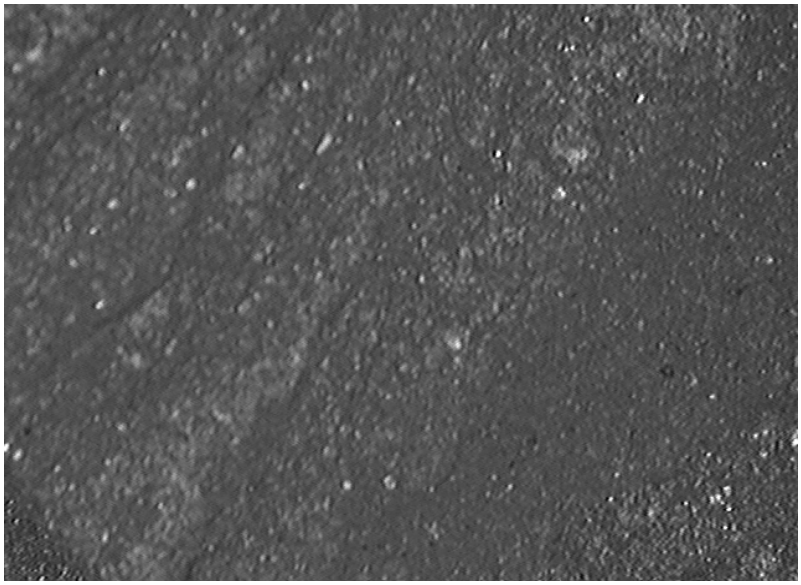

Figure 3.25b: Photograph of an extension fracture surface

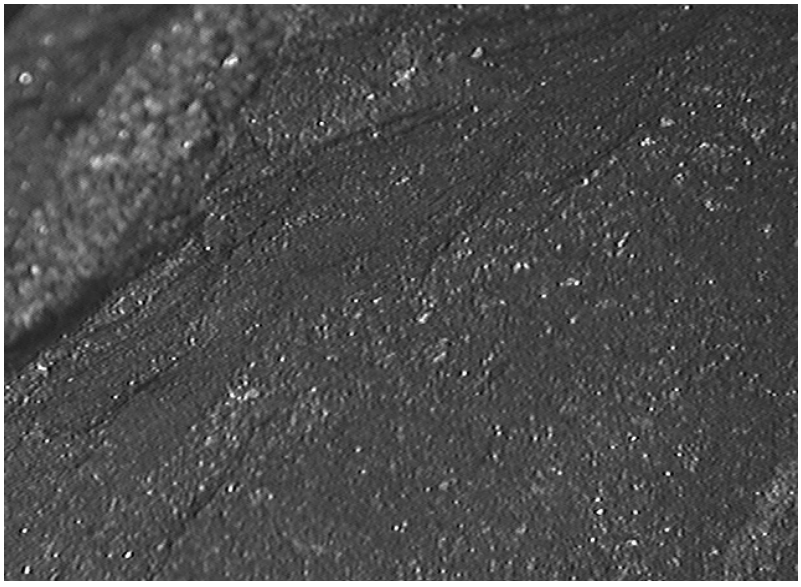

Figure 3.25c: Photograph of an extension fracture surface

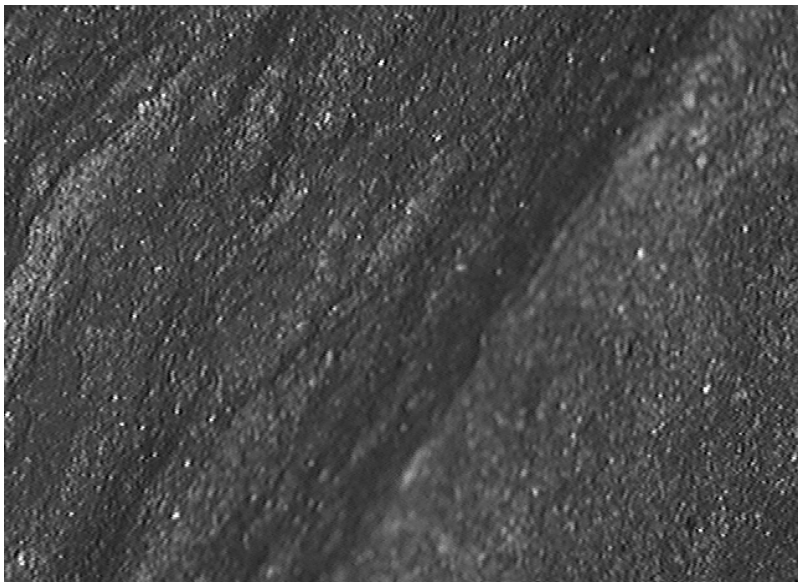

Figure 3.25d: Photograph of an extension fracture surface

Shear type of fractures were observed in a few samples (about 10%), mainly at the edges of the slabs. Shearing could possibly have taken place during guttering when a rock fell down and in the process sheared against the edge of the particular sample. Figures 3.26a and 3.26b show fracture surfaces which the author believes

to be of shear type. There are visible white surfaces caused by relative movement during the shearing process.

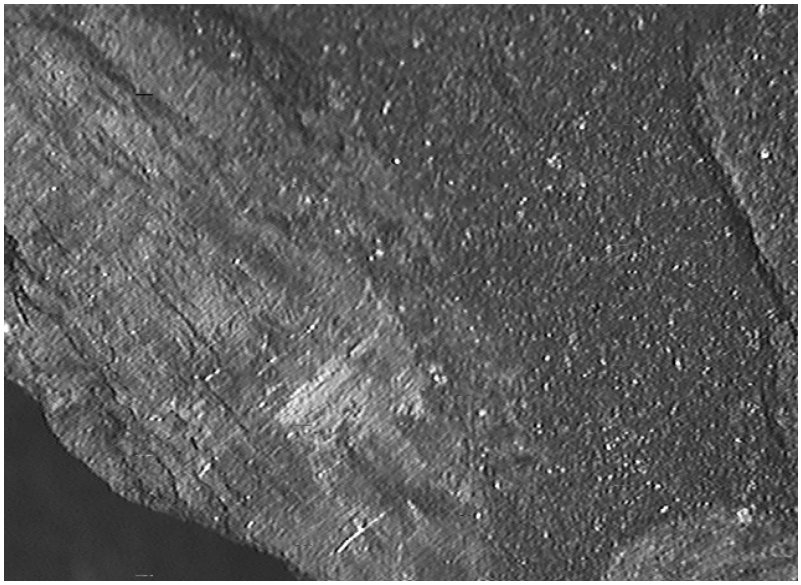

Figure 3.26a: Photograph of a shear fracture surface

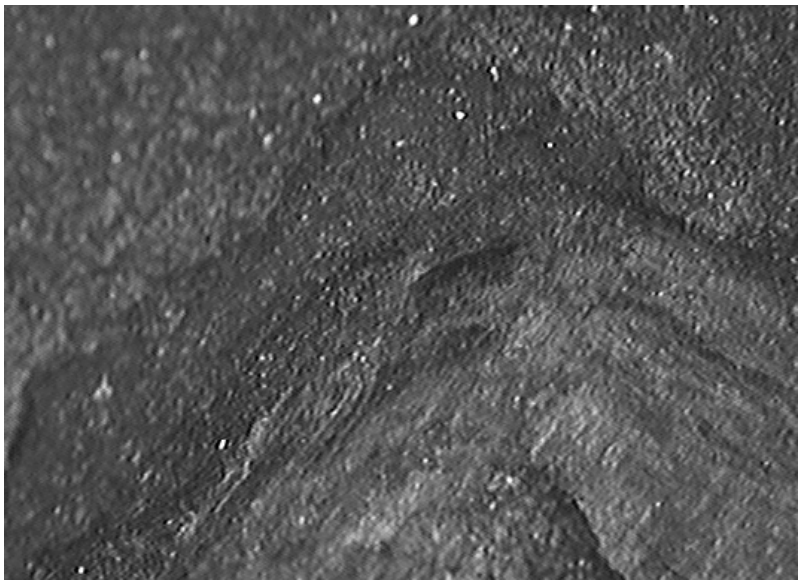

Figure 3.26b: Photograph of a shear fracture surface

Extension failure in rock is a form of stress induced failure. It is well known that rock is very weak in tension. A change in the virgin in situ stress distribution due

to mining excavation may cause stress concentrations in the vicinity of an underground opening. In some cases the stress concentrations may be considerably higher than the virgin in situ stress and may exceed the strength of the rock. In other cases the stress concentrations may induce fracturing by virtue of being higher than the fracture initiation stress, which is usually 30-40% of the strength of the rock mass. Both these situations will result in initiation of failure of the rock mass in the vicinity of the excavation (Afrouz, 1992). Large stresses can also be caused underground by movement of the rock. This creates mainly tensile stresses (Vervoort, 1998).

3.4.3 Possible mechanisms of development of guttering at Nooitgedacht Colliery

The above discussions (Sections 3.4.1 and 3.4.2) described the progressive failure of brittle rock and observations of fracture surfaces. The progressive failure of brittle rock discussed above is similar to observations of the failure of rock during the process of guttering at Nooitgedacht Colliery. Similarities are derived from the following observations:

(i) Guttering involved failure of intact rock which may be explained by stresses in the region of failure being greater than the strength of the rock in this region. The high horizontal compressive stresses in combination with a weak mudstone roof and low compressive stresses in a vertical direction could be the main cause of extension type of fractures at Nooitgedacht Colliery. These fractures are parallel to the major principal stress which is almost horizontal and normal to the minor principal stress. Extension fractures could be initiating the process of roof guttering;

(ii) Guttering cannot be a result of high horizontal stresses alone; if this was the case it is expected that guttering would initiate in the corners of the roadways, where induced stresses are highest. This was not the case as it was observed that guttering most often initiated and occurred towards the centre of the bords, i.e., away from the corners of the roadways;

(iii) Occurrence of guttering was not a once-off event. Several falls of crushed rock were necessary for the gutter to stabilise. The stabilising effect is not known. It might be possible that guttering stabilised when a more competent sandstone roof was encountered, or when stress equilibrium was re-established after a certain advance of the roadways as demonstrated by lack of active guttering in back areas. Subsequent excavations caused stress redistribution and influenced the growth of damage and formation of new gutters. It is also possible that the same mechanism of confinement described by Martin (1997) caused the stabilisation of gutter progression;

(iv) It is possible that guttering initiated in the region of maximum compressive stress concentration and propagated away from it. This is because no clear pattern of the geometrical location of the occurrence of guttering was observed. In some areas, within a roadway, guttering was observed to occur on one side of the roadway, then suddenly crossed the centre of the roadway and moved to the other side of the roadway;

(v) Scaling down favoured the progression of gutter formation. Removal of loose material (e.g., previously held in place by the steel mesh support) usually helped guttering to develop further in depth, width and length.

Figures 3.27a and 3.27b are diagrams showing the possible fracturing prior to a fall of rock during the guttering process, and the subsequent fall, respectively.

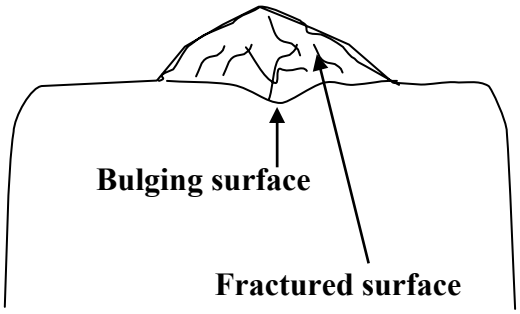

Figure 3.27a: Schematic diagram of a roadway cross-section showing possible fracturing just before occurrence of guttering

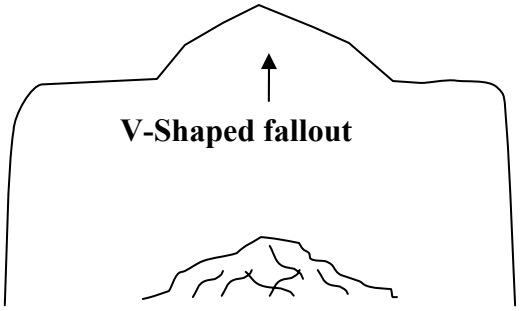

Figure 3.27b: Schematic diagram of a roadway cross-section showing the fallen rock and the "V-shaped" nature of guttered roof

Figure 3.27a represents the formation a few metres from the coal face where guttering has been observed to occur. This formation, without the bulging surface, probably also occurred on occasion at the roof/coal face intersection since guttering in some instances occurred from the coal face and propagated backwards a few minutes after blasting. An explanation could be that the roof fractures at the coal face and guttering follows immediately. This formation, without the bulging surface, probably also occurred on occasion ahead of the coal face since in some instances guttering occurred immediately on blasting. This may be explained by the assumption that the roof area ahead of the coal face is already fractured or that blasting removed confinement.

Occurrence of guttering grew in length, width and depth as the extension fractures continued to propagate until a stable V-notch was reached. Slabbing was observed to play an important role in the growth of the V-notch. The process of formation and progression of gutters was observed to be mostly active from the coal face to about three splits back. This could be an area of active stress redistribution as a result of continuing mining activities.

At micro- and macro-scale it may be observed that the stages of guttering involve the following:

(i) Crack initiation. Cracks are assumed to initiate behind, at, and probably ahead of the coal face in the region defined by compressive stresses exceeding the crack initiation stress.

(ii) Process zone. Critically oriented flaws are exploited in the zone where the mudstone roof is very weak. Crushing occurs in a process zone about 30 – 60 cm wide forming extension fractures. Extensive dilation, at the grain size scale, occurs in this process zone;

(iii) Crushing of the process zone to form gutters (V – notch). Development of the process zone causes strain energy to be stored in the rock during its deformation. A point is reached where the rock cannot store any additional strain energy. The rock fails in a violent crushing manner, similar to failure in laboratory UCS tests, in the process of releasing the stored strain energy. A gutter is formed in the process.

(iv) Slabbing. The gutter formed exposes the bedding planes to air and moisture. The bonds between the bedding planes are weakened as a result and slabbing takes place.

(v) Progression of gutter formation. Gutter formation progresses with time as extension fractures continue to propagate. It may be possible that as long as the redistributed stresses in a particular area are greater than the crack initiation stress then guttering will continue in that area.

(vi) Stabilisation. Development of gutter stops most likely when the stresses have redistributed and a new state of stress equilibrium is established where growth of extension fractures is inhibited.

3.5 Conclusions

Roof guttering was observed to involve failure of intact rock. From the literature gathered and observations made it can be concluded that guttering at the mine is due to the existence of high horizontal stresses in combination with a weak mudstone roof. Warning prior to occurrence of guttering is in the form of noises and "explosions" that can be heard just before failure. The main features of guttering were observed to be:

(i) 'upturned' boat-shaped nature of the gutter;
(ii) interlocking fracture surfaces towards the centre of the gutter;
(iii) fractured surface ahead of the gutter and towards centre of the gutter;
(iv) fall-out of fractured rock to form the 'v-shaped' gutter

Guttering was observed to occur generally with preferred orientations in two perpendicular directions, parallel to, or normal to, roadway and splits. Other orientations occurred in some places. Guttering occurred anywhere within a roadway or split, but most commonly was away from the pillar edges, approximately in the centres of the bords.

From previous mapping of guttering it was observed that the locations of occurrences of guttering were not evenly distributed within a panel. Some sections of a panel experienced a high intensity of guttering while others did not experience guttering at all. Most sections that did not experience guttering were observed to have siltstone or sandstone as the immediate roof rock. Guttering areas were observed to have mudstone or shale as the immediate roof rock. No guttering was experienced in the back area.

In some areas, initiation of guttering took place within seconds of blasting while in others it occurred a few days after mining of the particular area. It was also observed that the extent of guttering progressed with time. In most instances it took several roof falls over several days for the gutter to stabilise. Interaction of

guttering with natural planes of weaknesses in the immediate roof rock induced slabbing, which has also been observed to be a safety concern at the mine.

Pillars were observed to be intact showing no signs of slabbing. Roof guttering and roof slabbing appeared to have no adverse effects on pillar stability.

Roof guttering was observed to involve crack initiation, formation of a process zone, crushing of the process zone, slabbing and finally stabilisation. From underground observations and observations of fracture surfaces under the microscope, a combination of extension and shear type of failure cannot be ruled out, although extension failure was observed to be the major contributor, as most fracture surfaces (90%) were observed to be of extension type. It is possible that the observed shear fractures (10%) were due to shear failure involved in the falling of rock fragments during the process of guttering. Extension could also represent the initiation of fracturing, and subsequent movement or deformation could lead to shear or apparent shear deformation.

Chapter 4 deals with laboratory testing of the shale rock for the purposes of obtaining the material strength and deformation properties. The purpose of determining these parameters is to provide data to be used in numerical modelling, with the object of attempting to explain the guttering process.

CHAPTER 4

Laboratory testing

4.1 Introduction

Block samples of the immediate roof rock were collected from one of the sections that experienced a high intensity of guttering. Moisture loss was prevented by covering the samples with glad wrap. Rock specimens tested included cylindrical and cubical samples. Preparation of cylindrical samples involved drilling cores of the required diameter, cutting the cores to the required length and polishing the end surfaces so that they were flat and parallel. Cubical samples were prepared by cutting the block sample using the cutting saw. No polishing was done on cubical samples due to the unavailability of the equipment. Samples were then artificially dried in an oven at 50°C for one hour.

Testing was carried out within a month of sample collection and within 24 hours of sample preparation. The tests that were conducted included the following:

(a) Ultrasonic tests on both cylindrical and cubic samples with loading perpendicular and parallel to bedding;
(b) Uniaxial compression tests on both cylindrical and cubic samples with loading perpendicular and parallel to bedding;
(c) Brazilian tensile tests on cylindrical cores with loading perpendicular and parallel to bedding;

The following sections describe the individual tests. Results are summarised in Table 4.1.

4.2 Ultrasonic tests

Ultrasonic tests were conducted to determine indicative rock anisotropy and dynamic Young's modulus. Understanding the elastic anisotropy of rock is fundamental for correct constitutive modelling of rock mechanical behaviour. Anisotropic rocks possess direction dependent elastic properties. In sedimentary rocks elastic anisotropy is mainly due to the existence of bedding planes (Song *et al*, 2002). Such anisotropy is called transverse isotropy. The mechanical behaviour in the planes is isotropic in nature while it varies across the planes. Five independent elastic constants can be determined for such rock. These are two Young's moduli, two Poisson's ratios and one shear modulus (Martin, 1990). The seismic pulse method, (Brown, 1981a) which measures the travel time of a pulse generated at one end of the specimen and measured on its arrival at the other end, was used. The time measured is that of compressional and shear waves. Velocity of compressional and shear waves was then calculated since the travel distance i.e., length of sample, was known.

The following equation, derived from the theory of wave propagation, applies (Eissa and Kazi, 1988):

$$E_{dyn} = \rho V_s^2 (3V_p^2 - 4V_s^2) / (V_p^2 - V_s^2) \quad \text{.....(i)}$$

where

E_{dyn} = dynamic Young's modulus in Pa

V_p = velocity of compressional waves (also known as primary waves) in m/s

V_s = velocity of shear waves (also known as secondary waves) in m/s

ρ = density of rock in kg/m^3

The results for the test are summarised in Table 4.1 and the complete results are included in Appendix A1. They show that the dynamic Young's modulus determined along the bedding was twice that determined normal to the bedding. This indicates that the rock is anisotropic.

4.3 Uniaxial Compression Strength tests

The strain gauged uniaxial compression test (Brown, 1981b) is used to measure the uniaxial compressive strength of intact rock samples in the form of specimens of uniform geometry. Also derived from this test are the static deformation properties of the rock. The test results are important for strength classification, rock characterisation, and as input parameters in numerical modelling software. Forty specimens were tested in total, i.e., twenty cylindrical specimens and twenty cubic specimens. Half of each type of specimens was tested with loading along the bedding while the other half was tested with loading normal to the bedding. Cylindrical samples were of BX core size (i.e., 42 mm diameter) and 86mm in length although the NX size (i.e., 54 mm diameter) is preferred. The thickness of the available blocks was the limiting factor in this regard as a length to width ratio greater than 2 is a standard requirement in these tests. Cubic samples were of 80 mm dimensions. Testing was conducted such that failure took place within five to ten minutes of loading. Specimens loaded in a direction parallel to the bedding failed by splitting. Specimens loaded in a direction normal to the bedding failed by shear. Test results for UCS, static Young's modulus and Poisson's ratios are summarised in Table 4.1. The complete results are included in Appendix A1.

Static Young's modulus and Poisson's ratio could not be determined for the much larger cubic samples. Bedding plane separation was evident in all the cubic samples. This affected the measurements as strain gauges measure very small deformations (thousandth's of a millimetre) while the bedding plane separation in the cubic samples was visible to the naked eye. The uniaxial compressive strength of intact rock is much lower for rock tested in a direction along the bedding than it is for rock tested in a direction normal to the bedding. This is expected as the beddings are planes of weaknesses which lower the strength of the rock. The UCS values determined from the cylindrical cores are similar to those determined from the cubic samples, thus validating the tests.

4.4 Brazilian Tensile Strength test

The Brazilian tensile strength test measures, indirectly, the tensile strength of intact rock (Brown, 1981c). Two diametric line loads are applied along a diameter through two loading platens as shown in Figure 4.1(a) and 4.1(b). The test is based on the experimental fact that most rocks in biaxial stress fields fail in tension at their uniaxial tensile strength when one principal stress is tensile and the other is compressive with a magnitude not exceeding three times that of the tensile stress. Splitting of the specimen into two halves is the expected failure mode. An evaluation of tensile strength is important for the analysis of rock response near boundaries of underground openings where one of the induced principal stresses may be tensile. The tensile strength of the rock mass is compared with this induced principal stress. When the induced principal stress is larger than the tensile strength of the rock mass failure of the rock mass will take place.

Forty eight specimens, half of them prepared by drilling the rock sample in a direction along the bedding and the other half prepared by drilling the rock sample in a direction normal to the bedding, were tested. Specimen diameters were 53mm on average while the thicknesses were 30mm. Testing was conducted such that failure took place within 15 – 30 seconds of loading. Test results for the tensile strength of the intact rock specimens are summarised in Table 4.1. The complete results are included in Appendix A1. The tensile strength of a specimen is calculated from the formula:

$$\sigma_t = 2P / \pi D t$$

where, σ_t = tensile strength of the test specimen (MPa)

P = load at failure (N)

D = diameter of the test specimen (mm)

t = thickness of the test specimen (mm)

The values for the tensile strength of the intact rock obtained are reasonable. Samples prepared and loaded normal to the bedding (Figure 4.1b) have a higher tensile strength than those prepared and loaded along the bedding (Figure 4.1a).

4.5 Summary of results

The test directions for the different tests are shown in Figures 4.3(a) through 4.3(d).

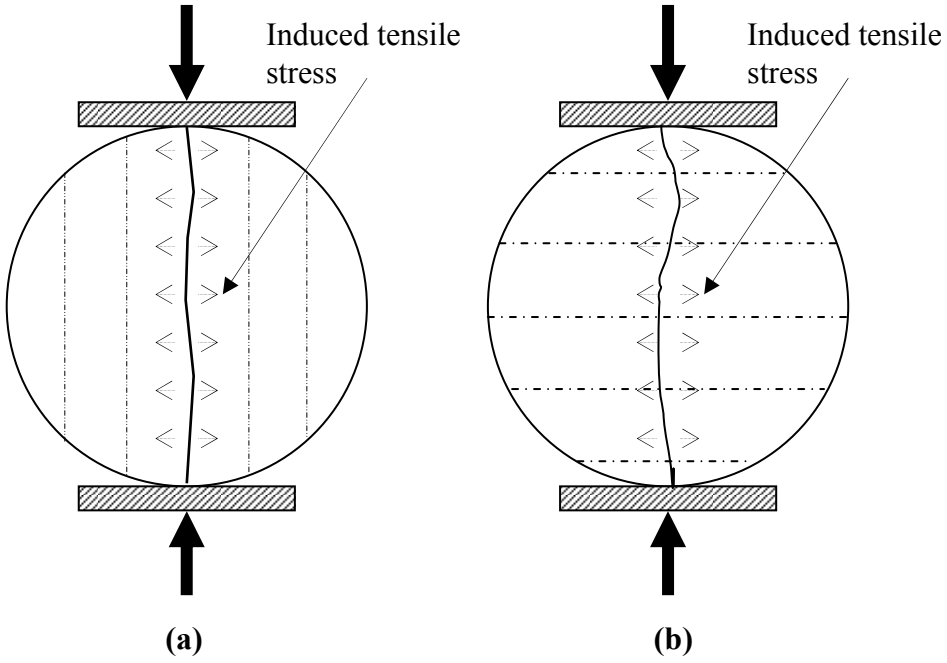

Figure 4.1(a): Loading along the bedding in Brazilian test

Figure 4.1(b): Loading perpendicular to the bedding in Brazilian test

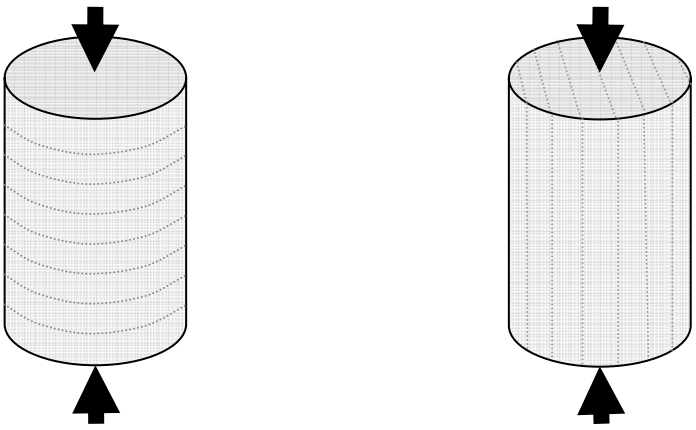

(c) **(d)**

Figure 4.1(c): Loading perpendicular to the bedding in UCS tests

Figure 4.1(d): Loading along the bedding in UCS tests

Table 4.1: Results of laboratory tests

	Cylindrical specimen		Cubic specimen	
	Along	Perpendicular	Along	Perpendicular
**Density, ρ (kg/m^3)	2350			
Dynamic E (GPa)				
range	16.7 - 19.8	10.6 - 11.4	19.0 - 20.7	9.3 - 9.8
mean	18.4	11	20	9.5
Static E (GPa)				
range	9.17 - 13.59	1.6 - 2.0	-	-
mean	11.3	1.8	-	-
Static Poisson ratio				
range	0.17 - 0.43	0.10 - 0.18	-	-
mean	0.27	0.16	-	-
UCS (MPa)				
range	23.28 - 28.15	37.18 - 40.95	23.81 - 28.01	36.89 - 39.25
mean	25.31	39.15	25	37.8
Tensile strength (MPa)				
range	0.76 – 1.42	2.35 – 3.11	-	-
mean	1.07	2.81	-	-

****Note: Density is not dependent on the orientation of bedding planes**

4.5 Conclusions

Laboratory testing was carried out successfully except for the determination of static Young's modulus and Poisson's ratio for cubic samples. The measurements of the strain gauges were greatly affected by bedding plane separation that was evident in all the cubic samples. The ultrasonic tests showed that the rock is transversely isotropic. The values determined along the bedding were used in the numerical analysis as the high horizontal loading was assumed to contribute significantly to the failure of the rock mass. Input parameters for the numerical modelling were obtained in the form of Young's modulus, Poisson's ratio, uniaxial compression strength and tensile strength of intact rock. The mean values are 11.3 GPa for Young's modulus, 0.27 for Poisson's ratio, 25 MPa for UCS and 1.07 MPa for tensile strength. Other input parameters, for example, friction angle, dilation angle and cohesion were estimated.

Chapter 5

Numerical Models and Constitutive Behaviours

5.1 Modelling in Rock Engineering

Models in engineering are used for design and mechanics. In design the aim is to optimise an engineering system based on some predefined criteria while in mechanics the aim is to develop or improve understanding of an engineering system (Lightfoot and Maccelari, 2000). It is the second part that this research focuses on, i.e., to improve the understanding of the development and occurrence of roof guttering at a coal mine. Rock engineering problems are generally data limited and the mechanics of rock behaviour are not well understood. Figure 5.1 shows Holling's (1978) classification of modelling. Rock engineering falls into region 4 in which the understanding of the problem and the available data are limited. For example, information on stresses, properties and joints can only be partially known, at best. Unlike in region 3 where good quality data are available and the mechanics of the system involved are well understood, it is usually impossible to use modelling to make quantitative predictions for fields that fall into region 4 (Starfield and Cundall, 1988). Numerical modelling is, therefore, used in rock engineering primarily to understand the dominant mechanisms affecting the behaviour of the system. Once the behaviour of the system is understood, it is then appropriate to develop simple calculations for a design process (Itasca, 2002).

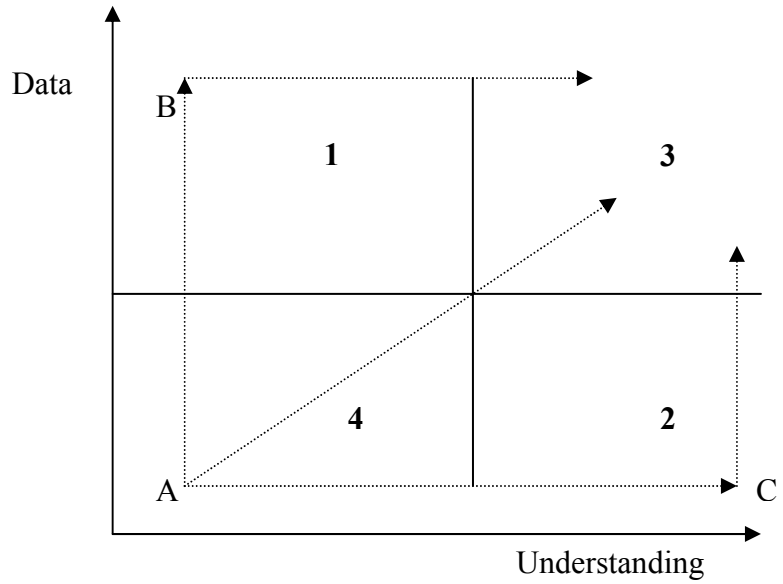

Figure 5.1: Holling's (1978) classification of modelling. Most rock engineering problems fall into region 4, whereas region 3 is better suited to routine quantitative modelling (after Starfield and Bleloch, 1986)

The traditional approach of solving rock engineering problems involves moving from A to B and then subsequently moving right towards region 3, i.e., collecting more data to move from region 4 to region 3. However, Starfield and Cundall (1988) suggest that a better approach would be to move diagonally from A to region 3 and aim to develop an understanding in proportion to the emphasis placed on data collection. This will help to develop models at the earliest possible stage so that these models can then be used to derive the data collection process.

5.2 Types of numerical models

Numerical methods for stress analysis in rock engineering can be divided into two main classes (Crouch and Starfield, 1983 and Jager and Ryder, 1999):

(i) Boundary Element (BE) or Integral methods – the boundary of the excavation is divided into discrete elements. Since the discrete elements are placed and solved at the boundaries (free surfaces) there

is a reduction in the dimension of the problem to be solved. This results in an increase in computational efficiency. The rock mass is represented mathematically as an infinite continuum. The stresses and displacements in the continuum outside the boundary are continuous. The method has the advantage of catering for the "infinite" extent of the rock mass in which mining takes place. The disadvantage is that it is generally suited to solving problems only in a homogeneous isotropic linear elastic material. There are three types of boundary element methods, these being the Fictitious Stress (FS) method, the Displacement Discontinuity (DD) method and the Direct Boundary Integral method.

(ii) Domain or Differential methods – the interior of the rock mass is divided into geometrically simple elements each with assumed properties. The rock mass is modelled as a volume in three dimensional models or an area in two dimensional models. The boundaries are placed far away enough so that they do not affect the area of interest where stresses and displacements are required. The stresses and deformations computed in the rock mass away from the excavation are discrete. Differential methods are sub-divided into Finite Element Method (FEM), Finite Difference Method (FDM) and Distinct Element Method (DEM). The first two treat the rock mass as continuum while the Distinct Element Method treats the rock mass as a discontinuum.

Any material property can be applied to any element in the mesh of FEM. FEM can represent inhomogeneous material as well as layering due to bedding. For better numerical solution finer mesh elements are used especially at the area of interest. The FDM allows the solution process to be stopped at any time between the initial and final equilibrium states to view results at a particular stage of solution. Each zone of the FDM mesh can have its own properties. The FDM can

represent inhomogeneous, non-linear and inelastic material. Layering due to bedding can easily be modelled. The disadvantage of the FDM is that solution time tends to be long. The DEM is used to model fractured rock mass as a collection of rock blocks. The blocks are detached from each other and interact through their boundaries.

For detailed description of integral and differential methods the reader is referred to Crouch and Starfield (1983), Jager and Ryder (1999) and Ryder and Jager (2002). The two classes of numerical methods can be combined together in the form of hybrid models. Hybrid models basically aim to maximise the advantages and minimise the disadvantages of each of the two methods.

5.3 Two dimensional versus three dimensional modelling

Two dimensional models are basically suited for analysis of stresses and displacements in plane strain conditions i.e., where the length of the excavation is much greater than its cross-sectional dimensions, for example, a tunnel. The stresses and displacements in a plane normal to the axis of the opening are assumed not to be influenced by the ends of the opening. Two dimensional models are easily understood and faster to run and analyse. Three dimensional models are used where the effect of end walls cannot be neglected. This is the case in bord and pillar geometries. Three dimensional analyses provide clear indications of stress concentrations and of the influence of three-dimensional geometry. The difficulty that comes with three-dimensional analysis is the interpretation of results as Hoek (2000) stated in his book *Practical Rock Engineering* "…three dimensional models are not easy to use… In addition, definition of the input parameters and interpretation of the results of these models would stretch the capabilities of all but the most experienced modellers". The three dimensional nature of bord and pillar mining necessitated the use of a three dimensional modelling code. FLAC3D was selected as it can be used for modelling failure.

5.4 Constitutive behaviour for rock mass

Different constitutive behaviours exist for rock masses. For the purposes of this dissertation the following constitutive behaviours for rock masses were considered. These are:

(i) Linear elastic;
(ii) Transversely isotropic elastic;
(iii) Mohr-Coulomb (MC);
(iv) Mohr-Coulomb strain softening (MCSS);
(v) Extension strain.

5.4.1 Linear elastic

The characteristic of a linear elastic constitutive behaviour is that no yielding is considered. A linear elastic constitutive behaviour is generally suitable for homogeneous, isotropic continuum materials, e.g., manufactured materials like steel, loaded below their elastic limits. The constitutive behaviour exhibits linear stress-strain behaviour.

5.4.2 Transversely isotropic elastic

Laboratory tests showed the shale layer is transversely isotropic. The transversely isotropic constitutive behaviour is used for analysis of materials that exhibit well-defined elastic anisotropy when loaded below their elastic limits.

5.4.3 Mohr-Coulomb

The Mohr-Coulomb constitutive behaviour is empirical and assumes that rock will fail in shear. It attempts to describe the stress environment at failure without necessarily explaining why failure takes place. The constitutive behaviour is represented by the following linear equation:

$$\tau = C + \sigma_n \tan\phi \quad \textbf{(5.1)}$$

where τ = shear stress along the shear plane at failure

σ_n = normal stress acting on the shear plane

C = initial cohesive strength

ϕ = angle of internal friction

The Mohr-Coulomb constitutive behaviour can also be represented by the following linear equation:

$$\sigma_1 = \sigma_c + q\sigma_3 \quad \textbf{(5.2)}$$

where $$q = \frac{1+\sin\phi}{1-\sin\phi} \quad \textbf{(5.3)}$$

$$\sigma_c = 2C\sqrt{q} \quad \textbf{(5.4)}$$

σ_1 = major principal stress at failure

σ_3 = minor principal stress at failure

C = initial cohesive strength

The yield stress depends on the major and minor principal stresses only; the intermediate principal stress has no effect. The two representations of the Mohr-Coulomb constitutive behaviour are illustrated in Figure 5.2 below. Since rock cannot sustain large tensile stresses, a tensile cut-off is often included.

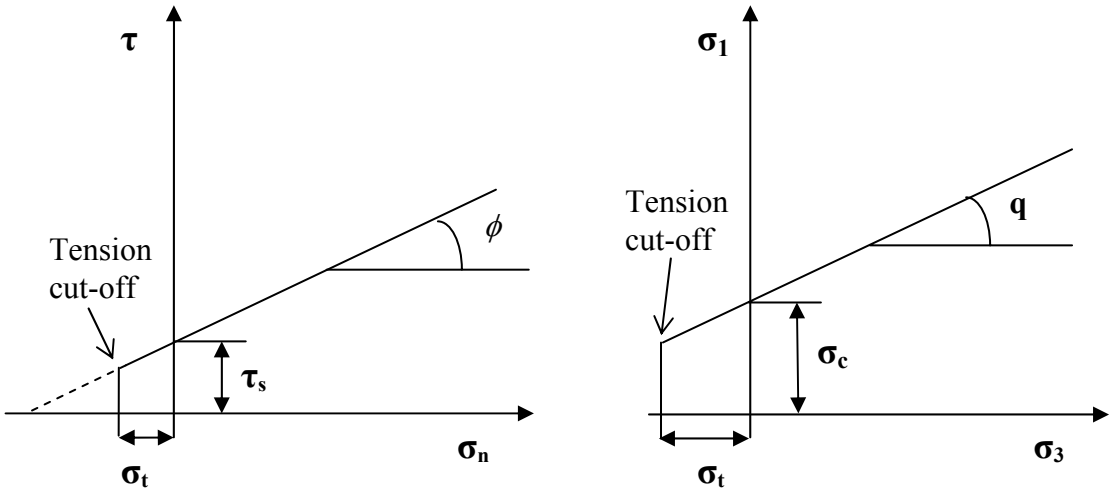

a) Normal and shear stresses **(b) Principal stresses**

Figure 5.2: Mohr-Coulomb criterion in terms of (a) principal stresses (b) normal and shear stresses

The Mohr-Coulomb constitutive behaviour is usually used to compare calculated stress states with estimated rock strength. It is in the form of a linear yield envelope defined in Mohr space. The area below the envelope represents the domain within which the material remains stable while the area above the envelope represents the domain within which the material will fail as shown in Figures 5.3a – 5.3c.

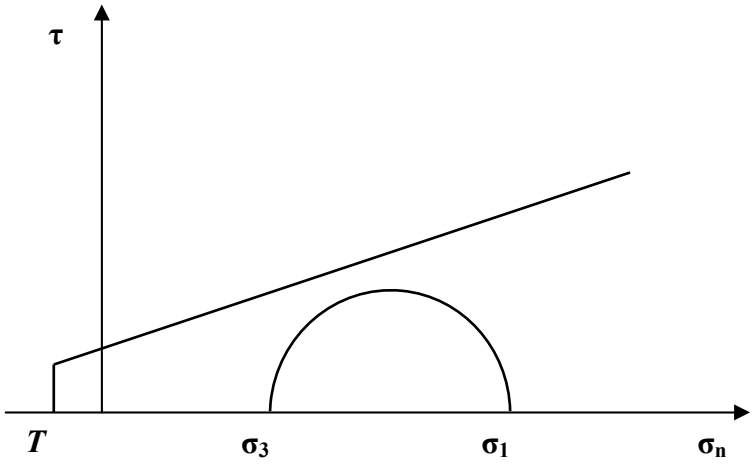

Figure 5.3a: Mohr circle that lies below the failure envelope and represents a stable stress state

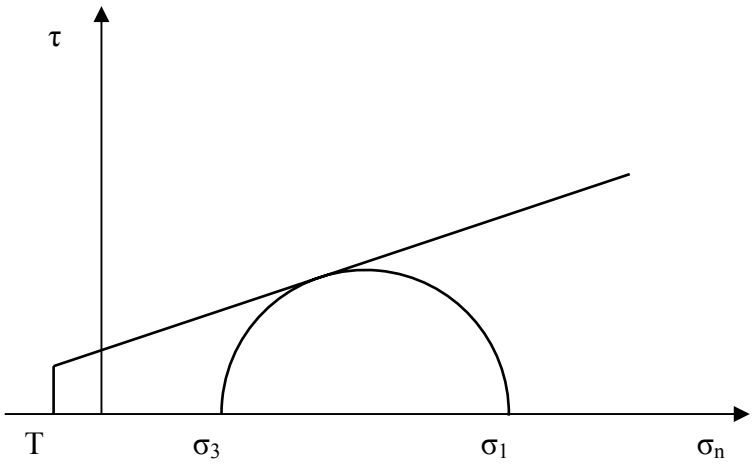

Figure 5.3b: Mohr circle that is tangent to the failure envelope and represents the state of stress at the instant of failure

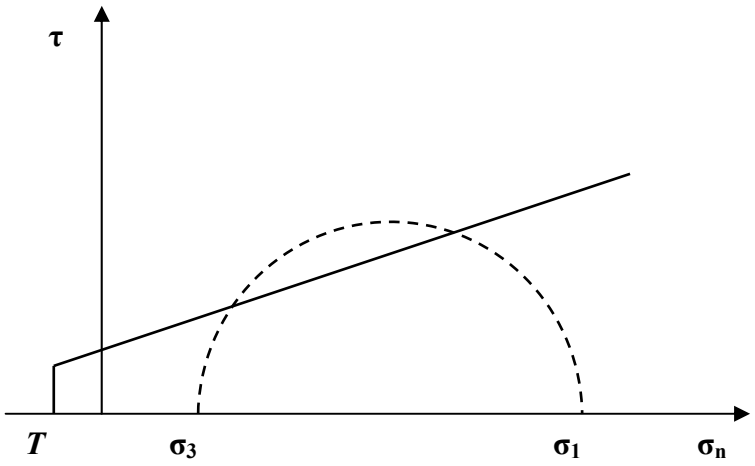

Figure 5.3c: Mohr circle that intersects the failure envelope and represents an unstable stress state

One of the reasons for the widespread use of the Mohr-Coulomb constitutive behaviour in rock engineering is its simplicity in application. It is, however, not a particularly satisfactory peak strength criterion for rock material (Brady and Brown, 1985). The reasons are:

(i) it implies that a major shear fracture exists at peak strength; observations show that this is not always the case;

(ii) it implies a direction of shear failure which does not always agree with experimental observation, and;

(iii) experimental peak strength envelopes are generally non-linear; they can be considered linear only over limited ranges of σ_n or σ_3.

For these reasons, other peak strength criteria are preferred for intact rock. Plastic strain is not calculated directly in Mohr-Coulomb constitutive behaviour. The strain softening constitutive behaviour is used in situations where plastic strain is required, e.g., studies in post-failure behaviour like progressive collapse (FLAC3D User Manual).

5.4.4 Mohr-Coulomb strain softening (MCSS)

The Mohr-Coulomb strain softening (MCSS) constitutive behaviour is a variation of the Mohr-Coulomb constitutive behaviour. It is used to simulate shear softening material and deals with post-failure behaviour of the material. Initiation of material softening is a gradual process once yielding begins. At failure, deformation becomes inelastic as a result of micro-cracking. This leads to degradation of strength and initiation of shear bands. In FLAC3D, shear softening is simulated by making Mohr-Coulomb parameters i.e., cohesion, friction angle and dilation angle, functions of plastic strain. The Mohr-Coulomb strain softening constitutive behaviour is suitable for studies in post-failure e.g., progressive failure as in the occurrence of guttering.

5.4.5 Extension strain criterion

Rock failure in intact rock sometimes occurs at stress levels that under normal circumstances would not be expected to be critical, based on the use of a shear stress criterion. An extension strain criterion is usually applicable to such circumstances. This criterion was originally known as the 'limiting tensile strain criterion' and was stated simply as *'fracture of the rock will occur in indirect tension when the tensile strain exceeds a limiting value which is dependent on the properties of the rock'*. Stacey (1981) changed the terminology from tensile strain

to extension strain as the former term could have implied the presence of a tensile stress, which is not a necessary condition for extension strain to occur. Stacey (1981) showed that extension strain may occur even when all three principal stresses are compressive. He discussed observations of extension fracturing that had been reported by others. Points he noted were that:

(i) Extension fractures can occur even when there is a very high compressive stress acting normal to the fracture plane;
(ii) The majority of fractures in rocks take place in the direction of the major principal stress;
(iii) Axial cleavage fracturing and slabbing of rock from sidewalls of mine haulages are examples of extension fractures.

Stacey (1981) noted that literature on failure of concrete indicated that an extension strain criterion for failure was apparently accepted. The term 'discontinuity' was introduced to define the point at which the axial stress versus axial strain relationship deviates from linearity and severe cracking begins. Stacey (1981) concluded from unconfined compression and confined triaxial compression tests that the extension strain at fracture initiation should not vary for a particular rock type. The results of the tests were expressed in the form of axial versus lateral strain plots. The extension strain necessary to initiate fracture could therefore be approximated from the point of intersection of two straight lines defining the point at which the change in slope occurred. For each set of rock specimens, the change point occurred at approximately the same magnitude of lateral extension strain.

Stacey (1981) then stated the extension strain criterion as follows, '*Fracture of brittle rock will initiate when the total extension strain in the rock exceeds a critical value which is characteristic of that rock type.*' Mathematically, this criterion can be expressed as follows:

$$e \geq e_c \qquad \textbf{5.5}$$

where e_c is the critical value of extension strain. The fractures were observed to form in planes normal to the direction of the extension strain. This corresponds with the direction of the minimum principal stress (the least compressive principal stress). For a material which shows ideal linear deformation behaviour, the strain in this direction is related to the three principal stresses by the following equation:

$$e_3 = \frac{1}{E}[\sigma_3 - \nu(\sigma_1 + \sigma_2)] \qquad \textbf{5.6}$$

where σ_1, σ_2, σ_3 are the principal stresses, E is the modulus of elasticity, ν is Poisson's ratio. From the above equation, Stacey (1981) noted that an extension strain will occur if $\nu(\sigma_1 + \sigma_2) > \sigma_3$. From this it can be seen that extension fractures can form when all three principal stresses are compressive and thus also in planes across which the net macro stress is compressive. The magnitudes of the critical extension strain obtained for the different rocks were observed to be very low and in a uniaxial compressive test corresponded to a stress level in the region of 30% of the uniaxial compressive strength (Stacey, 1981). In some cases fracturing occurs when the major field stress is as low as 10% of the intact rock strength (Stacey, 1989). The critical values of extension strain obtained from the tests represent the strain at which extension fractures initiate. At higher values of macro extension strain, continuous fractures are likely to form causing the progressive failure of brittle rock.

Stacey (1981) gave the conditions under which the criterion is applicable as those of brittle rocks under low confinement. He noted that the fractures will only progress as far as permitted by the distribution of extension strain and that fracture propagation is stable. He also noted that the presence of extension fractures will be limited to the proximity of openings in stressed rock since the presence of extension strain is inhibited by compressive confining stress. He noted that it is usually in such locations where design, and hence prediction of rock fracture, is required. The criterion is well suited for prediction of brittle rock fracture using

theoretical stress analyses as much of the pre-failure deformation behaviour is essentially linear for brittle rock. The two equations dealt with above are the only relations required. All the values in the latter equation are either input or output data from a conventional numerical stress analysis.

Kuijpers (2000) has questioned the use of the extension strain criterion. He noted that the mechanism fails to address the physics involved in the formation of fractures in compressive stress environment. Kuijpers noted that the formation of extension fractures must be associated with energy release. In the extension strain criterion he noted that fracture opening takes place against the action of a compressive stress hence there should be energy generation. This, according to him, appears farfetched. He concluded that extension fracturing is preceded by a micro damage process which, in turn, affects the global stress distribution in such a way that tensile stresses can be generated. Ryder and Jager (2002) noted that the predictions of the extension strain criterion into more general loading regimes are at variance with the findings of laboratory poly-axial testing. According to them, the criterion predicts halving of strength in extension mode yet significant increases in strength are observed. Their concerns can be dismissed since the locations under which the extension strain is applicable are those at the boundary of an excavation. At such locations there is no confinement.

Researchers that are agreeable to the use of an extension strain criterion to estimate the spalling of underground cavities are Martin (1997), Martin et al (1999), Aydan et al (2001), Wesseloo (2000), Diederichs (2003) and Eberhardt et al (2004). Martin (1997) noted that although the application of the extension strain criterion has met with some success it is still not obvious what fundamental mechanisms control the failure of brittle rock. Martin et al (1999) observed that since an extensional strain criterion could be used to predict the depth of spalling and the observational evidence that the spalling process involves the growth of extension-like fractures then the brittle failure process should be controlled by the cohesion of the rock mass. Aydan et al (2001) noted that the above definition of

extension strain actually corresponds to the definition of initial yielding in the theory of plasticity.

Diederichs (2003) showed that rock mass strength near underground excavations is controlled by damage initiation mechanisms that are relatively insensitive to confinement but by fracture propagation (extension) mechanisms that dominate at low confinement. Using confined compression tests he showed that the total lateral extension strain at crack interaction did not vary with an increase in confining stress, i.e., the value was constant for the different values of confining stress. He concluded that this was consistent with the extension strain criterion developed by Stacey (1981).

Eberhardt et al (2004) noted that the brittle fracture process involves both the initiation of new fractures and the propagation of pre-existing fractures. They noted that the extensional strains induced by a combination of high horizontal stresses and low vertical stress will result in fracture initiation and propagation driving the progressive development of the failure surface (i.e., roof guttering, in this case). Wesseloo and Stacey (2000) report that the extension strain approach has also been given additional credibility by the work of Fujii et al (1994, 1997), who used it for the prediction of rock failure in addition to fracture initiation. Wesseloo (2000) successfully used the extension strain criterion to model the notch formation around AECL's underground tunnel.

Numerical simulation using the extension strain criterion in bord and pillar workings involves the following stages:

(i) estimation of the critical extension strain from UCS tests;
(ii) creation of model geometry;
(iii) setting up model equilibrium with in situ stress field;
(iv) roadway and split excavation and running the model to its new equilibrium state;

(v) calculation of the minor principal strain field and noting all elements with an extension strain larger than the specified critical extension strain;

The critical extension strain is estimated from the following equation:

$$e_c = \frac{f * UCS * v}{E} \qquad \textbf{5.7}$$

where e_c = critical extension strain;

UCS = uniaxial compression strength of intact rock sample of the rock;

v = Poisson's ratio;

E = Young's modulus

f = factor that varies between 0.25 to 0.3 for crack initiation strain

Progressive failure can be modelled by removal of all elements with an extension strain larger than the critical extension strain. All the material that fails is assumed to be removed. If failure of material is in the roof or side wall, then the failed material is assumed to be removed by gravity. If the failed material is in the floor, removal is assumed to be by mechanical means. It should be noted that if the failed material in the floor is not removed this material will have a stabilising effect and the extension strain criterion will over predict the depth of fracturing.

5.5 Conclusions

This chapter reviewed numerical modelling as applied to a data limited field like rock engineering and types of numerical codes available to a rock engineer. The chapter also included a discussion of the constitutive laws that were used in the analysis of rock mass behaviour. These are the linear elastic, transversely isotropic elastic, the Mohr-Coulomb, the MCSS and the extension strain constitutive laws. The following chapter discusses the modelling methodology in FLAC3D and results obtained from the implementation of the five constitutive laws discussed above.

Chapter 6

Numerical modelling methodology and results

6.1 Introduction

This chapter briefly discusses the modelling procedure followed in FLAC3D. The results of stress and strain (deformations) distributions in a bord and pillar geometry are then discussed. The results are discussed in the following order; elastic results, non elastic results and finally extension analyses results. The results are then analysed and a comparison is made between the results of different analyses and underground observations.

6.2 Numerical modelling procedure in FLAC3D

The numerical modelling procedure in FLAC^{3D} for bord and pillar mining consists of the following steps:

(i) Grid generation;
(ii) Selection of appropriate constitutive model and incorporation of material properties;
(iii) Setting initial and boundary conditions;
(iv) Stepping to equilibrium to establish in situ stresses in the model;
(v) Loading and sequential excavation of the roadways and splits;
(vi) Presentation of results for interpretation.

6.2.1 Grid generation

The bord and pillar mining layout is shown in Figure 6.1. The actual in-mine dimensions for bords and square pillars are 6.5 m and 8.7 m, respectively. Pillar height is 1.65 m in one panel and 2 m in the other two panels. For the purposes of

numerical modelling bord and pillar widths assumed are 7 m and 9 m, respectively, and the modelled pillar height is 2 m. The modelled depth is 52 m below ground surface. A system of coordinate axes is defined with the origin at the horizontal plane through the pillar at pillar mid-height; the z-axis points upward and the y-axis points along the direction of mining. The two model geometries considered for the analyses are described below:

(i) **Model 1** - A quarter of the bord and pillar geometry is used for modelling, taking advantage of the symmetry of the excavation geometry and the loading. There are four planes of symmetry. These are the four vertical planes defining the quarter of the model. Horizontal displacements at the vertical symmetry planes are zero. To optimise memory usage and runtime requirements only 16 m of cover has been modelled and the horizontal plane through the pillar at pillar mid-height has been assumed to be another plane of symmetry. This plane is fixed in the vertical direction and the vertical displacements on it are zero. The distance of 16 m was found to be free from the influence of roadways. The quarter symmetry model is shown in plan view in Figure 6.1. The quarter symmetry model grid in three dimensions is shown in Figure 6.2. The model has 230 400 zones and requires approximately 1.1 GB of RAM. The immediate shale roof is made up of zones of 0.1 m dimensions.

(ii) **Model 2** – The geometry shows a coal heading. Loading is symmetrical. The model is shown in plan view in Figure 6.3. The four planes of symmetry explained for Model 1 exist in this model. The model contains 475 200 zones and requires approximately 1.4 GB of RAM. The immediate shale roof is made up of zones of 0.1 m dimensions.

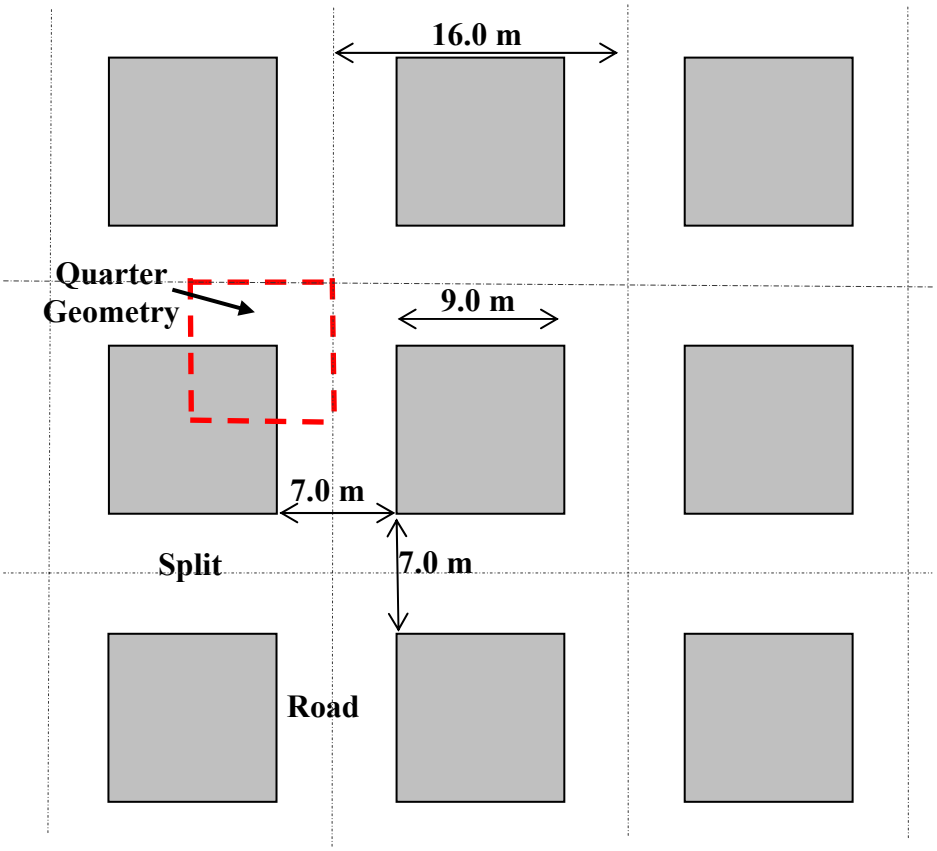

Figure 6.1: Plan view of bord and pillar geometry showing the quarter symmetry model

6.2.2 Constitutive behaviours and material properties

Constitutive behaviours discussed in the previous chapter are used for the analyses. In addition to these, a null model is used and represents material that is excavated from the model. The material properties used with each model are given in Appendix A2.

6.2.3 Initial and boundary conditions

Initial conditions are variables that are prescribed for the model before an excavation is created. Boundary conditions are variables that are prescribed on the boundaries of the model. The initial stress state corresponds to gravitational loading. The vertical stress gradient is 0.025 MPa/m while the horizontal stress

gradients are 0.142 MPa/m and 0.105 MPa/m for σ_x and $\sigma_{y,}$ respectively. These represent k_x and k_y ratios of 5.7 and 4.2, respectively.

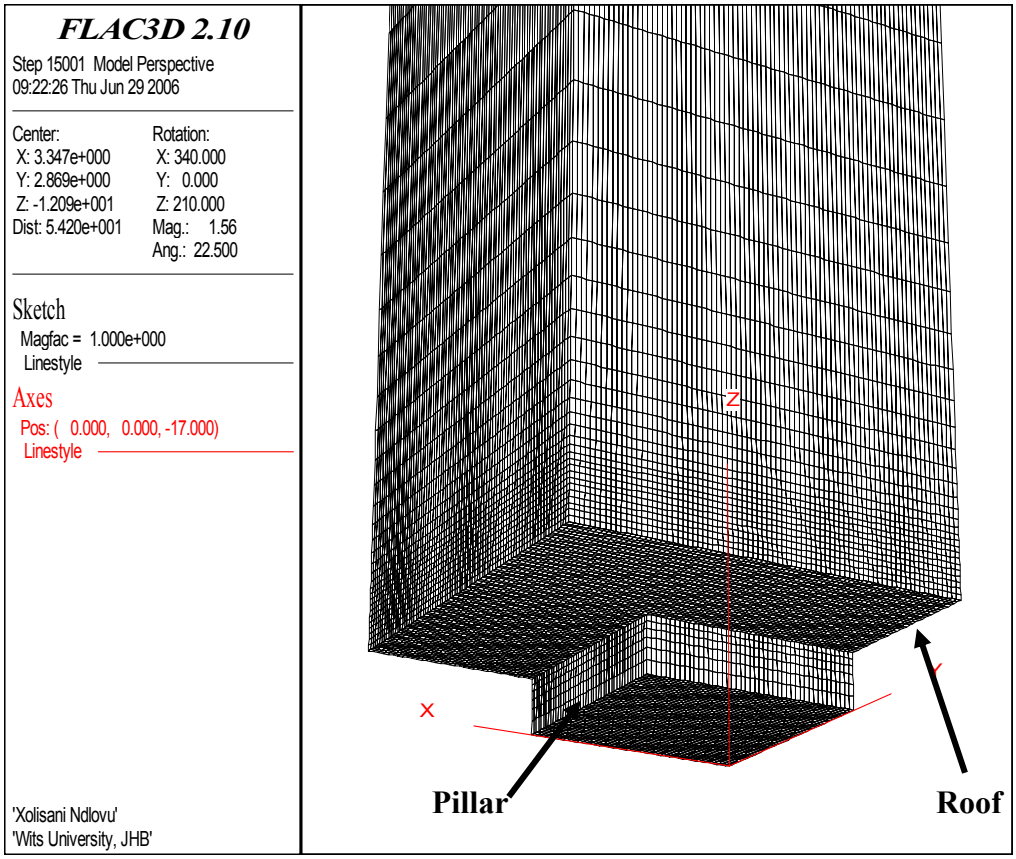

Figure 6.2: Quarter geometry model grid in three dimensions

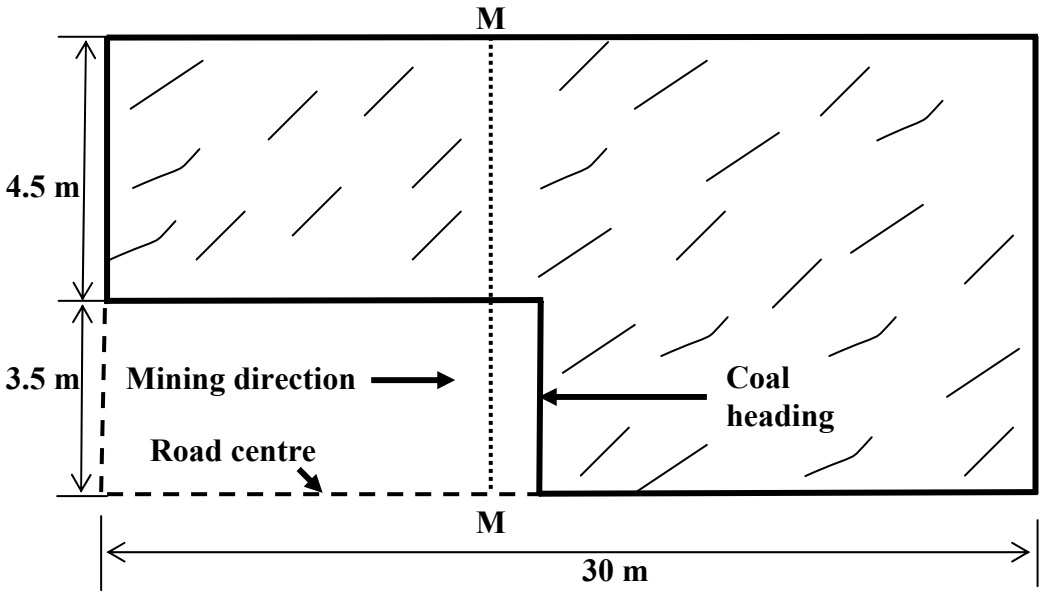

Figure 6.3: Plan view of model geometry with a coal heading (Line M-M/Section M-M can be moved to different locations behind and ahead of the coal face)

6.2.4 Solution to initial equilibrium

Equilibrium is established by running the model until the unbalanced force ratio reaches a pre-defined value. This is a ratio of forces that exist at the end of a certain number of steps to the forces that exist at the beginning of a model run. A value of 0.00001 is used.

6.2.5 Loading and sequential excavation

Loading is achieved by excavation of the roadways and splits so that the excavation is loaded by in situ stresses. Stresses re-distribute and a new equilibrium state is attained or failure takes places depending on the new state of stress.

6.3 Modelling Results

Three types of analyses were carried out for each of the constitutive behaviours considered. These were analyses based on:

(i) Model 1 described above;
(ii) Model 2 described above;
(iii) Model 1 with an interface at the coal-shale contact.

The first two analyses assume a strong contact between the coal and shale layers. The third analyses used an interface to allow for bed slip between the coal and the shale roof, which should have a major influence on the overall system behaviour. An interface is a FLAC3D entity for modelling physical discontinuities. Selected relevant results are discussed in the following sections. The history locations for Model 1 are shown in Figures 6.4 and 6.5 across the pillar and at different levels above the roof, respectively. For Model 2 analyses the history locations are along the line M-M shown in Figure 6.3 at different locations from the coal face and above the roof level.

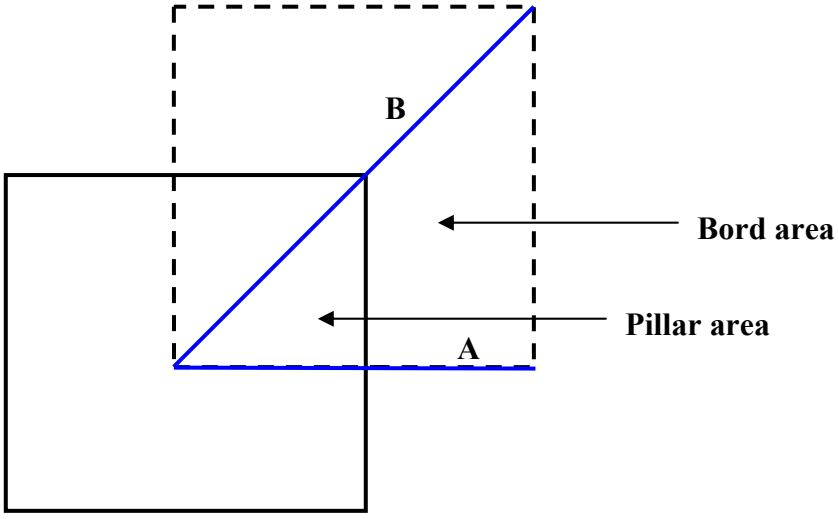

Figure 6.4: Plan view showing the bord and pillar geometry and Lines A and B across the pillar, along which history points are located. For contour plots A becomes Section A.

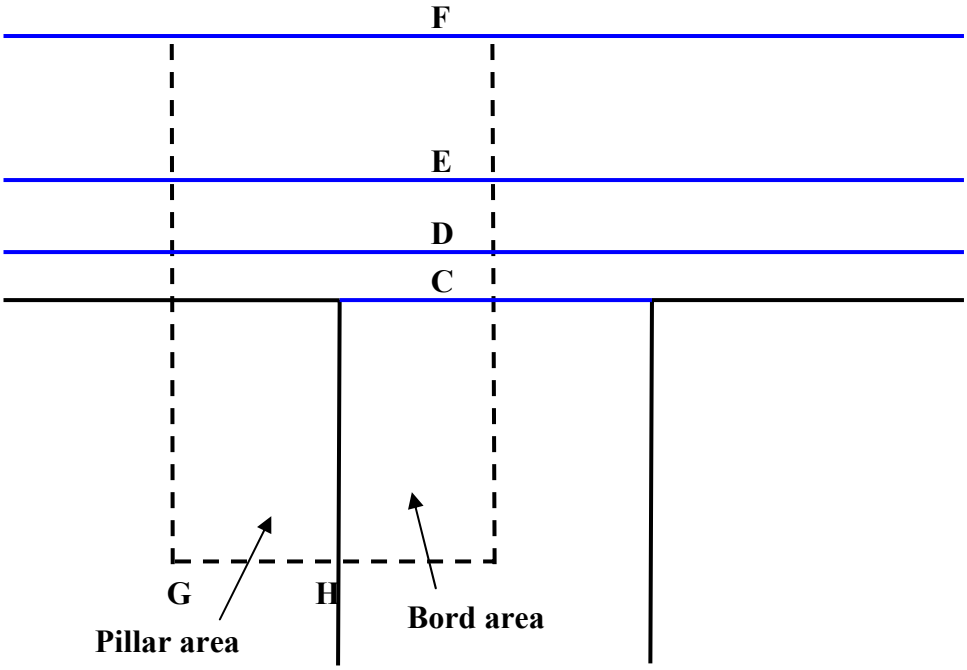

Figure 6.5: Section showing the bord and pillar geometry and Lines C, D, E and F above the roof, along which history points are located

Dotted lines define the region considered for numerical modelling. History points along Line A are normal to the pillar while those along Line B are diagonally across the pillar. History points along Lines C, D, E and F are at the roof level, 0.2 m, 0.5 m and 1 m above the roof level, respectively.

An equilibrium state is established before an excavation is created. The principal stress tensors show that the major principal stress is compressive throughout the model with a maximum value of 6.2 MPa. No tensile stresses exist in the equilibrium state. The major principal stress is in a horizontal direction while the minor principal stress is in a vertical direction. The vertical stress is 1.3 MPa. Stress re-distribution takes place when an excavation is created. The rock above the excavation is then supported by the pillars.

6.3.1 Results of elastic analyses

The isotropic and transversely isotropic models without an interface at the coal-shale contact make up the elastic models. The results for the two model analyses are discussed below.

6.3.1.1 Results of isotropic analyses

An elastic analysis does not simulate failure and results show that the system is at equilibrium after excavation of the bords. This was checked using the unbalanced force, displacement and velocity histories. Figure 6.6 shows a contour plot of the vertical stress distribution after an excavation is created. High stresses exist in the pillar while the immediate roof experiences de-stressing. The sides of the pillar at pillar mid-height position also experiences de-stressing. Significant stress concentrations occur at the roof-pillar contact.

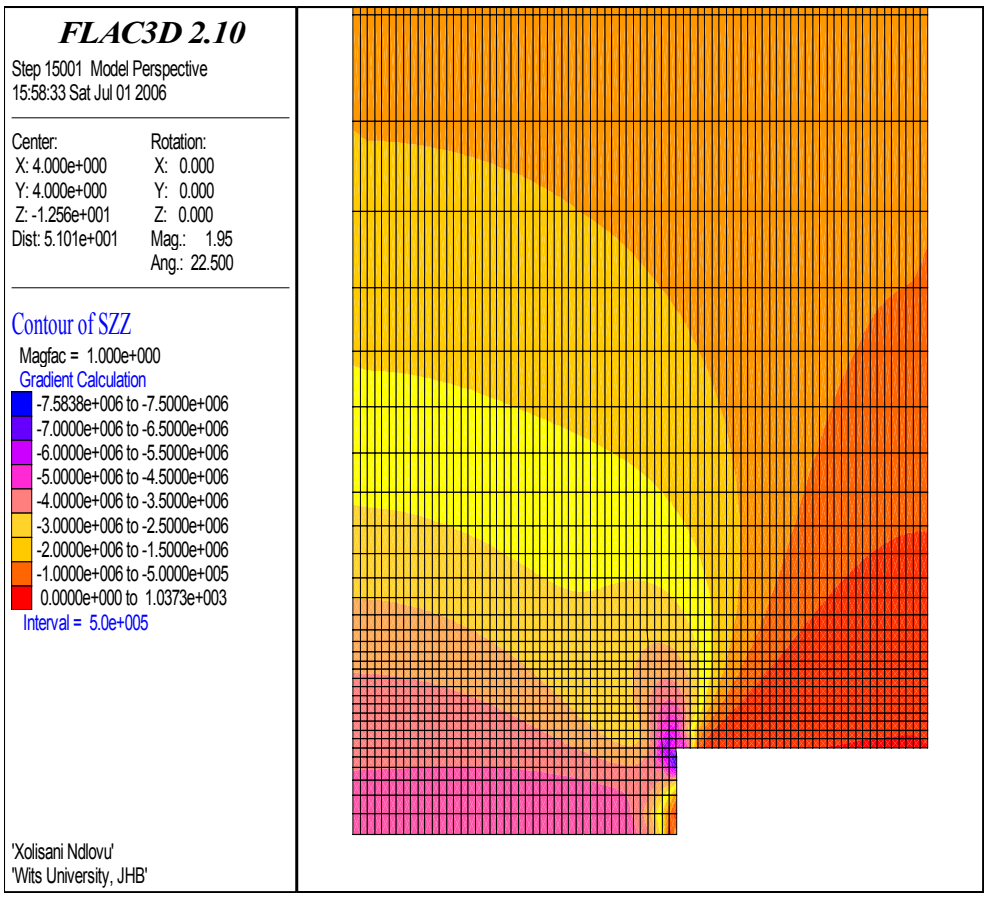

Figure 6.6: Contour plot of vertical stress distribution for the isotropic model (along Section A, Figure 6.4)

Figures 6.7 and 6.8 show the contour plots of the horizontal stress distributions. Significant horizontal stress concentrations occur at the roof-pillar contact while there is de-stressing around the sides of the pillar. The major and minor horizontal stresses above the roof have not significantly changed from their in situ values.

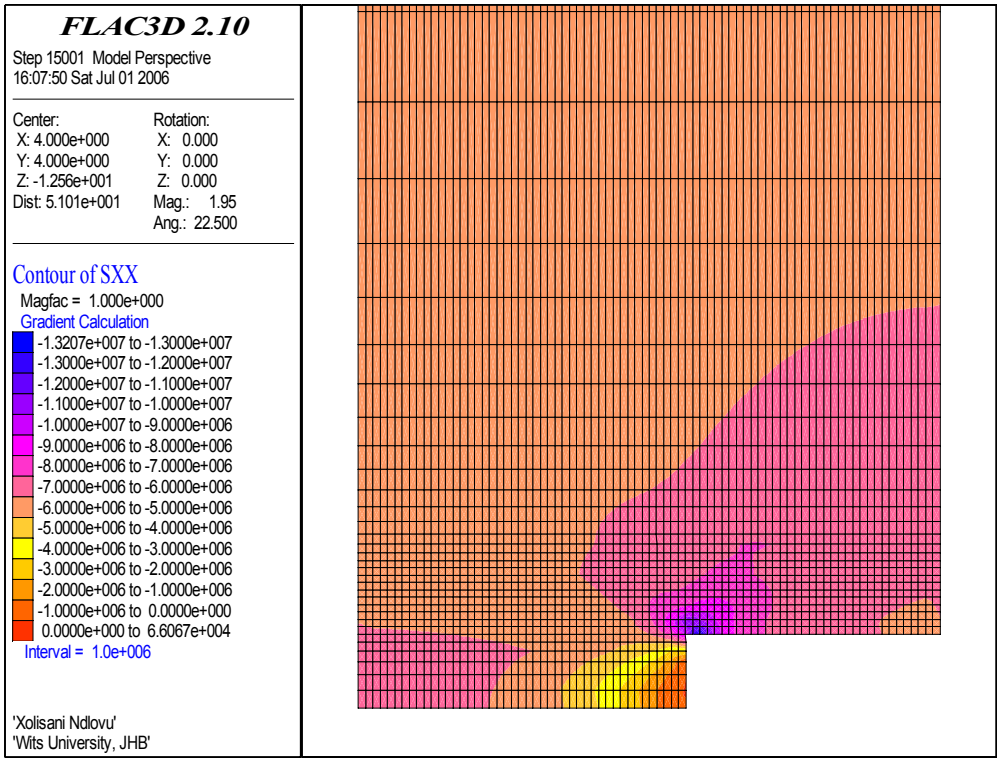

Figure 6.7: Contour plot of major horizontal stress distribution (along Section A, Figure 6.4)

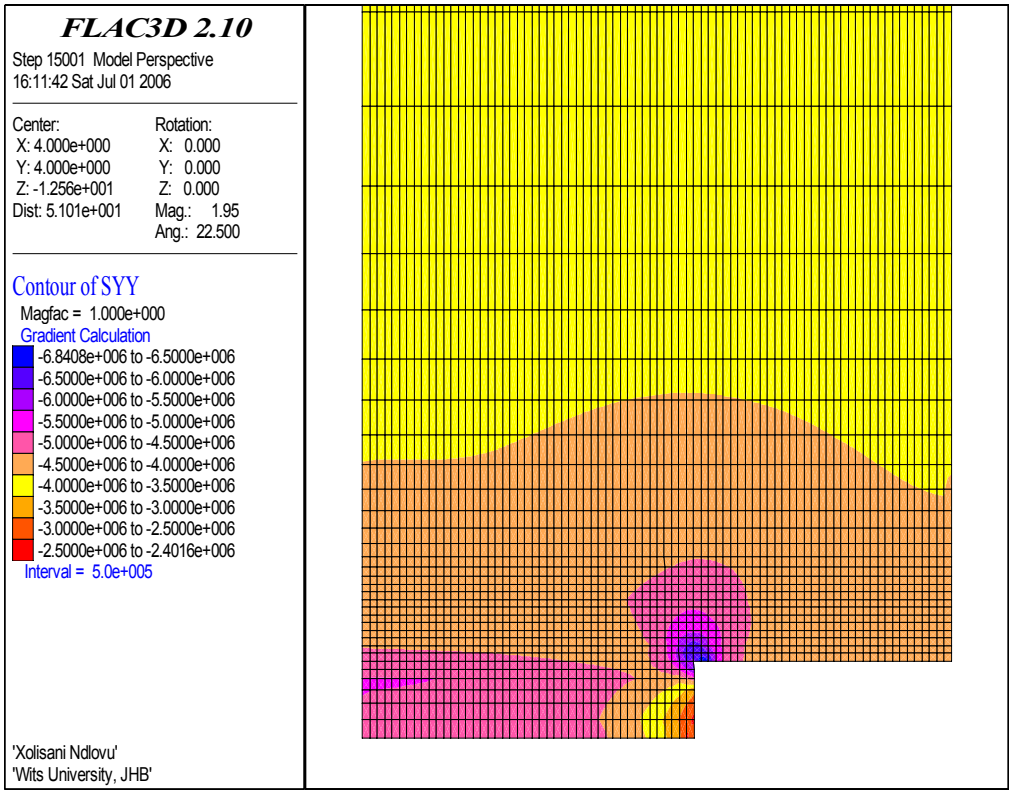

Figure 6.8: Contour plot of minor horizontal stress distribution along Section A

Figure 6.9 shows plots of stress distribution at the roof height position for the isotropic model. The plots show that the area that experiences high stress concentrations is very small. This area is around the roof-pillar contact and is about 1 m in width. The maximum value of the major horizontal stress is about 13 MPa while the maximum value of the minor horizontal stress is about 6.8 MPa.

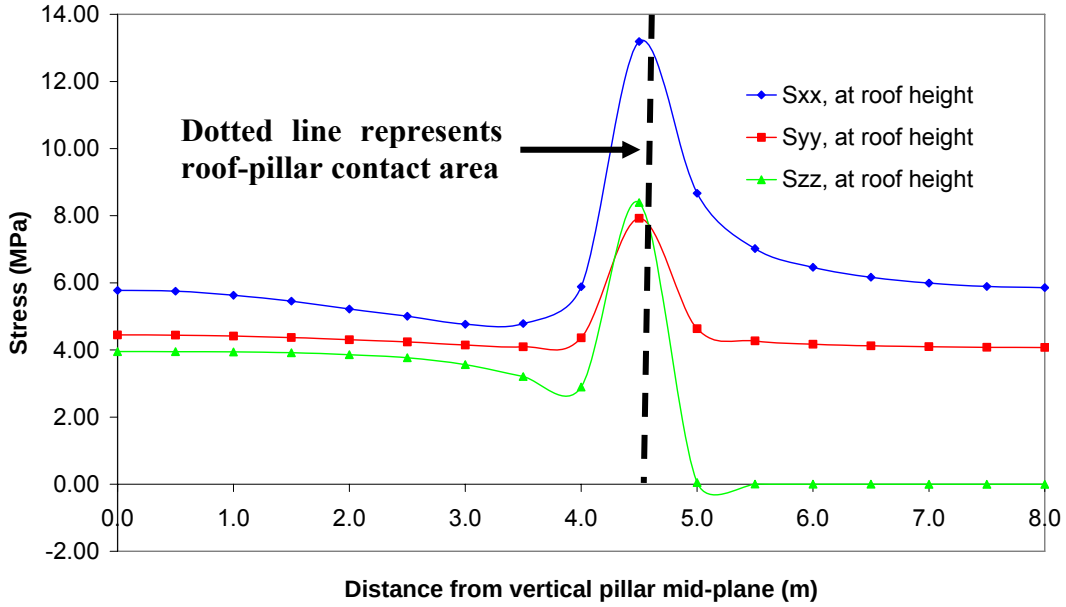

Figure 6.9: Distribution of stresses (along Line A, Figure 6.4)

An analysis based on Model 2 geometry confirmed the above results. The distributions of the major horizontal stress at various locations behind, at and ahead of coal face are shown in Figure 6.10. There are, however, minor stress concentrations just behind, at and just ahead of the coal face towards the centre of the roadway. These are, however, still well below the stress concentrations at the roof-pillar contact.

A plot of principal stress tensors after excavation, shown in Figure 6.11, indicates that the maximum compression is 20.3 MPa and the maximum induced tension is about 0.2 MPa. A plot of vertical displacement shows that the maximum displacement is 1.6 mm.

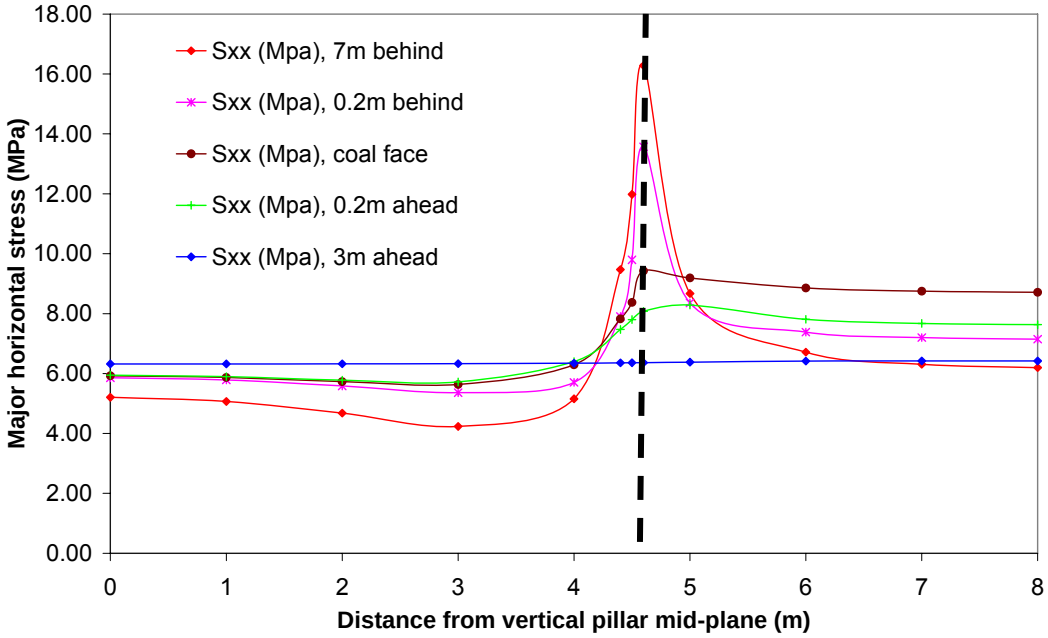

Figure 6.10: Distribution of major horizontal stresses (along Line M-M in Figure 6.3) at various positions behind, at and ahead of coal face

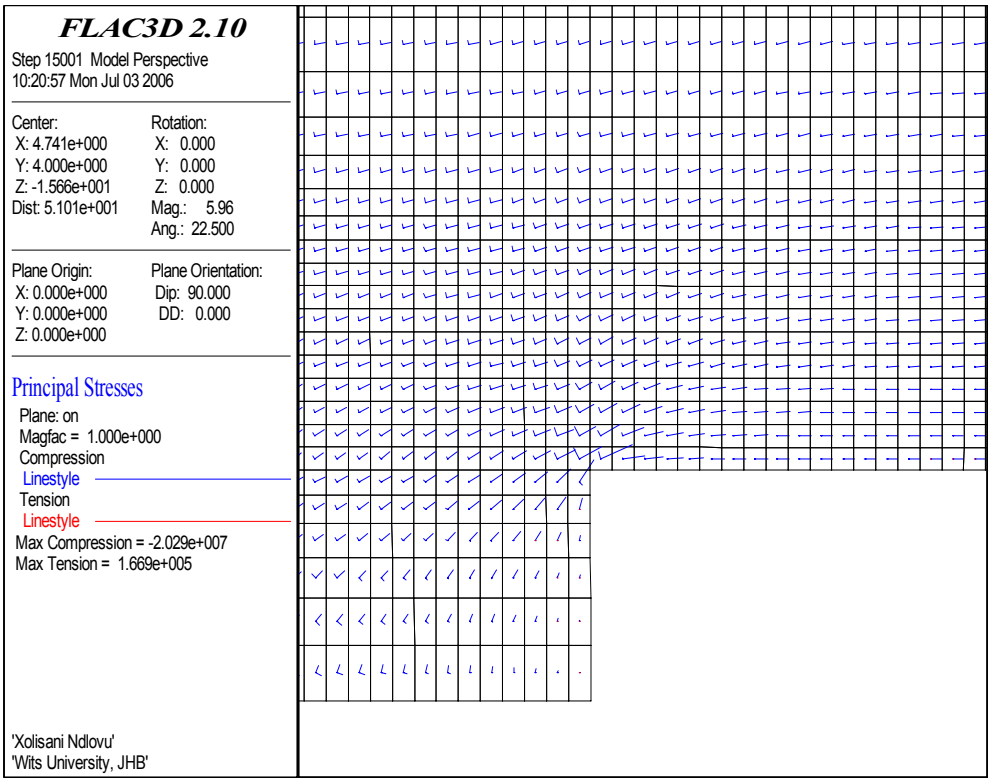

Figure 6.11: Principal stress tensors for the isotropic model (along Section A, Figure 6.4)

Figure 6.12 shows the vertical stress distribution from pillar centre to the roadway centre at the pillar horizontal mid-plane along Line A shown in Figure 6.4. The peak vertical stress acting in the pillar horizontal mid-plane occurs a little inside the free face of the pillar. Results similar to these were reported by Stacey (1972) using three dimensional finite element analyses.

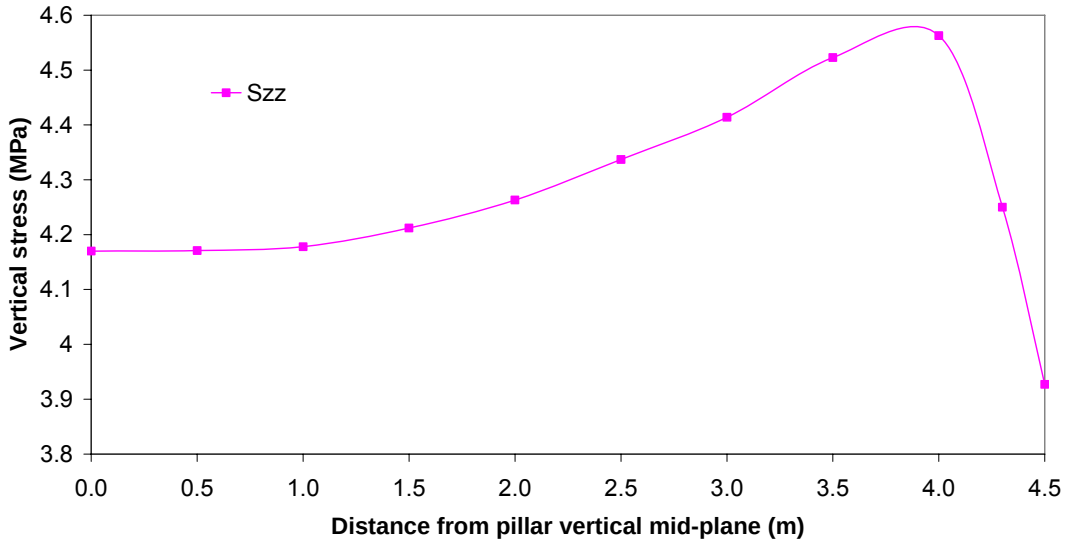

Figure 6.12: Distribution of vertical stresses at the horizontal pillar mid-plane for the isotropic model (along Line G-H Figure 6.5)

6.3.1.2 Results of transversely isotropic analyses

Stress distributions are similar to those of the isotropic model. The difference exists in the magnitude of the stresses, in particular the maximum stress concentrations. The distribution of stresses is shown in Figure 6.13. The maximum horizontal stress concentrations are higher for the transversely isotropic model than for the isotropic model. The maximum vertical stress concentration is less for the transversely isotropic model than for the isotropic model. Model 2 results show similar stress distributions to those of Model 2 results of the isotropic model. There are no stress concentrations of the major and minor horizontal stresses towards the centre of the roadways.

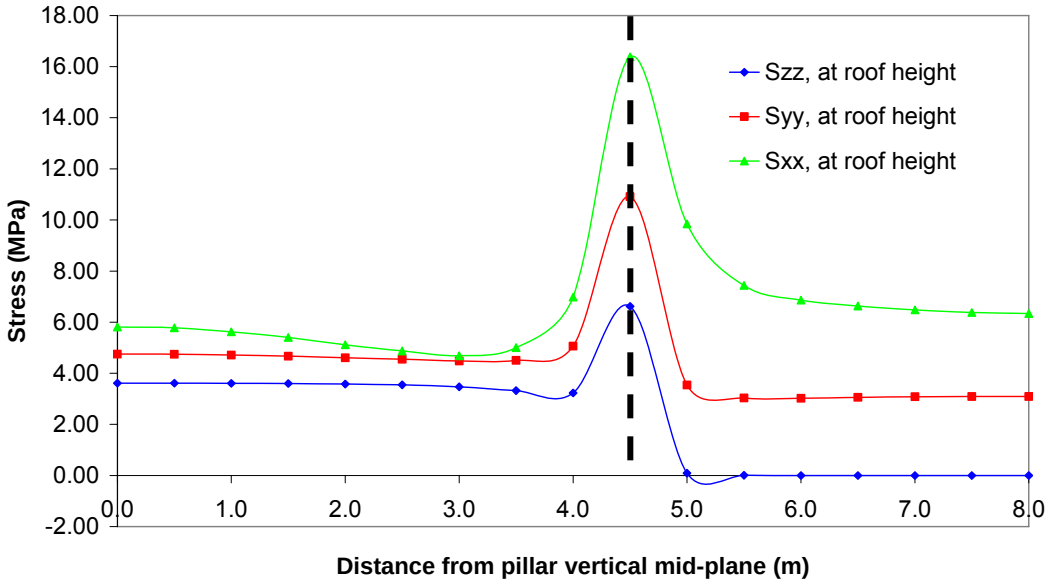

Figure 6.13: Distribution of stresses for the transversely isotropic model (along Line A in Figure 6.4)

An analysis of the plot of principal stress tensors after excavation indicates that the maximum compression is 23.7 MPa and the maximum induced tension is about 0.0005 MPa. A plot of displacement shows that the maximum vertical displacement is about 2.9 mm and occurs at the centre of the intersection of two roads. The peak vertical stress acting in the pillar horizontal mid-plane occurs a little inside the free face of the pillar.

6.3.2 Results of non elastic analyses

Non elastic models include the isotropic and transversely isotropic models with an interface at the coal-shale contact, the Mohr-Coulomb and the Mohr-Coulomb strain softening models. The results for the analyses of non elastic model simulations are discussed below.

6.3.2.1 Results of isotropic analyses for model with an interface

Figure 6.14 shows a contour plot of the vertical stress distribution for the isotropic model with an interface at the coal-shale contact. High stresses exist in the pillar while the immediate roof experiences de-stressing. Small magnitudes of tensile stresses are developed towards the centre of the road while there are no tensile stresses developed in the pillar. There are no significant stress concentrations at the roof-pillar contact.

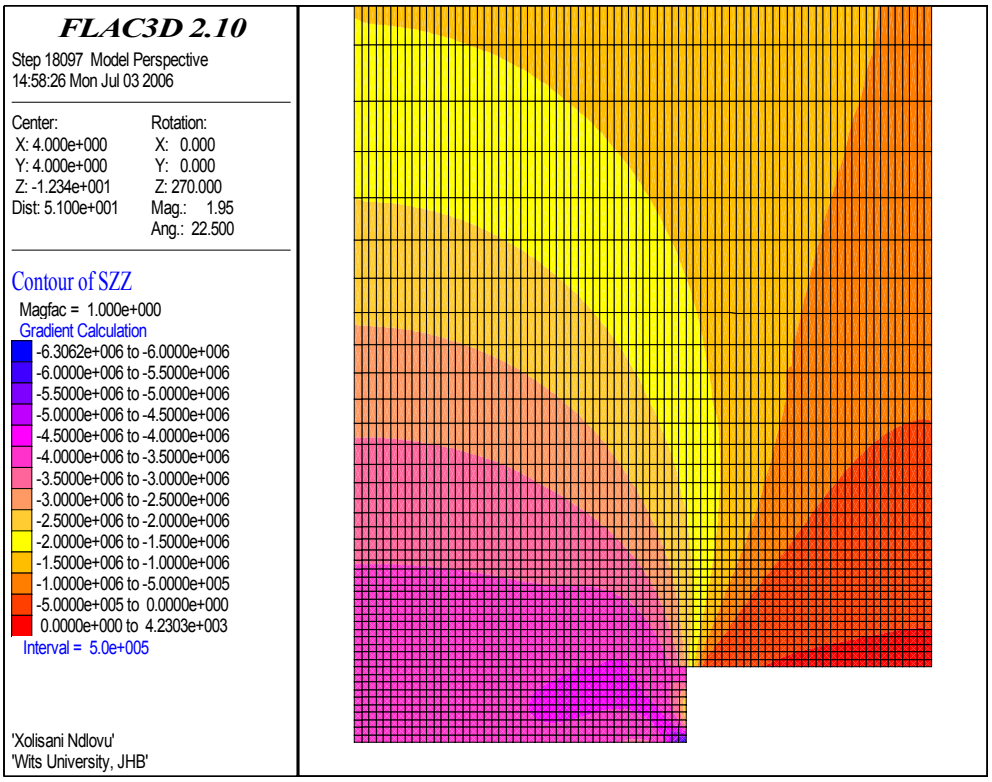

Figure 6.14: Contour plot of vertical stress distribution along Section A for the elastic model with an interface

Horizontal stress distributions show that there are no significant stress concentrations at the roof-pillar contact area. A contour plot of the major horizontal stress is shown in Figure 6.15. A graphical plot of the variation of stresses at different points along Line A is shown in Figure 6.16. The plot shows that the highest stress concentrations occur at about 0.5 m into the pillar from the roof-pillar contact area.

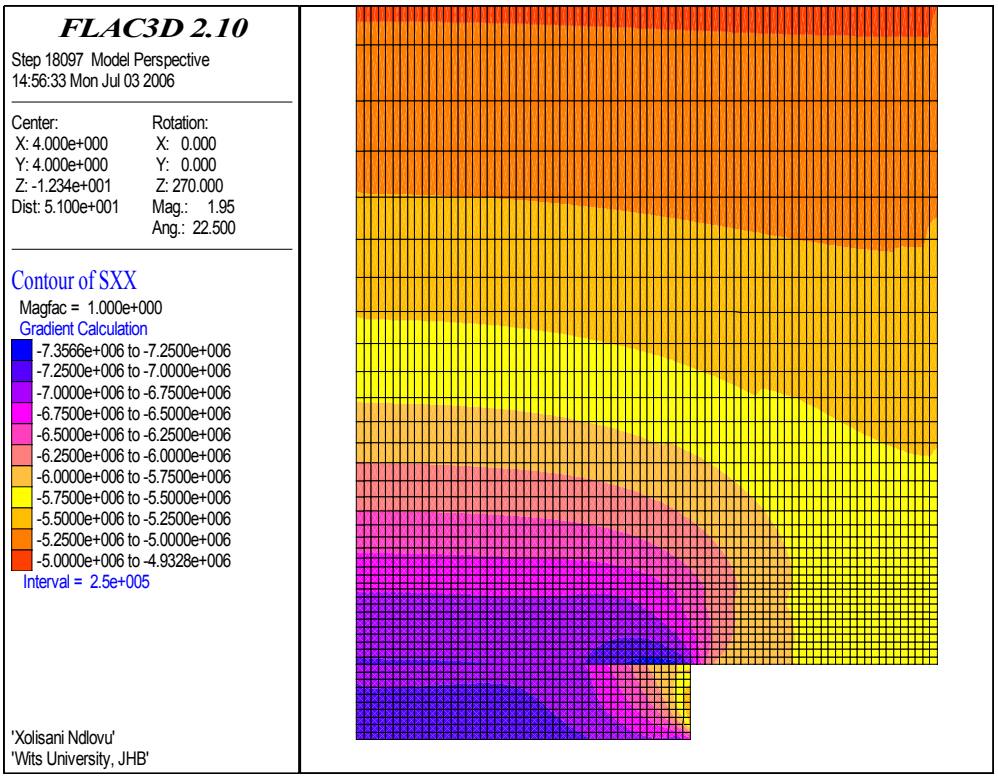

Figure 6.15: Contour plot of major horizontal stress distribution along Section A for the elastic model with an interface

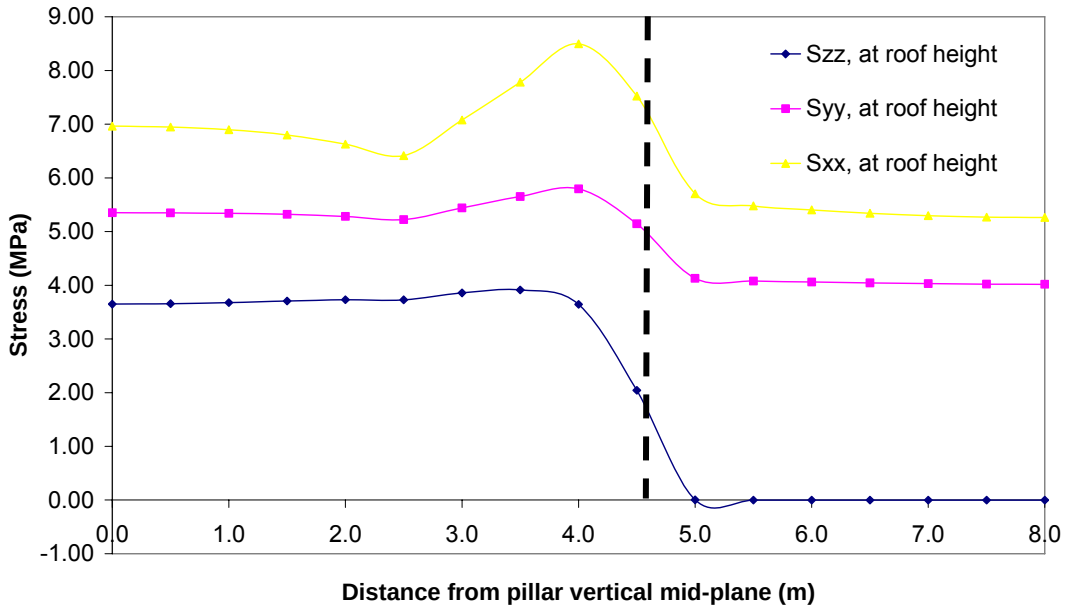

Figure 6.16: Distribution of stresses (along Line A, Figure 6.4)

Figure 6.17 shows the vertical stress distribution from pillar centre to the roadway centre at the pillar horizontal mid-plane along Line A. The peak vertical stress acting in the pillar horizontal mid-plane occurs at the free face of the pillar. Results similar to these were obtained by van Heerden's (1970) in situ tests. The minimum vertical stress occurs at about 0.5 m from the free face.

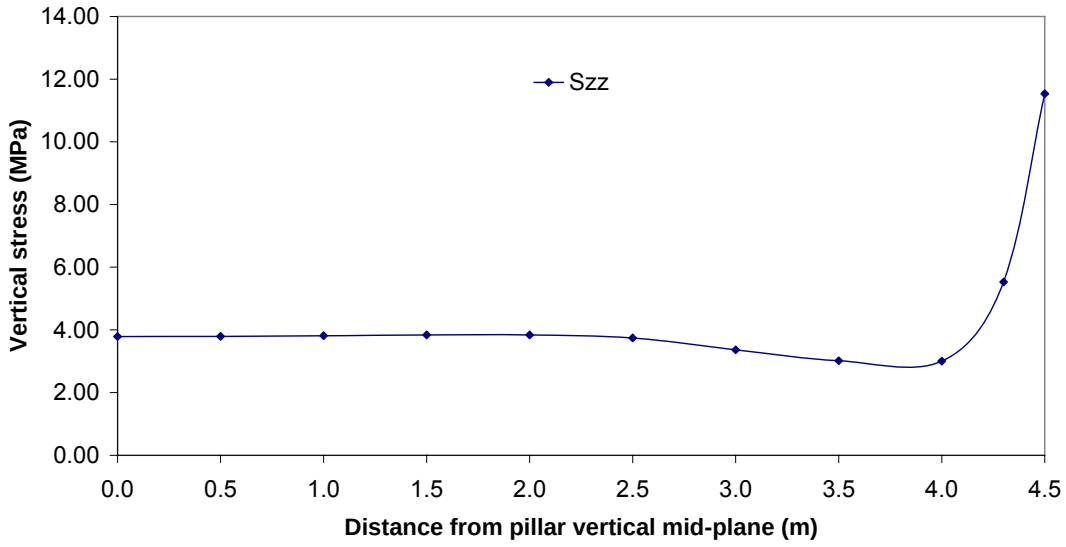

Figure 6.17: Distribution of vertical stress in the pillar horizontal mid-plane for the isotropic model with an interface (along Line A)

Principal stress tensors show that maximum compression is 11.8 MPa while maximum tension is 0.0004 MPa. An analysis of the displacement plots shows that the maximum vertical displacement is about 1.6 mm.

6.3.2.2 Results of transverse isotropic analyses for model with an interface

A contour plot of vertical stress distribution for this model is shown in Figure 6.18. The vertical stress in the pillar is compressive throughout. Tensile stresses occur towards the centre of the excavation and these are insignificant.

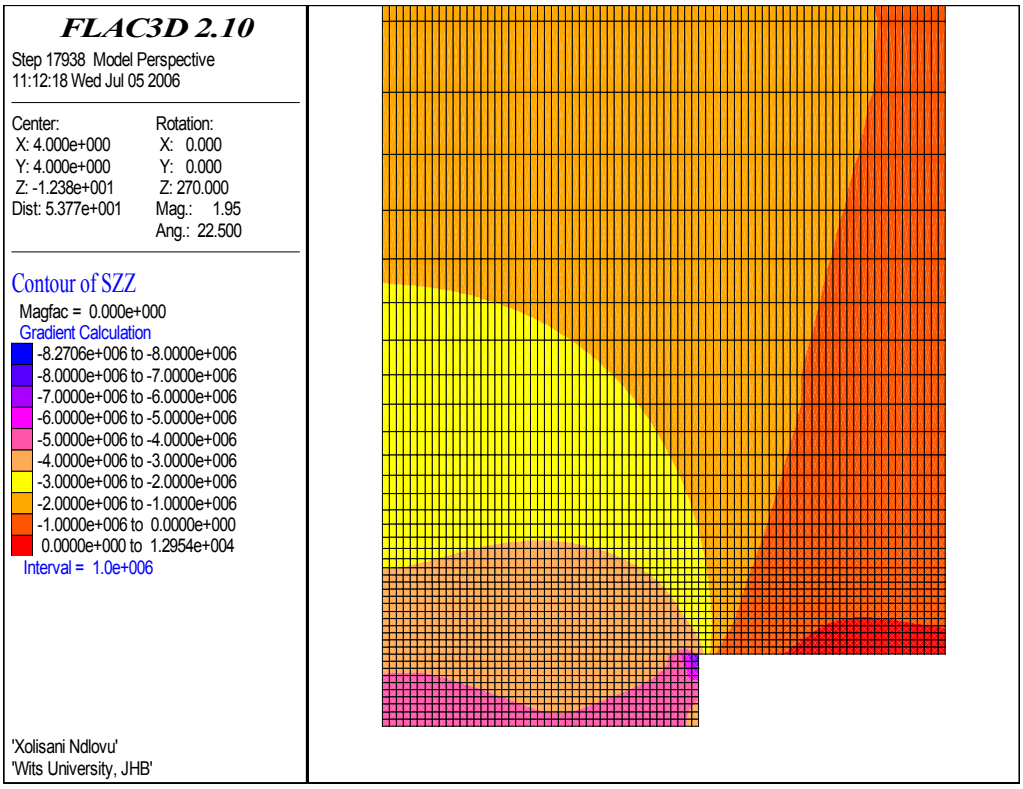

Figure 6.18: Vertical stress distribution (along Section A, Figure 6.4)

Analyses of major and minor horizontal stresses indicate that there are no stress concentrations towards the centre of the road. Figure 6.19 shows the contour plot of the major horizontal stress distribution. The highest stress concentrations occur mainly in the rock mass above the pillar.

An analysis of the principal stress tensors show that maximum compression is 13.7 MPa while the maximum tension very negligible at 0.0001 MPa. The displacement plots show that the maximum vertical displacement is about 3.3 mm.

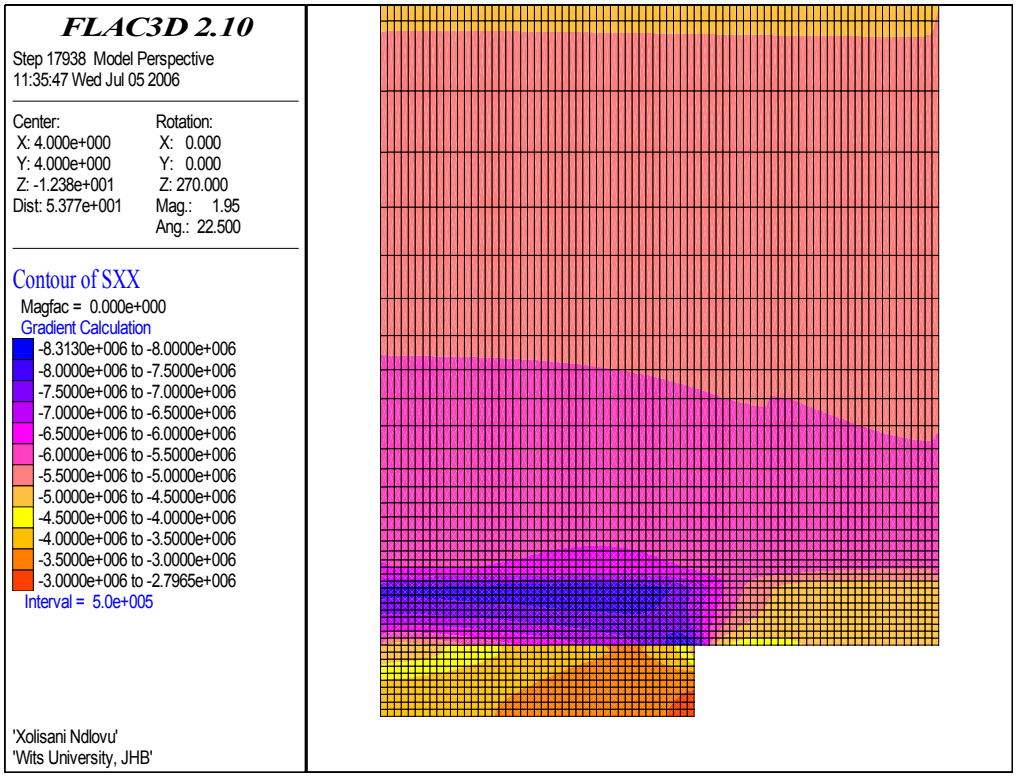

Figure 6.19: Major horizontal stress distribution (along Section A, Figure 6.4)

6.3.2.3 Results of Mohr-Coulomb analyses

The major principal stress distribution is shown in Figure 6.20. The immediate roof and sides of the pillars experience significant de-stressing. Significant horizontal stress concentrations occur at the pillar centre. Induced tensile stresses are in the order of 0.0004 MPa in magnitude.

A plot of the vertical stress distribution is shown in Figure 6.21. Stress concentration areas include areas along the roof-pillar contact. The vertical stress approaches zero in the immediate the roof.

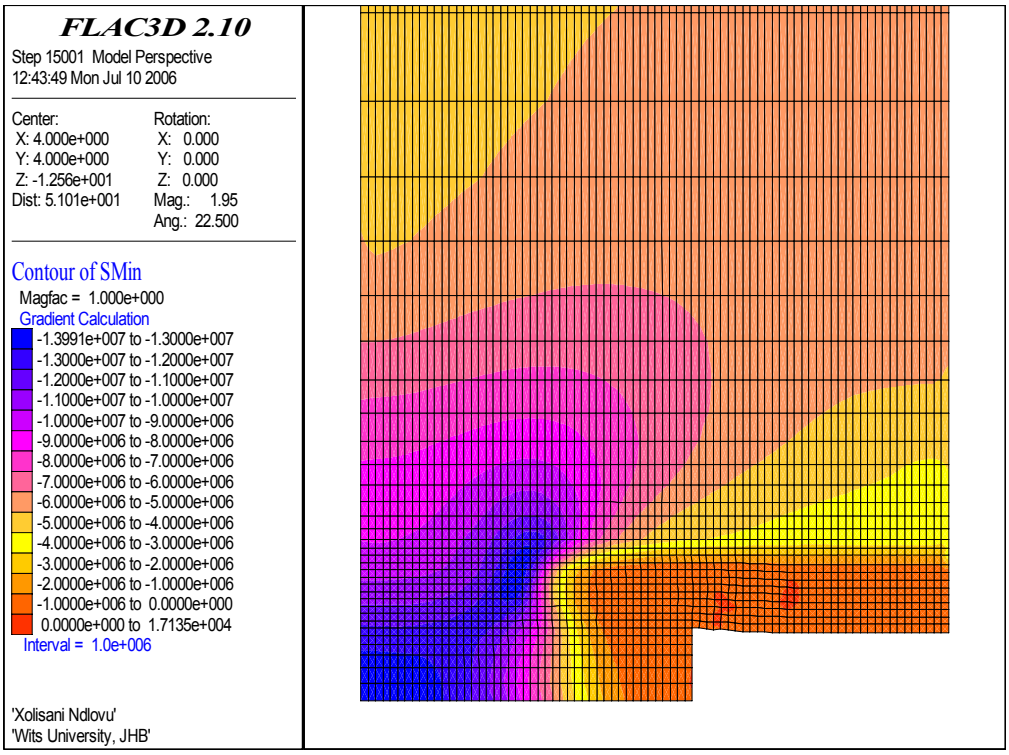

Figure 6.20: Plot of major principal stress distribution along Section A

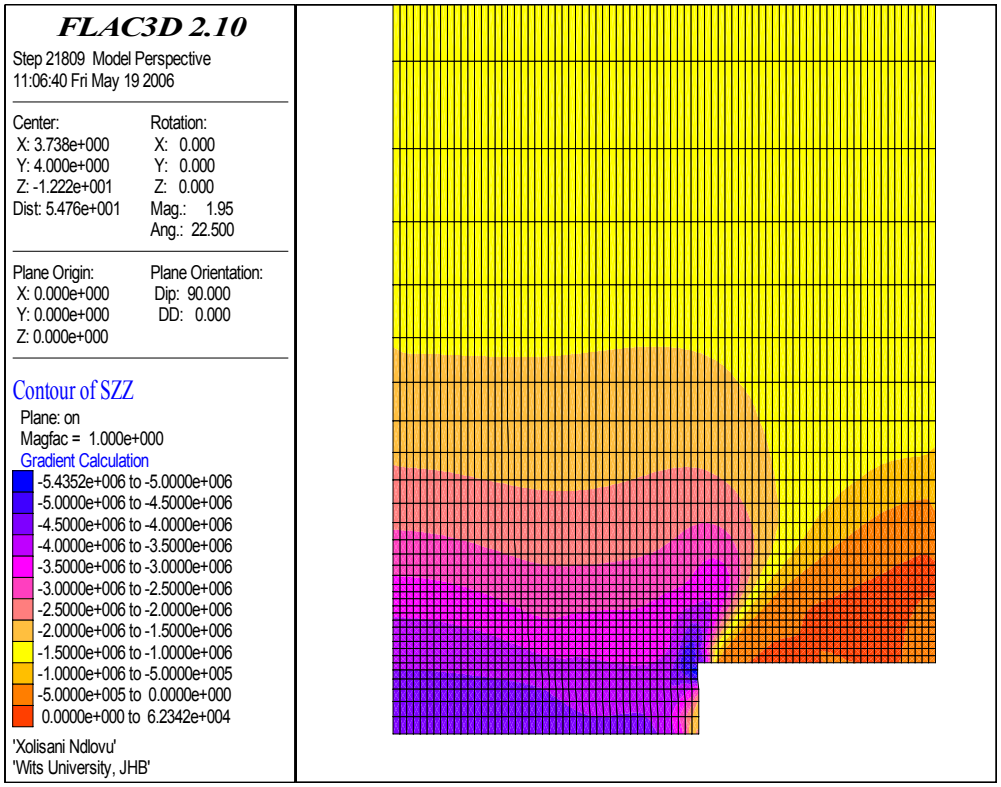

Figure 6.21: Plot of vertical stress distribution along Section A

Figure 6.22 is a plot of the principal stress distribution at the roof level along Line A. The plot confirms the destressing that takes place at the roof level. The major principal stress experiences significant concentration at the roof-pillar contact.

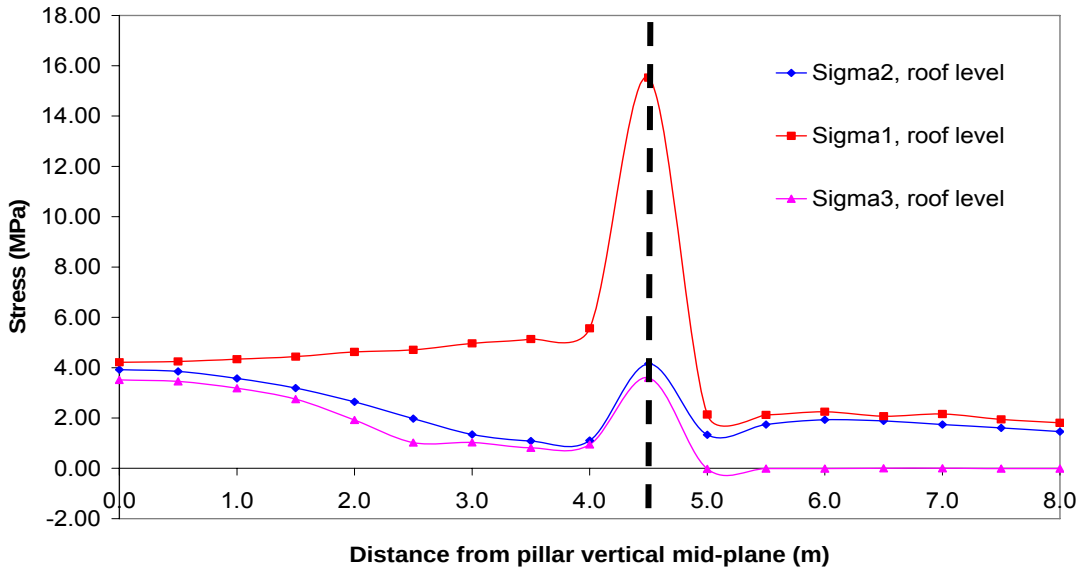

Figure 6.22: Stress distribution above bord and pillar geometry

Principal stress tensor plots show that the maximum compression is about 16 MPa. Maximum tension is about 0.0004 MPa and occurs at the pillar sides. Analysis of the deformation plot shown in Figure 6.23 indicates that the maximum vertical deformation is about 3.5 mm and occurs at the centre of the intersection.

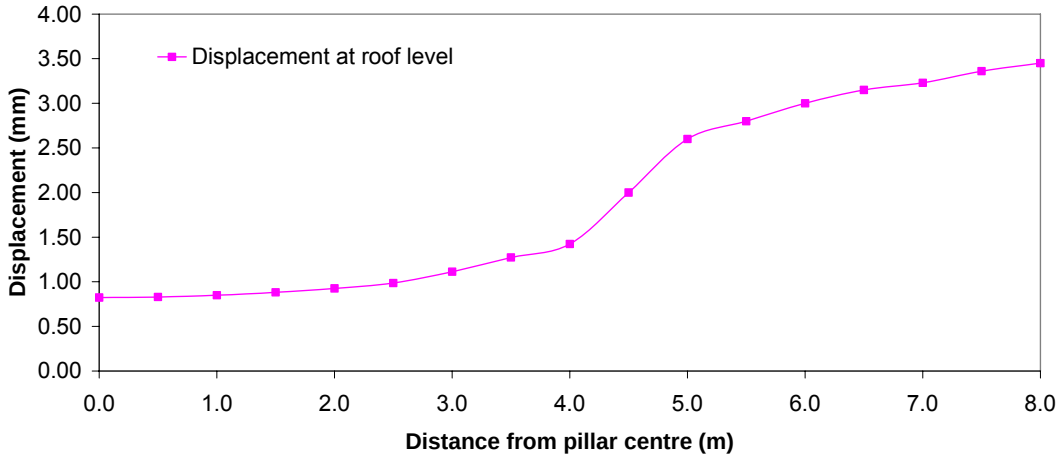

Figure 6.23: Induced vertical displacements (along Line B, Figure 6.4)

A useful analysis tool for the Mohr-Coulomb simulations is the plot of plasticity indicators. Plasticity indicators show the zones that have failed in the past during the model run and those that are currently in a state of failure. The plot of plasticity indicators shown in Figure 6.24 indicates zones failing in shear in the immediate roof around the roof-pillar contact. The size of the failure region (shown by shear-n) is about 1.1 m in width and 0.5 m in height. The whole shale roof, including part of the sandstone roof, seem to have satisfied the failure criterion earlier in the model run (shown by shear-p) but now the stresses fall below the yield surface. Initial plastic flow can occur at the beginning of a simulation, but subsequent stress redistribution unloads the yielding elements so that their stresses no longer satisfy the yield criterion.

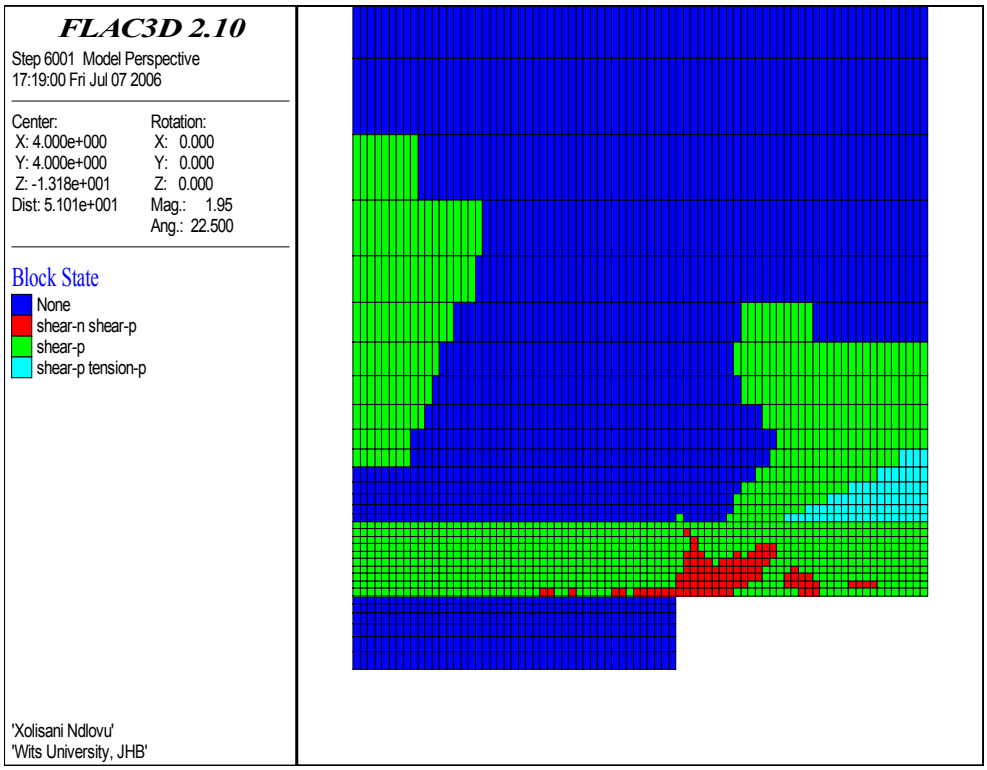

Figure 6.24: Failure state in the immediate roof (along Section A, Figure 6.4)

The following analyses are for simulations based on the model with a coal heading. Figure 6.25 shows the failure state of the zones at the roof level. Failure occurs at the area towards the roof-pillar contact.

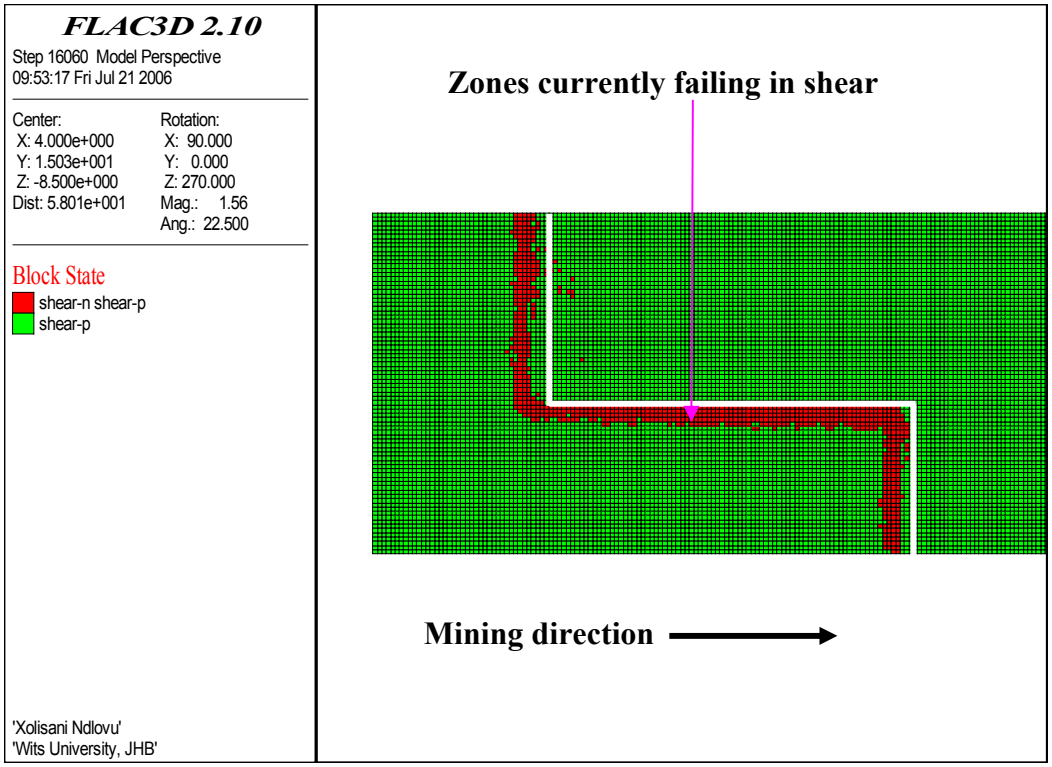

Figure 6.25: Plan view showing failure zones at the roof level for model with a coal heading

Figure 6.26 shows the failure zones at 0.2 m behind the coal face. Failure is indicated to be taking place for a height of about 0.4 m of the immediate roof. Failure zones at 1 m behind the coal face are shown in Figure 6.27. The zones are located at the roof pillar contact area. The height of failure is about 1.5 m and the width is about 0.5 m. Failure at 3 m behind the coal face is similar to the failure at 1 m behind the coal face. Figure 6.28 shows the failure zones at 6 m behind the coal face. Failure is shown to be taking place at the roof-pillar contact. The failure is about 0.4 m in width and 1 m in height. The failure zones are inclined at about 30 degrees to the vertical. No tensile failure took place for the model with a coal heading.

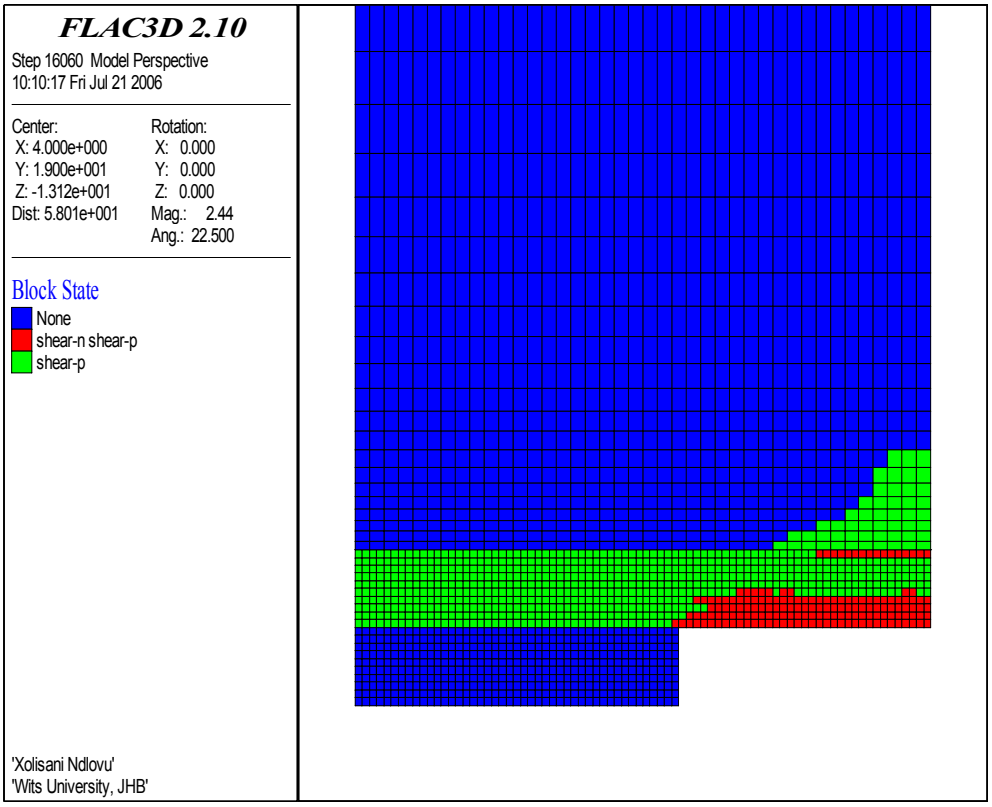

Figure 6.26: Failure zones 0.2 m behind the coal face (along Section M-M)

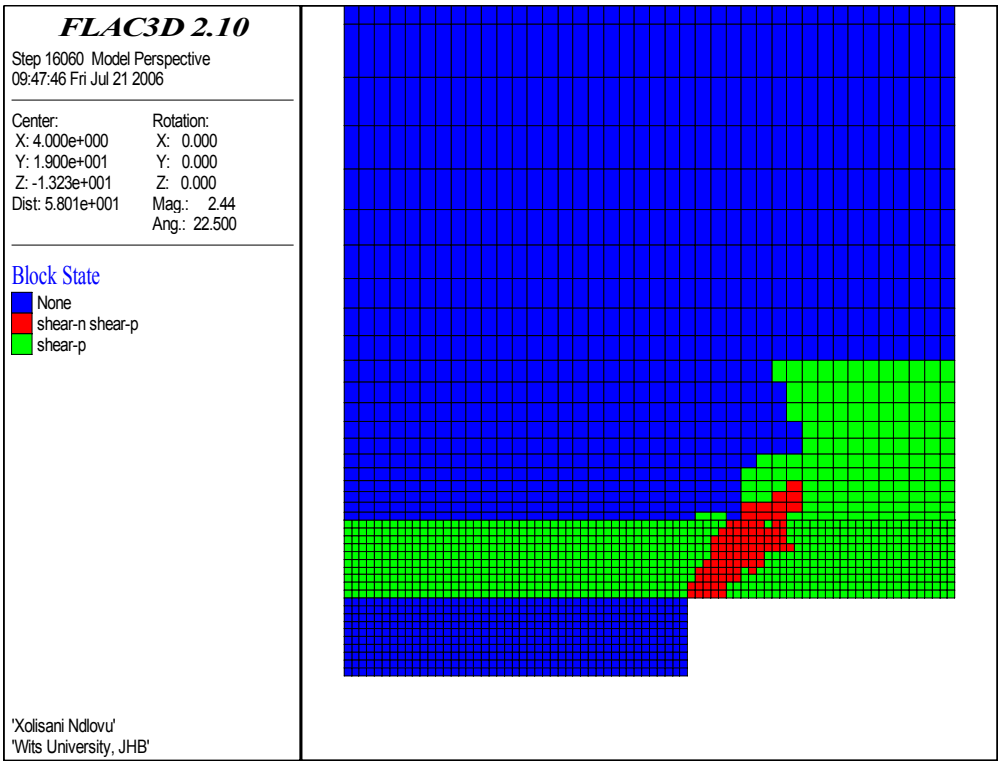

Figure 6.27: Failure zones 1 m behind the coal face (along Section M-M)

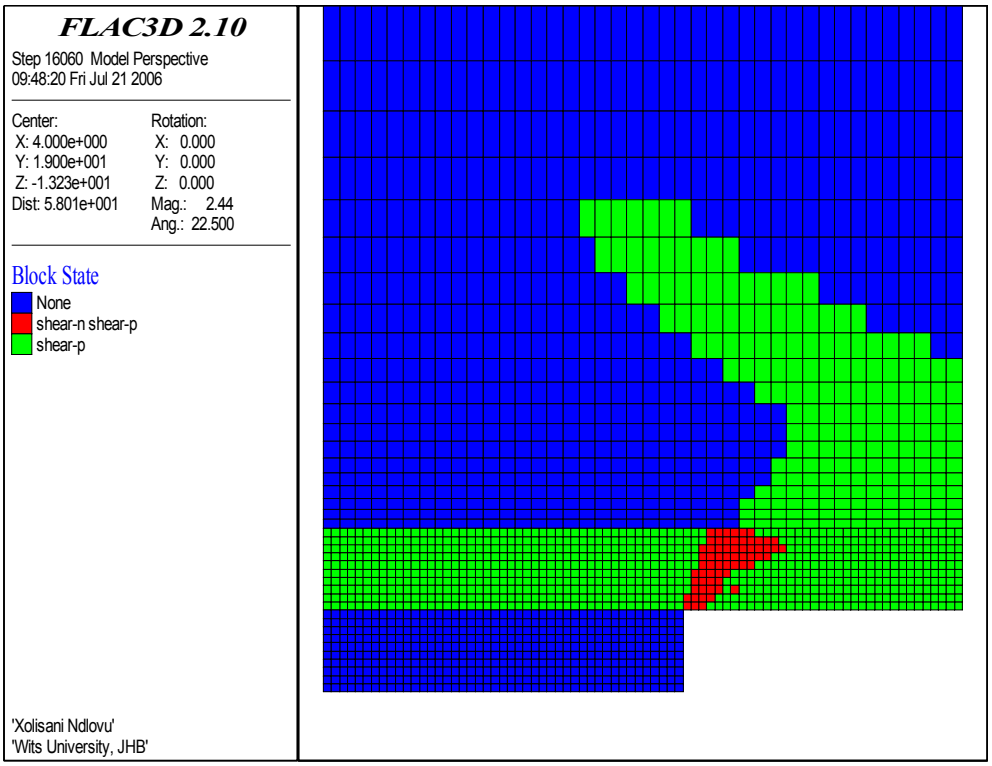

Figure 6.28: Failure zones 6 m behind the coal face (along Section M-M, Figure 6.3)

6.3.2.4 Results of Mohr-Coulomb strain softening analyses

The strain softening model analyses indicate that failure takes place towards the roof pillar contact area as shown in a section plot in Figure 6.29. The width of failure is about 0.5 m and the height of failure is about 0.2 m. At some time during the model run tensile strength of rock was exceeded and is indicated by 'tensile-p' in Figure 6.29.

The state of failure at different locations behind the coal face shows that failure initiates at the roof-pillar contact and progresses in a direction that is away from the roof and towards the area above the pillar. Figure 6.30 shows a section view of the failure state at 1 m behind the coal face.

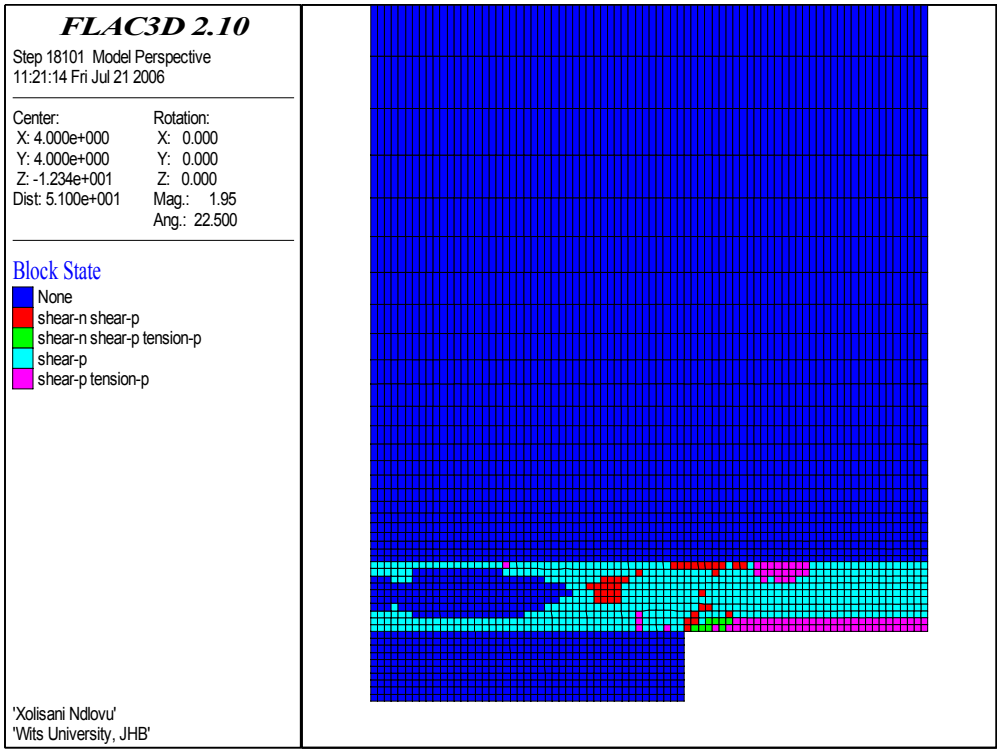

Figure 6.29: Failure state above immediate roof for strain softening model (along Section A, Figure 6.4)

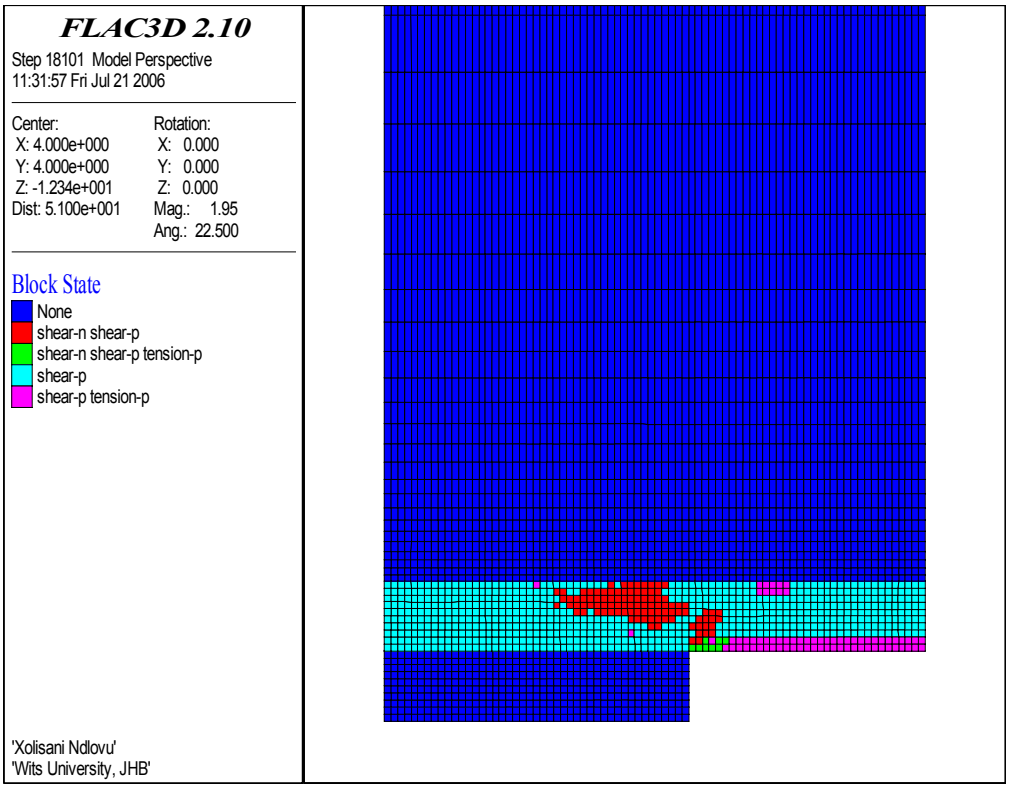

Figure 6.30: Failure zones 1 m behind the coal face (along Section M-M)

The results for the model with an interface between the coal and shale contact also show failure towards the area around the roof-pillar contact as shown in plan view in Figure 6.31. The region that is currently failing is about 0.5 m in width around the roof-pillar contact area.

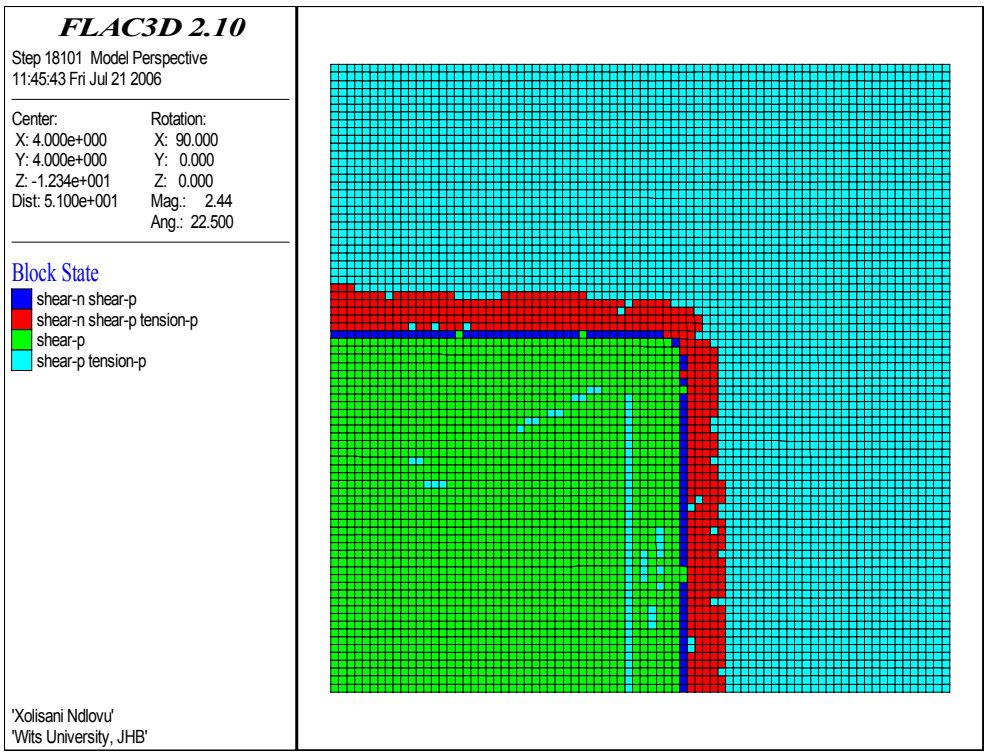

Figure 6.31: Plan view showing failure state at the roof level for Model 1 geometry with an interface

Principal stress tensor plots show that the maximum compression is about 10.2 MPa. Maximum tension is about 0.5 MPa and occurs at the pillar sides. Analyses of the deformations show that the maximum vertical deformation is about 4.2 mm and occurs at the centre of the intersection.

6.3.3 Results of extension strain analyses

Extension strain analyses are based on the following models:

(i) Isotropic model without an interface;
(ii) Isotropic model with an interface;
(iii) Transversely isotropic model without an interface;
(iv) Transversely isotropic model with an interface.

The analyses are presented in the form of extension strain magnitudes and distributions. Results are presented in the form of plan views of extension strain values and distributions at the roof level. Plan views at other locations in the immediate roof are included for comparison purposes. Section plots are included where these are deemed necessary. The results are summarised below:

(i) **Isotropic model without an interface** – Extension strain distribution in the immediate roof varies between 240 micro strains to just above 320 micro strains as shown in Figure 6.32. Extension strain values are highest at the roof-pillar contact area and decrease towards the centre of the road. Towards the centre of the road the extension strain value is constant at between 240 and 250 micro strains for the entire immediate shale roof. At other locations the extension strain values decrease with height into the roof. For example, the extension strain value of above 320 micro strains only occurs for 0.3 m of the immediate roof and just above this area extension strain values of less than 180 micro strains occur.

Figure 6.33 shows the extension strain distribution at the roof level while Figure 6.34 shows the extension strain distribution at 1 m above the roof level. The distribution of high extension strain values is more prominent in the road that is oriented normal to the direction of the maximum in situ horizontal stress than it is in the road oriented along this direction.

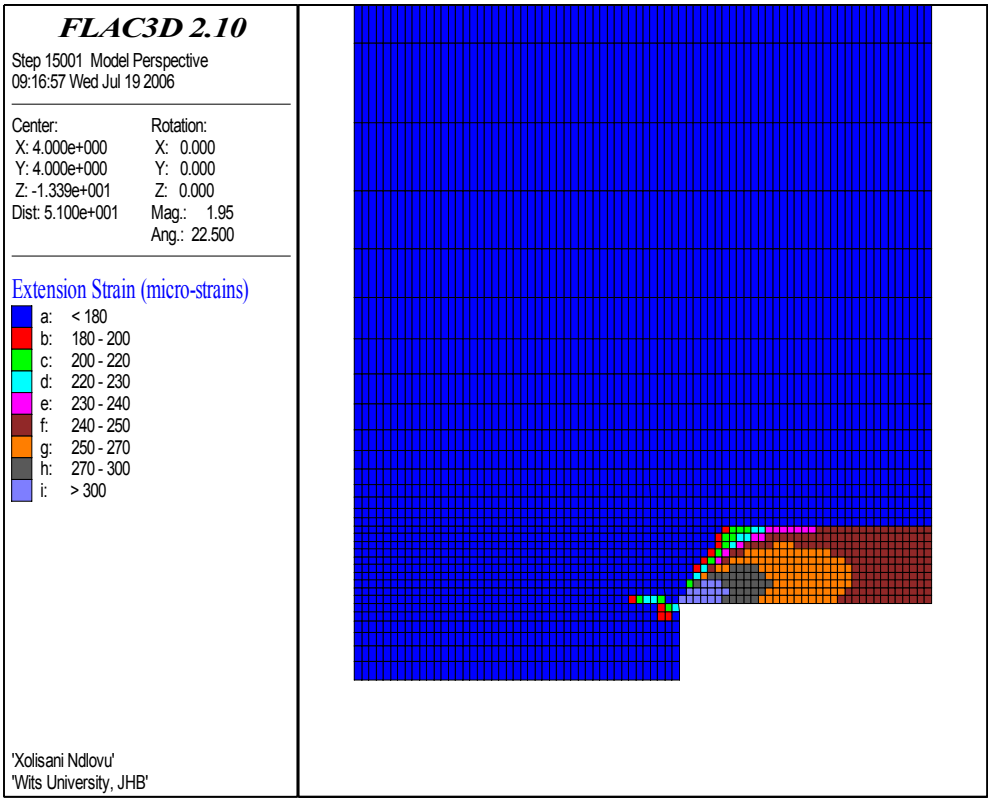

Figure 6.32: Extension strain distribution (along Section A, Figure 6.4)

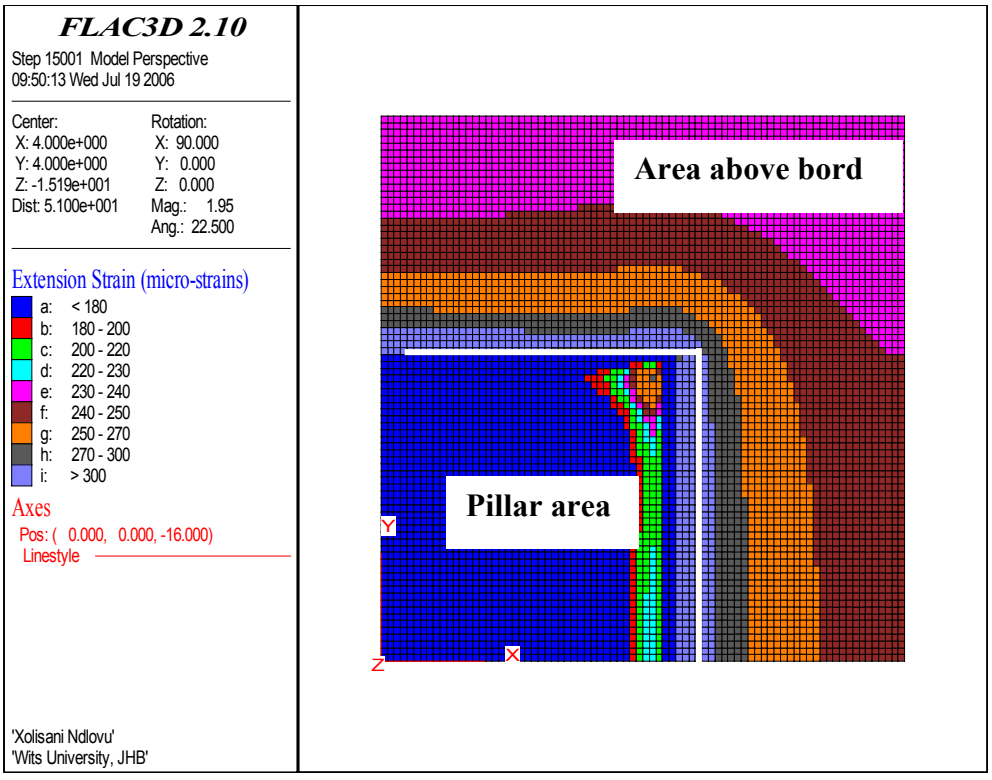

Figure 6.33: Plan view of extension strain distribution at roof level

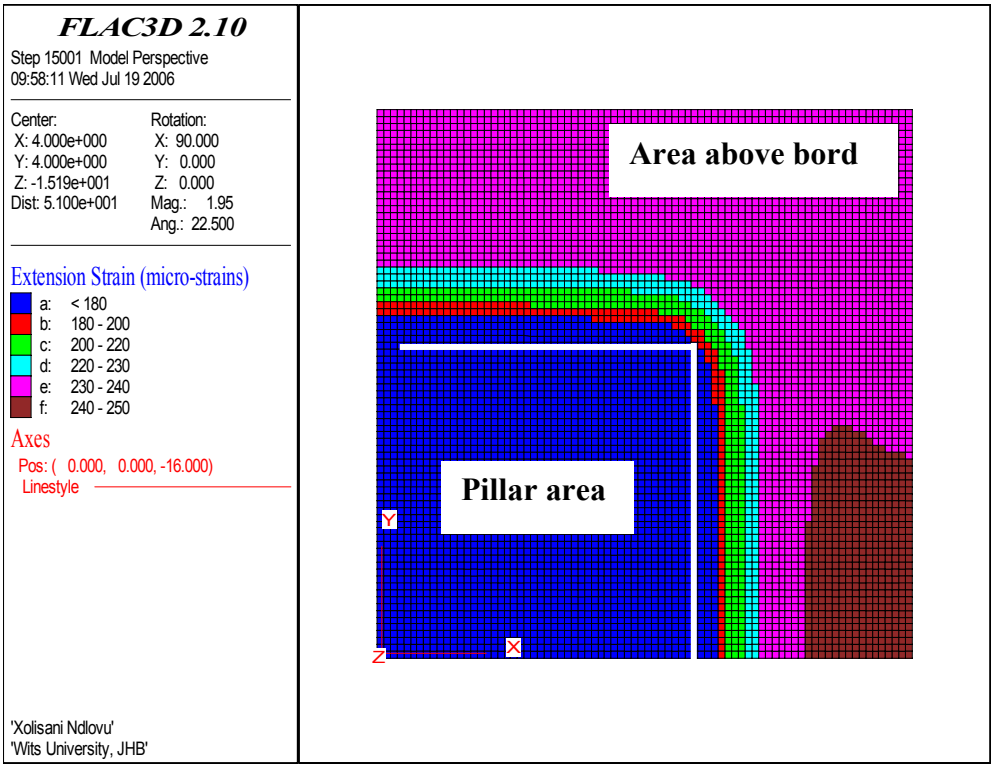

Figure 6.34: Plan view of extension strain distribution at 1 m above roof level

The quarter model represents a situation that exists well behind the coal face where pillars have been demarcated. At such areas few instances of initiation of roof guttering were observed. Analyses based on Model 2 geometry shows similar extension strain magnitudes. The model shows that a constant extension strain magnitude of between 240 – 250 micro strains occurs at the centre of the road for the whole immediate shale roof. The extension strain distribution at the roof level is shown in Figure 6.35. High extension strains also occur at the centre of the road just behind the coal face, at roof level position possibly because this area is a roof-pillar contact area. Extension strains as high as 270 micro strains also occur just ahead of the coal face at about 0.5 m from the roof-pillar contact area to the centre of the road.

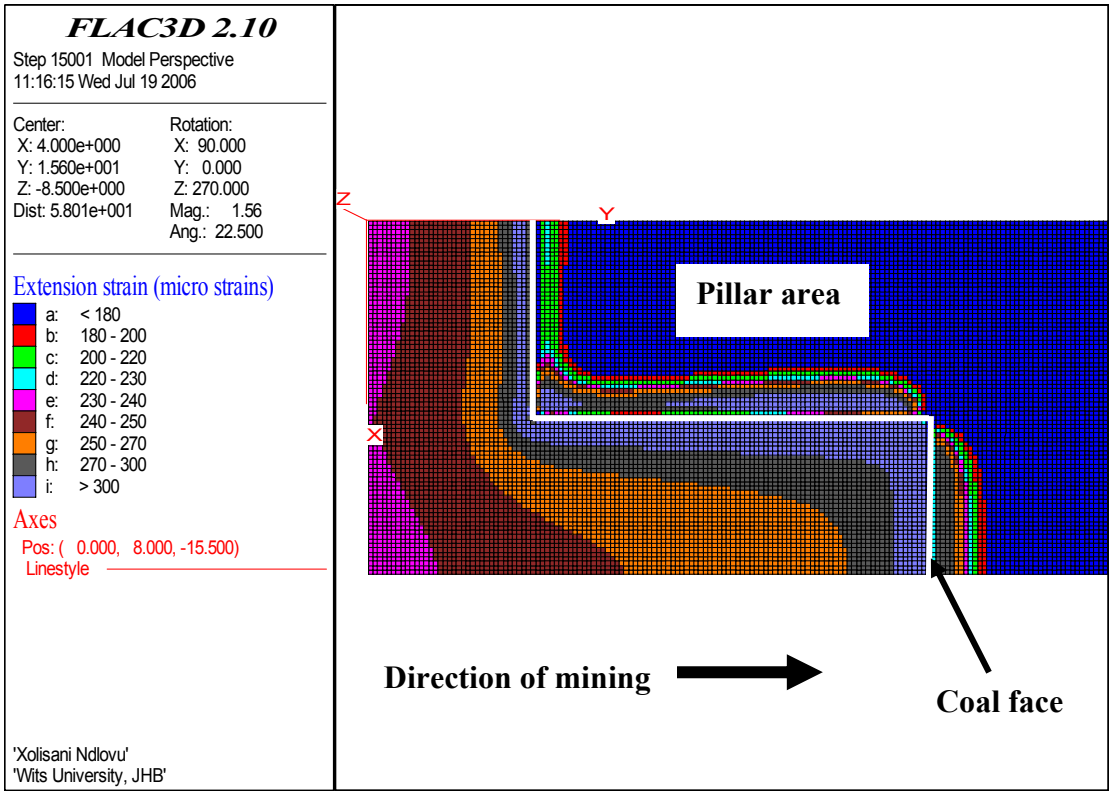

Figure 6.35: Plan view of extension strain distribution at roof level (based on Model 2 geometry)

Plots of extension strain distributions at various positions in relation to the coal face were analysed. High extension strains occur at the roof pillar contact area and also occur just behind the coal face for a length of 1 m which covers the whole bord width. These high extension strains occur for a height of about 0.3 m in the said locations. At 1m from the coal face and behind, the high extension strains only occur at the roof-pillar contact area and cover an area of about 0.6 m in width and 0.3 m in height. A plot of the extension strain distribution at 3 m behind the coal face is shown in Figure 6.36.

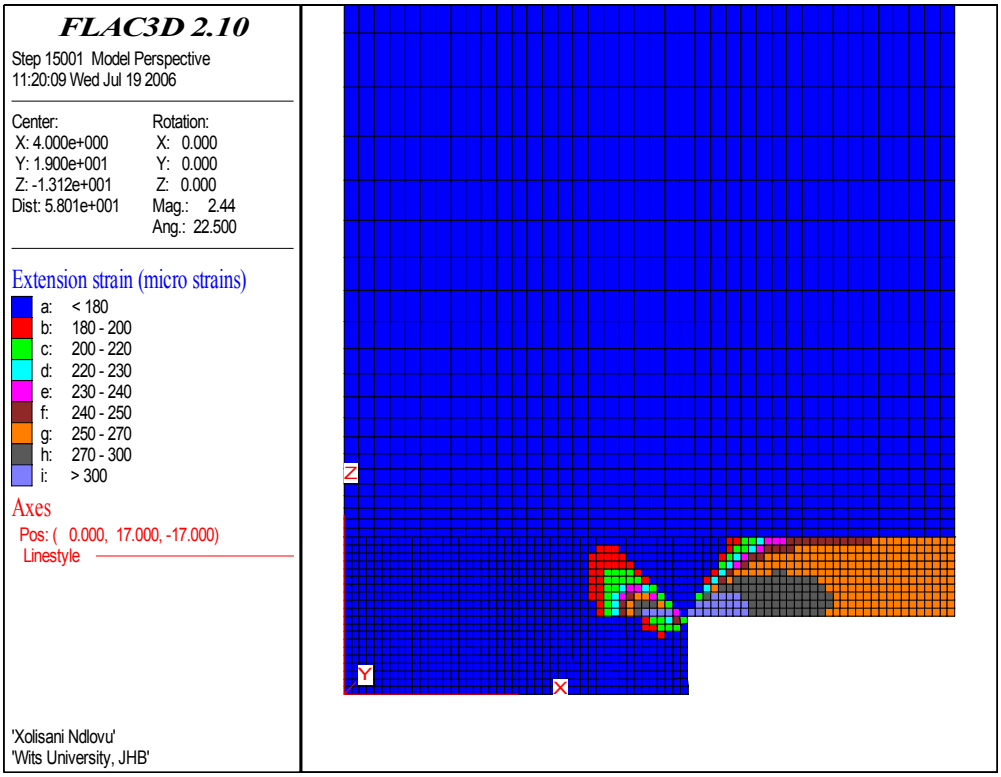

Figure 6.36: Extension strain distribution at 3 m behind the coal face (along Section M-M, Figure 6.3)

At the coal face the area that experiences significant extension strain is the roof height position for a height of only 0.1m. At this location the extension strain varies from 180 – 200 micro strains. Extension strains as high as 270 micro strains occur just ahead of the coal face at about 0.5 m from the roof-pillar contact area to the centre of the road. At about 1.4 m ahead of the coal face the only significant (180 – 200 micro strains) occurrence of extension strain is at the centre of the road as shown in Figure 6.37. It occurs at 0.4 m above the roof level position for a height of 0.5 m and width of 1.2 m.

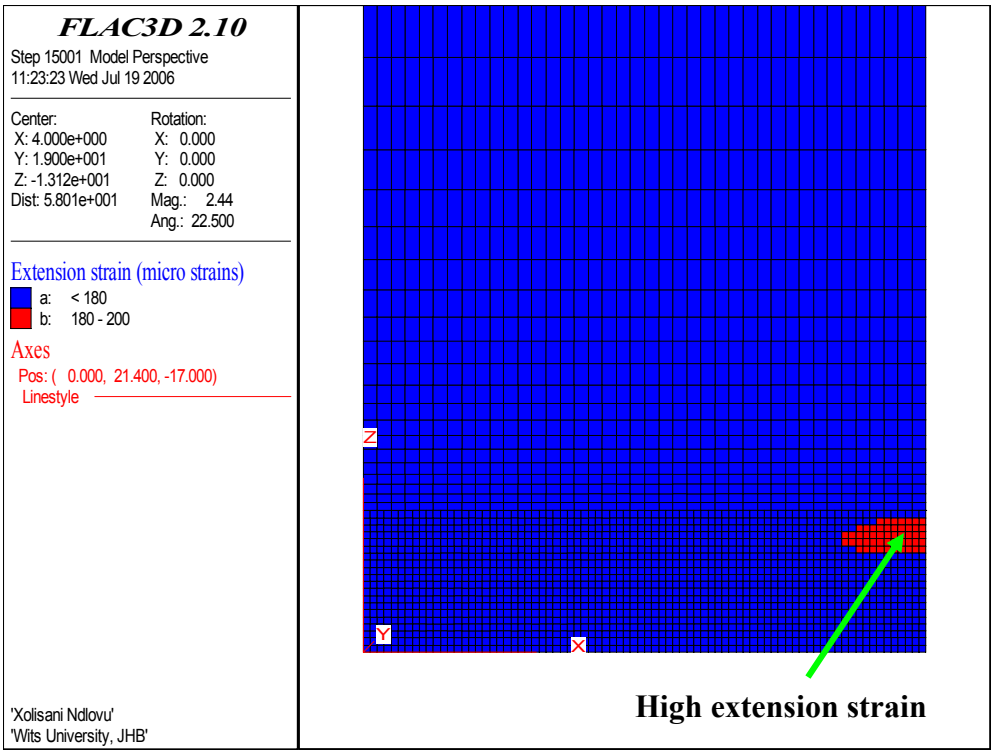

Figure 6.37: Extension strain distribution at 1.4 m ahead of the coal face (along Section M-M, Figure 6.3)

(ii) **<u>Isotropic model with an interface</u>** – the extension strain values vary between 220 and 270 micro strains in the immediate shale roof as shown in Figure 6.38. This is a big difference when compared to the model without an interface where extension strain values vary between 240 and 320 in the immediate shale roof. High extension strains occur towards the roof-pillar contact area. Plan views of extension strain distributions show that the area covered by each range of the extension strains is equal in the two perpendicular roads. This can be observed from Figure 6.39 which shows the extension strain distribution at 1 m above the roof level position. The Figure also shows that the highest extension strains (230 – 240 micro strains) at this height occur away from the roof-pillar contact area and towards the road centre.

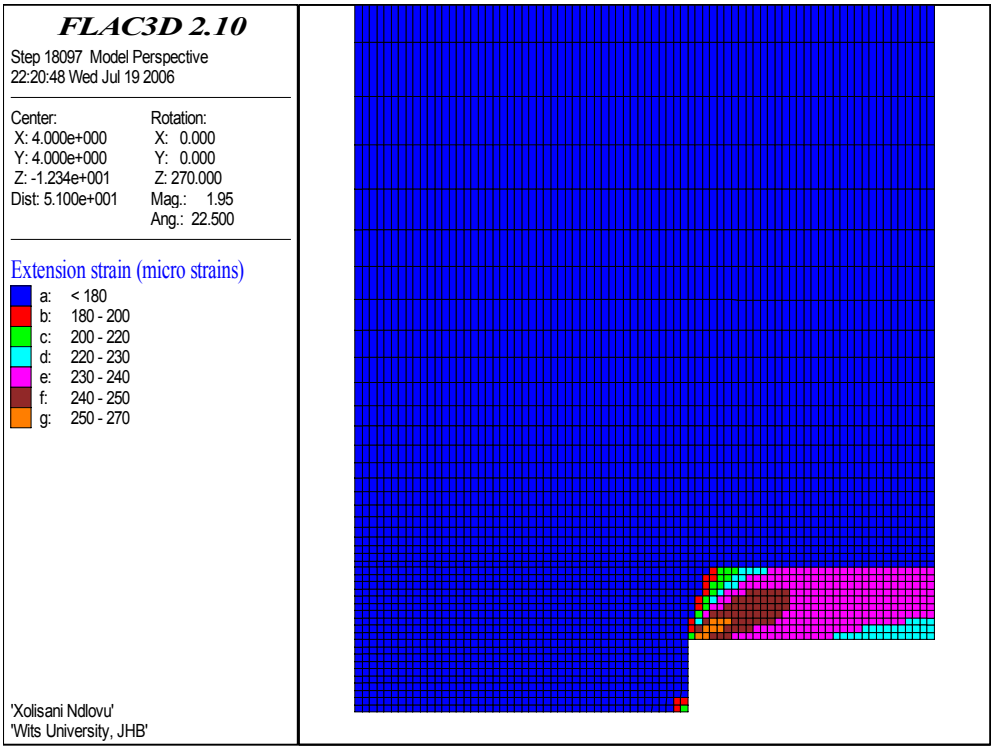

Figure 6.38: Extension strain distribution (along Section A, Figure 6.4)

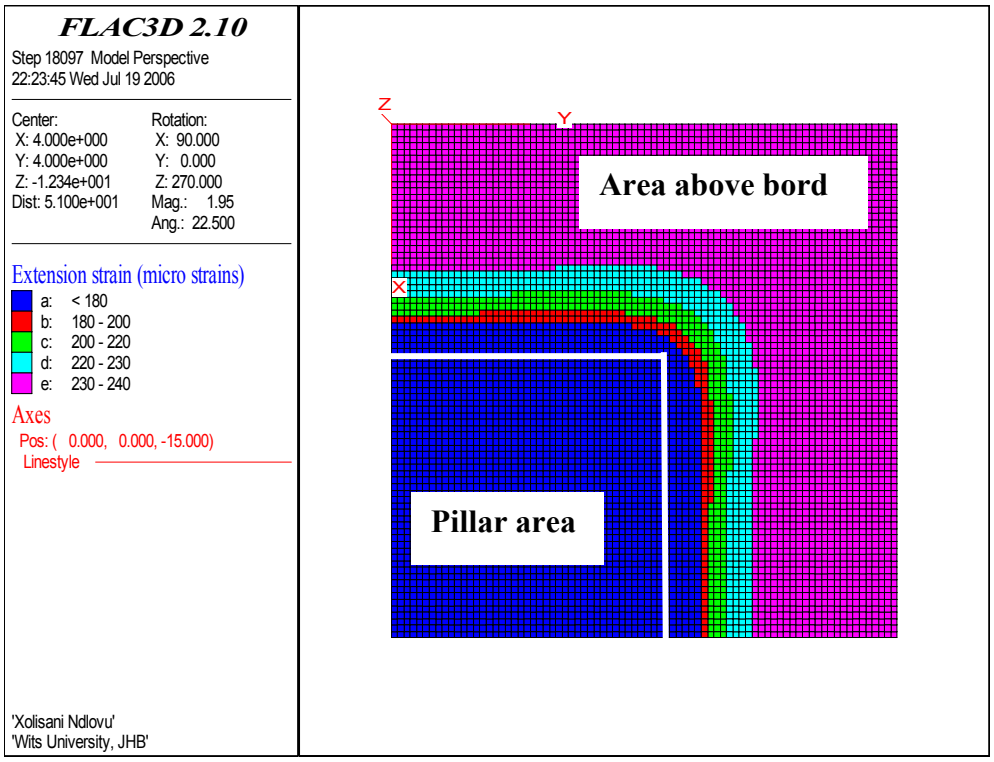

Figure 6.39: Plan view showing extension strain distribution at 1 m above the roof level position

(iii) **Transversely isotropic model without an interface** – High extension strains occur in the road along the direction of mining. The road is oriented normal to the direction of the maximum in situ horizontal stress. The plot of extension strain distribution at roof level is shown in Figure 6.40. There are also high extension strain values (250 – 270 micro strains) just ahead of the coal face.

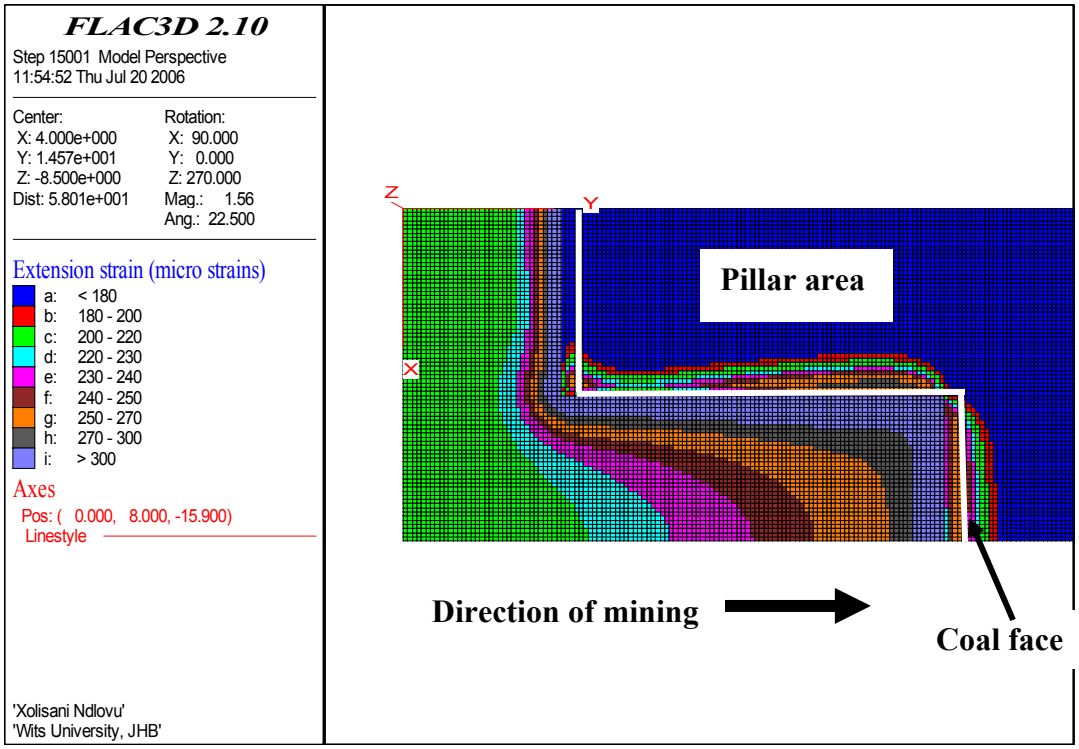

Figure 6.40: Plan view of extension strain distribution at roof level

At 0.2 m above the roof level position two "boat shaped" formations of the distribution of extension strain were observed as shown in Figure 6.41. The formation at the centre of the road is larger than the one at about 0.5 m from the roof-pillar contact area.

Analyses of extension strain distributions at various positions from the coal face show that high extension strains occur towards the roof pillar contact area and just behind the coal face. The height of occurrence of high extension strains is about 0.4 m. Significant extension strain values also occur ahead of the coal face.

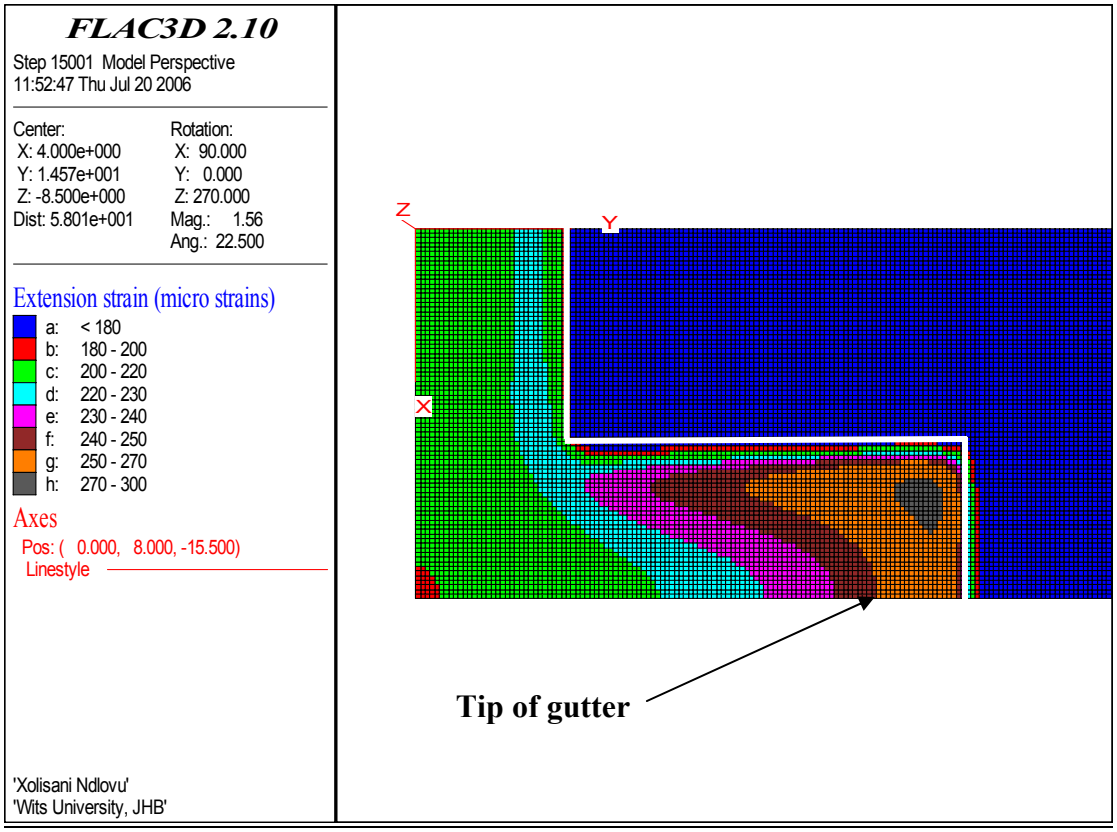

Figure 6.41: Plan view of extension strain distribution at 0.5 m above the roof level position

(iv) **Transversely isotropic model with an interface** – Extension strain values calculated based on this model are in the range of 220 to 300 micro strains in the immediate roof as shown in Figure 6.42. The majority of zones have an extension strain in the region of 200 – 220. A few zones towards the roof-pillar contact have an extension strain greater than 220 micro strains.

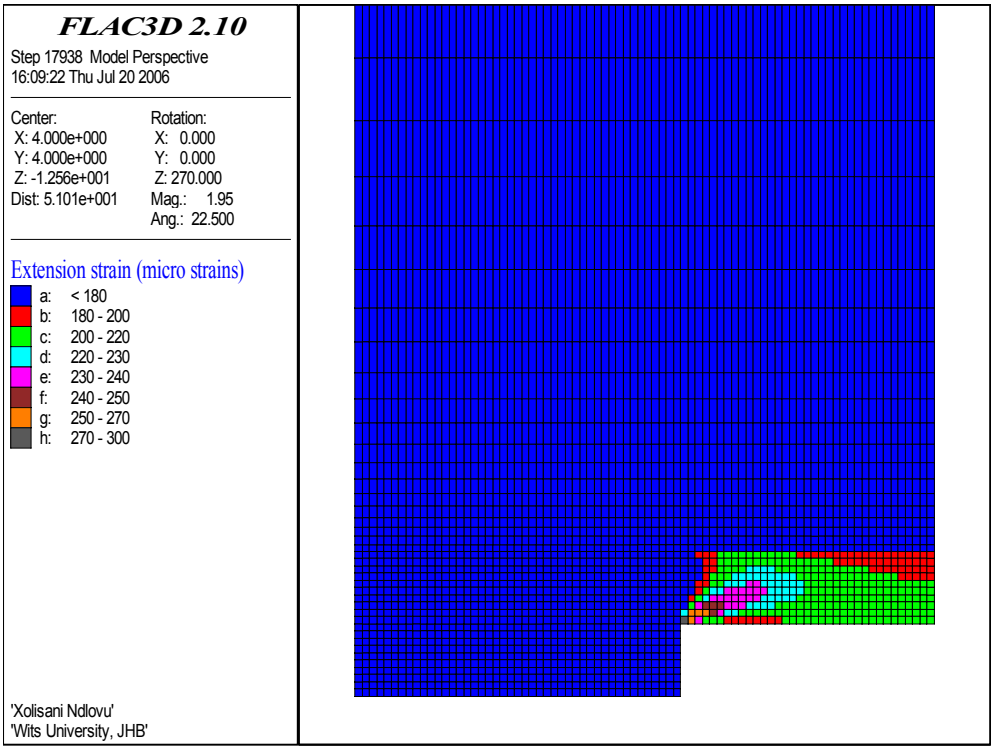

Figure 6.42: Distribution of extension strain (along Section A, Figure 6.4)

6.4 Analyses of results and comparison to mine observations

A comparison of the results of the different analyses is made and presented here. The comparisons are based on the state of stress in the immediate roof, maximum compression, tension and vertical displacements, maximum induced stress along Section A, location of the highest induced stress and the state of horizontal stress at the centre of the bords in the immediate roof. Table 6.1 is a summary of the results.

Table 6.1: Comparison of results for the different constitutive behaviours

Constitutive law	Maximum compression (MPa)	Maximum tension (MPa)	Maximum displacement (mm)	Maximum induced stress along Section A (MPa)			Location of highest induced stress	Horizontal stress state at the roof above centre of the road
				σ_1	σ_2	σ_3		
Isotropic	20.3	0.2	1.6	14.5	6.8	4.3	Roof-pillar contact area	slight stress concentration
Transversely Isotropic	23.7	0.0005	2.9	16.5	9.2	4.7	Roof-pillar contact area	slight stress concentration
Isotropic with interface	11.8	0.0004	1.6	11.2	5.8	3.9	0.5 m into the pillar from roof-pillar contact	Insignificant destressing
Transversely isotropic with interface	13.7	0.0001	3.3	11.2	7.5	4.2	Above the roof-pillar contact area	Insignificant destressing
Mohr-Coulomb	16.0	0.0004	3.5	14.0	8.4	7.9	Roof-pillar contact area	Significant destressing
Mohr-Coulomb with interface	10.2	0.2	3.0	9.0	5.2	4.0	Above the roof-pillar contact area	Significant destressing
MC strain softening	10.0	0.5	3.8	9.7	6.0	5.9	Roof-pillar contact area	Significant destressing
MC strain softening with interface	10.2	0.5	4.2	9.3	6.0	5.4	Above the roof-pillar contact area	Significant destressing

The results show that higher compression is developed in the elastic (isotropic and transversely isotropic) models than in the non elastic models. The Mohr-Coulomb model with an interface and the Mohr-Coulomb strain softening models have the lowest compression at about 10 MPa. All the models show insignificant induced tension in the immediate roof. The high horizontal stresses at the mine could be inhibiting sagging of the roof and development of tensile stresses. In all the analyses the induced displacements (strains) are insignificant despite the use of the large strain mode in FLAC3D analyses. Underground observations did not indicate any observable sagging of the roof, nor any delamination due to the anisotropy of the rock. The results of induced displacements obtained from the "continuous" model can, therefore, be said to represent the situation at the mine. The highest stress concentrations occurred around the roof-pillar contact area for all the models without an interface. For the models with an interface the highest stress concentrations occurred in the area above the pillar and away from the roof-pillar contact area. The interface allowed sliding at the coal-shale contact hence the observed results.

Slight stress concentrations towards the centre of the road were predicted for the elastic models. These were well below the stress concentrations predicted at the roof-pillar contact area. Failure is expected to initiate and occur at the roof-pillar contact area. The isotropic and transversely isotropic analyses with an interface at the coal-shale contact did not show any significant stress concentrations close to the vicinity of the excavation. Stress concentrations in the two models occur inside the pillar. There is insignificant destressing in the immediate roof. It is difficult to predict where initiation of failure should take place using the two models as there are no stress concentrations in the vicinity of the excavations.

The non elastic Mohr-Coulomb and Mohr-Coulomb strain softening analyses show that there is destressing in the immediate roof. Stress concentrations, like in the elastic analyses, occur at the roof pillar contact area. The models predict shear failure at the roof-pillar contact area. From underground observations the majority of failures initiated and occurred towards the centre of the roadways away from

the roof-pillar contact area. The Mohr-Coulomb and Mohr-Coulomb strain softening analyses, however, predicted the failures that occur towards the roof-pillar contact area. Predicted failure is up to 1 m in depth while underground observations showed that the depth of failure is up to 0.5 m. The predicted width of failure is about 1.1 m while underground observations showed failure widths of up to 3.5 m. The models therefore over predicted the depth of failure and under predicted the width of failure.

The extension strain analyses showed that high extension strain values occurred towards the roof-pillar contact area. Extension strain values are as high as 320 micro strains. Initiation of failure could be at strains in the region of 90 micro strains calculated from the formula below:

$e_{ini} = \sigma_t / E$

where e_{ini} = extension strain at initiation of fracture

σ_t = tensile strength of rock

E = Young's modulus

Failure of rock could be taking place at strain values that are about three times the failure initiation strain values. This translates to about 270 micro strains. Using the value of 270 micro strains as the value that signifies the onset of failure then the predicted depth of failure is about 0.5 m and the width of failure is up to about 2 m. Failure that occurred towards the roof-pillar contact area underground is therefore well predicted by the extension strain criterion both in depth and width. The distribution of high extension strain values is more prominent in the road that is oriented normal to the direction of the maximum in situ horizontal stress than it is in the road oriented along this direction.

The model with a coal heading showed that the highest value of extension strain (180 – 200 micro strains) occurrence at about 1.5 m ahead of the coal face is at the road centre. Fracture initiation could be taking place ahead of the coal face. It is

possible that on blasting the rock that has been fractured during initiation fails and in the process forms a roof gutter at the centre of the road.

It should be noted that extension strain analyses are implemented on models that have been stepped to equilibrium. The induced principal stresses used in the calculations have been shown to be elevated at the roof-pillar contact area. This could be a reason why high extension strains are predicted at the roof-pillar contact. An implementation of the extension strain criterion based on removal of zones whose extension strain exceeds a critical value also predicted failure at the roof-pillar contact area.

6.5 Conclusion

Numerical modelling results have indicated that there are insignificant stress concentrations towards the centre of the roadway using the elastic and transversely isotropic elastic models. Stress concentrations were predicted at the roof-pillar contact area. It is therefore expected that failure should initiate and occur at the roof-pillar contact area. This does not correspond with the underground observations of guttering.

The Mohr-Coulomb and Mohr-Coulomb strain softening models predicted shear failure at the roof-pillar contact area. The predicted depths of failure ranged from about 0.2 m to about 1.5 m while the predicted widths of failure ranged from about 0.4 m to about 1.1 m. The observed underground failures ranged from about 0.1 m to 0.5 m in depth and from about 0.5 m to 3.5 m in width. The two models, therefore, over predicted the depth and under predicted the width of failures.

FLAC3D's FISH language was used to implement the extension strain criterion. Extension strain analyses predicted failure mainly at the roof-pillar contact area. The depths and widths of failure were successfully predicted. High extension strain values were also predicted at the centre of the road position ahead of the coal face. It is possible that fracture initiation could be taking place ahead of the

coal face. On blasting, the rock that has been fractured falls and, in the process, a gutter is formed at the centre of the road.

The results of numerical analyses have shown that the traditional failure criterion, i.e., Mohr-Coulomb, predicted failure towards the roof-pillar contact area. The Mohr-Coulomb strain softening and extension strain failure criteria also predicted failure towards the roof-pillar contact area. The extension strain criterion, however, showed that high extension strains do occur at the road centre position ahead of the coal face. Initiation of extension could be assumed to be taking place at this position.

Chapter 7

Conclusions

The study of the occurrence of roof guttering in South African collieries has apparently not been given the attention that it deserves. Available research papers on the subject indicate that guttering occurrence in local coal mines has been likened to that which occurs in the United Kingdom coal mines. This may be a result of the lack of detailed mapping of the occurrence of roof guttering in the local coal mines. The occurrence of roof guttering in the roof of a local coal mine has been mapped and results presented in this dissertation. It has been shown that about 80% of the occurrence of roof guttering initiates and occurs towards the centre of the roads as opposed to the roof-pillar contact area. In situ stress measurement results together with underground observations confirmed the high state of horizontal stresses at the mine and laboratory testing results showed that the immediate shale/mudstone roof rock was weak. Underground observations of the occurrence of roof guttering formed the greater part of this dissertation. The following conclusions were drawn from these results:

- A thorough mapping exercise showed that guttering occurs mainly towards the centre of the bords (80%). Only about 20% of the guttering occurs at the roof-pillar contact area. This observation contradicts earlier reports by various researchers that guttering occurred at the roof-pillar contact. Guttering involved failure of intact rock as opposed to failure of a rock mass composed of rock joints and faults.
- Guttering cannot be a result of high tangential stresses alone; if this was the case it is expected that guttering would initiate in both corners of the roadways, where such tangential stresses are highest.
- Statistics showed that on a mine-wide scale guttering occurs in equal proportions in the two perpendicular directions of mining the roads and splits. When the panels were considered separately it was observed that in some panels guttering occurred in equal proportions in the two

perpendicular directions of mining while other panels had significant occurrence in one direction compared to the other direction.

- Laboratory results confirmed that the shale/mudstone roof rock was weak with UCS strength of 27 MPa and that the rock was transversely isotropic. The tensile strength was as low as 1 MPa.
- Stress measurements showed that high horizontal stresses exist at the mine. This was confirmed by observations of core discing and off-sets in exploration holes. The weak shale/mudstone roof should be contributing significantly to roof guttering as roof guttering was observed to initiate and occur in areas with a shale roof in most instances.
- Special features of the formed gutters are the boat shape, fracture surfaces ahead of the gutter and towards the centre of the gutter, the explosive sound during formation of the gutters, and the progressive nature of formation of the gutters.
- The formation of gutters seem to be as follows; crack initiation just behind, at and possibly ahead of coal face, critically oriented cracks are exploited in the zone where the shale/mudstone rock is weak, crushing of the cracked zone, slabbing due to weakening of the bedding, buckling of slabs, gutter progression as the cracking process persists due to the constant redistribution of stresses as a consequence of mining, and finally stabilisation, possibly when a new state of stress equilibrium is attained.
- Observation of fracture surfaces of the rock obtained from guttering roof indicated that about 90% of the surfaces showed extension type of failure. The remaining 10% showed shear failure. The shear failure can possibly be attributed to shearing surfaces when rock falls during the process of guttering.

Three dimensional stress and strain analyses around bord and pillar geometry in a coal mining environment using the FLAC3D code have been presented in this dissertation. In addition, the analyses were carried out to study the phenomenon of roof guttering, which formed the greater part of the numerical analyses. The following conclusions have been drawn from these analyses:

- The immediate roof was destressed while the pillar developed significant induced stresses, especially the vertical stresses. The greatest stress concentrations occurred at the roof-pillar contact area.
- Displacements (strains) were in the order of a few millimetres. There was no observable sagging of the roof and the small displacements obtained from numerical analyses therefore agree with underground observations. The high horizontal stresses that exist at the mine could be inhibiting sagging of the roof.
- Isotropic and transversely isotropic numerical analyses showed that there were slight stress concentrations towards the centre of the road yet there were significant stress concentrations at the roof-pillar contact area. It is therefore expected that if any failure takes place it should initiate at the roof-pillar contact.
- Analyses based on the traditional Mohr-Coulomb constitutive behaviour predicted shear failure at the roof-pillar contact area. The predicted depths of failure ranged from about 0.4 m to about 1.5 m while the predicted widths of failure ranged from about 0.4 m to about 1.1 m. The observed underground failures ranged from about 0.1 m to 0.5 m in depth and from about 0.5 m to 3.5 m in width. The model, therefore, over predicted the depth and under predicted the width of failures.
- The modified Mohr-Coulomb model in the form of the Mohr-Coulomb strain softening model also predicted shear failure towards the roof-pillar contact. The predicted depth of failure was about 0.2 m while the predicted width of failure was about 0.5. The model, therefore under predicted both the depth and width of failures.
- An implementation of the extension strain criterion showed that high extension strain values occur at the roof pillar contact for models without an interface. These models represent a situation where the coal-shale contact is strong. Few occurrences of roof guttering was observed at the roof pillar contact.

- The extension strain criterion implementation with an interface at the coal-shale contact showed that high extension strain occurs at about 0.5 m away from the roof-pillar contact.
- The extension strain criterion predicted correctly the depth and width of failures although the failures were predicted at the roof-pillar contact area while the observations indicated failure mainly towards the centre of the roads.
- Initiation of failure was predicted ahead of the coal face at the centre of the road position using the extension strain criterion.

Although none of the constitutive behaviours predicted correctly the observed underground failures the extension strain criterion has shown the best agreement. Guttering that occurred at the roof-pillar contact was modelled successfully using the extension strain criterion. The extension strain criterion predicted initiation of failure ahead of the coal face at the road centre position. It is possible that fracture initiation could be taking place in this location ahead of the coal face, and, on blasting the rock that has been fractured falls forming a gutter at the centre of the road.

References

Afrouz , A. A., 1992, *Practical Handbook of Rock Mass Classification Systems and Modes of Ground Failure*, CRC Press, pp 165.

Agapito, J. F. T., Aggson, J. R., Mitchell, S. J., Hardy, M. P. and Hoskins, W. N., 1980, Study of ground control problems in coal mines with high horizontal stresses. *Proceedings of 21st Symposium on Rock Mechanics: A State of the Art.* Univ. MO, Rolla, MO, pp 820 – 828.

Agapito, J. F. T. and Gilbride, L. J., 2002, Horizontal stresses as indicators of roof stability. SME Annual Meeting, Preprint 02 – 056, 11pp.

Aggson, J. R., 1978, Coal mine floor heave in the Beckley Coalbed: An Analysis. Bureau of Mines Report of Investigation No. 8274, 32pp.

Aggson, J. R., 1979a, How to plan ground control. *Coal Mining and Process*, Vol. 16, No. 12, pp 70 – 73.

Aggson, J. R., 1979b, Stress induced failures in mine roof. Bureau of Mines Report of Investigation No. 8338, 16pp.

Altounyan, P. and Taljaard, D., 2000, Developments in controlling the roof in South African coal mines – a smarter approach. *Coal – The Future, 12th International Conference on Coal Research*. The S. Afr. Inst. Min & Metall., Symposium Series 26, Johannesburg, pp 39 – 46.

Badr, S. A. E., 2004, *Numerical analysis of coal yield pillars at deep longwall mines*. PhD thesis, Colorado School of Mines, 248pp.

Barron, K. and Baydusa, A., 1999, A theory of cutter roof failure and its application. *CIM Bulletin*, Vol. 92, No. 103, pp 45 – 49.

Bieniawski, Z. T., 1968, In situ strength and deformation characteristics of coal. *Engineering Geology*, Vol. 2. pp 325 – 340.

Bieniawski, Z. T. and van Heerden, W. L., 1975, The significance of in situ tests on large rock specimens. *Int. J. Rock Mech. Min. Sci. & Geomech. Abstr*. Vol. 2. pp 101 – 113.

Brady, B. H. G. and Brown, E. T., 1985. *Rock Mechanics for Underground Mining*. George Allen and Unwin, London, 527pp.

Brown, E. T., ed. 1981a, *Rock Characterisation, Testing and Monitoring, ISRM Suggested Methods*, Pergamon Press, New York, pp 105 – 110.

Brown, E. T., ed. 1981b, *Rock Characterisation, Testing and Monitoring, ISRM Suggested Methods*, Pergamon Press, New York, pp 113 – 116.

Brown, E. T., ed. 1981c, *Rock Characterisation, Testing and Monitoring, ISRM Suggested Methods*, Pergamon Press, New York, pp 119 - 121.

Brown, E. T., 1993, The nature and fundamentals of rock mechanics. *Comprehensive Rock Engineering – Principles, Practice and Projects*, Hudson, J. A., Brown, E. T., Fairhurst, C., and Hoek, E. (eds) Vol. 1, Pergamon Press, pp 1 – 23.

Budavari, S., 1983, Response of the rock mass to excavations underground. *Rock Mechanics in Mining Practice*. The S. A. Inst. Min. & Metall., Monograph Series M5, pp 55 – 76.

Chamber of Mines of South Africa. 2004. INTERNET. http://www.bullion.org.za. Cited 10 May 2005.

Chandler, N., 2004, Developing tools for excavation design at Canada's Underground Research Laboratory. *Int. J. Rock Mech. and Min. Sci.* Vol. 41, pp 1229 – 1249.

Cook, N. G. W., Hodgson, K. and Hojem, J. P. M., 1971, A 100-MN Jacking System for testing coal pillars underground. *J. S. Afr. Inst. Min. & Metall*, Vol 72, pp 215 – 224.

Department of Minerals and Energy. 2004. INTERNET. http://www.dme.gov.za/publications/pdf/annual_reports/SAMI2003-4e.pdf. Cited 10 May 2005.

Diederichs, M. S., 2003, Rock fracture and collapse under low confinement conditions. *Rock Mech. Rock Engng*, Vol. 35 (5), pp 339 – 381.

Dolinar, D. R., Mucho, T. P., Oyler, D. C. and Pablic, J., 2001, Advance and relieve mining, a method to mitigate the effects of high horizontal stress on the mine roof. SME Annual Meeting, Denver, Colorado, Preprint 01 – 113, 13pp.

Eberhardt, E., Spillmann, T., Maurer, H., Willenberg, H., Loew, S., Stead, D., 2004. The Randa Rockslide Laboratory: Establishing brittle and ductile instability mechanisms using numerical modelling and microseismicity. *9th International Symposium of Landslides,* Rio de Janerio, June 28 – July 2, A. A Balkema, Leiden, pp. 481 – 487.

Eissa, E. A., and Kazi, A. 1988, Relation between static and dynamic Young's moduli of rocks. *Int. J. Rock Mech. Min. Sci. & Geomech. Abstr*. 35(6), pp 479 – 482.

Esterhuizen, G. S., 1998, *The Effect of Discontinuities on the Strength of Pillars in Coal mines.* PhD. Thesis, University of Pretoria, 203pp.

Esterhuizen, G. S. and Iannacchione, A. T., 2004, Investigation of pillar-roof contact failure in Northern Appalachian stone mine workings. *23rd International Conference on Ground Control in Mining*, pp 320 – 326.

Franklin, J. A., Vogler, U. W., Szlavin, J., Edmond, J. M. and Bieniawski, Z. T., 1978, Suggested methods for determining water content, porosity, density, absorption and related properties and swelling and slake-durability index properties. *Rock Characterisation, Testing and Monitoring. ISRM Suggested Methods*, Pergamon Press, pp 92 – 94.

Frith, R. C., Thomas, R., Hill, D., Buddery, P., 2002, Final Project Report – Survey of horizontal stresses in coal mines from available measurements and mapping, *SIMRAC Project COL802*, 51pp.

Fujii, Y., Kiyama, T., and Ishijima, Y, 1994, A new criterion for brittle failure of rock, *Proc. MMIJ/AusIMM Joint Symp*., Ube, Japan, pp. 469 – 476.

Fujii, Y., Kiyama, T., and Ishijima, Y, 1997, Condition insensitive damage indicator for brittle rock, *Int. J. Rock. Mech. Min. Sci.,* Vol. 34, No. 3 – 4, Paper No. 086.

Gale, W. J., 1996, Geological issues relating to coal pillar design. Symposium of Geology in Longwall Mining. pp 185 – 191.

Gale, W. J., 1999, Experience of field measurement and computer simulation methods for pillar design. *Proceedings of the Second International Workshop on Coal Pillar Mechanics and Design*. *Bureau of Mines Information Circular 9448, US Department of Interior.*

Hajiabdolmajid, V., Martin, C. D. and Kaiser P. K., 2000, Modelling brittle failure of rock. *Pacific Rocks 2000*, Girand, Liebman, Breeds and Doe (eds). Balkema, Rotterdam.

Hajiabdolmajid, V., Kaiser, P. K. and Martin, C. D., 2002a, Modelling brittle failure of rock. *Int. J. Rock Mech. and Min. Sci*. Vol. 39, pp 731 – 741.

Hajiabdolmajid, V., Kaiser, P. K. and Martin, C. D., 2002b, Mobilisation of strength in brittle failure of rock – in laboratory vs. in situ. *Mining and Tunnelling Innovation and Opportunity*. *Proceedings of the 5th North American Rock Mechanics Symposium and the 17th Tunnelling Association of Canada Conference: NARMS-TAC 2002*. Hammah, R., Bawden, W., Curren, J., and Telesnicki, M. (eds), Vol. 1, University of Toronto, pp 227 – 234.

Hajiabdolmajid, V., Kaiser, P. K. and Martin, C. D., 2003, Mobilised strength components in brittle failure of rock. *Geotechnique*, Vol. 53, No. 3, pp 327 – 336.

Hill, J. L. III. and Bauer, E. R., 1984, An investigation of the causes of cutter roof failure in a Central Pennsylvania coal mine: a case study. *Rock Mechanics in Productivity and Protection, 25th Symposium on Rock Mechanics.* Soc. Min. Eng. AIME, pp 603 – 614.

Hill, J. L. III, 1986, Cutter roof failure: an overview of the causes and methods for control. *Bureau of Mines Information Circular 9094, US Department of Interior*. 27pp.

Hill, R. W., 1989, Multi-seam mining in South Africa. *SANGORM Symposium: Advances in Rock Mechanics in Underground Coal Mining*. Witbank. South Africa.

Hoek, E., and Brown, E. T., 1980, *Underground Excavations in Rock,* The Inst. Min & Metall., London.

Hoek, E., 2000, INTERNET. http://www.rocscience.com/hoek/PracticalRock-Engineering.asp. Cited 10 October 2005.

Holling, C. S., 1978, *Adaptive Environmental Assessment and Management*, Wiley, Chichester, England.

Hooker V. E. and Johnson C.F., 1969, Near surface horizontal stresses including the effects of rock anisotropy. *U.S. Department of the Interior, Report of Investigations 7224*, 29pp.

Hustrulid, W. A., 1976, A review of coal strength formulas. *Rock Mechanics*, Vol. 8. pp 43 – 50.

Iannacchione, A. T., Popp, J. T. and Rulli, J. A., 1984, The occurrence and characterisation of geologic anomalies and cutter roof failure: their effect on gate road stability. *Stability in Underground Mining II*. Soc. Min. Eng. AIME, pp 428 – 445.

Iannacchione, A. T., Dolinar, D. R., Prosser, L. J., Marshall, T. E., Oyler, D. C. and Compton, C. S., 1998, Controlling roof beam failures from high horizontal stresses in underground stone mines". *Proceedings of the 17th International Conference on Ground Control in Mining*, pp 102 – 112.

Iannacchione, A. T., Marshall, T. E., Burke, L., Melville, R. and Litsenberger, J., 2001, Safer mine layouts for underground stone mines subjected to excessive levels of horizontal stress. SME Annual Meeting, Denver, Colorado. Preprint 01–88, 7pp.

Itasca Consulting Group, Inc, 2002, *FLAC3D – Fast Lagrangian Analysis of Continua in 3 Dimensions: User's Guide*, FLAC3D Version 2.1 User's Manual, Itasca Consulting Group, Inc., Minneapolis, U.S.A.

Jager, A. J., and Ryder, J. A., 1999, *A Handbook on Rock Engineering Practice for Tabular Hard Rock Mines.* The Safety in Mines Research Advisory Committee (SIMRAC), Johannesburg.

Kripakov, N. P., 1982, Alternatives for controlling cutter roof in coal mines. *Proceedings of the 2nd Conference on Ground Control in Mining*. West Virginia Univ., Morgantown, pp 142 – 151.

Kuijpers, J, 2000, Fracturing around highly stressed excavations in brittle rock. *AITES-ITA 2000 World Tunnel Congress*. Durban. South African Institute of Mining and Metallurgy.

Lekhnitskii, S. G., 1981, *Theory of Elasticity of an Anisotropic Body*. Moscow: Mir Publishers.

Lightfoot, N., and Maccelari, M. J., 2000, *Numerical Modelling of Mine Workings, 2nd Edition*, Vol. 1, SIMRAC Project Report GAP 728.

Madden, B. J. 1989, Re-assessment of coal pillar design. *School: The Total Utilisation of Coal Resources.* S.A. Inst. Min. & Metall., Witbank.

Madden, B. J., 1990, *An Investigation into the Effects Affecting the Strength of Pillars in South African Coal Mines*. PhD Thesis, University of the Witwatersrand.

Madden, B. J., Canbulat, I., Jack, B. W. and Prohaska, G. D., 1995, A reassessment of coal pillar design procedures. *SIMRAC Final Project Report – COL021*, CSIR Division of Mining Technology.

Madden, B. J., Canbulat, I. and York, G., 1998, Current South African coal pillar research. *J. S. Afr. Inst. Min. & Metall.*,. Vol 98, pp 7 – 10.

Mark, C. and Iannacchione, A. T., 1992, Coal pillar mechanics: theoretical models and field measurements compared. *Proceedings of the Workshop on Coal Pillar Mechanics and Design*. *US Bureau of Mines Information Circular 9315*. pp 78 – 93.

Mark, C., Mucho, T. P. and Dolinar, D., 1997, Horizontal stress and longwall headgate ground control. SME Annual Meeting, Denver, Colorado. Preprint 97 – 187, 8pp.

Martin, C. D., 1990, Characterising in situ domains at the AECL Underground Research Laboratory. *Can. Geotech. J*, No. 27, pp 631 – 646

Martin, C. D., 1997, Seventeenth Canadian Geotechnical Colloquium: The effect of cohesion loss and stress path on brittle rock strength. *Can. Geotech. J*, No. 34. Vol. 5, pp 698 – 725.

Martin, C. D., Read, R. S. and Martino, J. B., 1997, Observation of brittle failure around a circular test tunnel. *Int. J. Rock Mech. Min. Sci. & Geomech. Abstr*. 34(7), pp 1065 – 1073.

Martin, C. D., Kaiser, P. K. and McCreath, D. R., 1998, Hoek – Brown parameters for predicting the depth of brittle failure around tunnels. *Can. Geotech. J*, No. 36, pp 136 – 151.

Martino, J. B. and Chandler, N. A., 2004, Excavation-induced damage studies at the Underground Research Laboratory. *Int. J. Rock Mech. and Min. Sci*. Vol. 41, pp 1413 – 1426.

Mohan, G. M., Sheorey, P. R., and Kushwaha, A., 2001, Numerical estimation of pillar strength in coal mines. *Int. J. Rock Mech. & Min. Sci.* Vol. 38, pp 1885 – 1192.

Munsamy, L., 2003, *Determination of the High Horizontal Stresses at Nooitgedacht Colliery and Strategies to overcome the Roof Instability. MINN 594 Investigative Research Project*, Witwatersrand University, 76pp.

Munsamy, L. and Minney, D., 2004, Stress damage at a coal mine roof at shallow depth", *Second International Seminar on Deep and High Stress Mining*, The S. Afr. Inst. Min & Metall., Johannesburg.

Nicholls, B., 1978, Pillar extraction on the advance at Oakdale Colliery. *Stability in Coal Mines. Proceedings of the First International Symposium on Stability in Coal Mining*, Vancouver, British Columbia, Canada, pp 182 – 196.

Oravecz, K. I., 1973, Loading of pillars in bord and pillar workings. *COMRO Contract Report No. 40/73*. Johannesburg.

Ortlepp, W. D., 1997, *Rock Fracture and Rockbursts – An Illustrative Study*. The S. Afr. Inst. Min & Metall., Johannesburg.

Pariseau, W. G. and Eitani, I. M., 1981, Comparison between finite element calculations and field measurements of room closure and pillar stress during retreat mining. *Int. J. Rock Mech. Min. Sci. & Geomech. Abstr*. Vol. 18, pp 305 - 319.

Parker, J., 1973, How to design better mine openings: practical rock mechanics for miners". *Engineering and Mining Journal*, Vol. 174, No. 5 pp 76 – 80.

Peng, S. S., 1986, *Coal Mine Ground Control*. 2nd Edition. John Wiley & Sons.

Phillips, D. W., 1947, American coal mining. *Colliery Guardian*, Vol. 175, No. 4523, pp 37 – 43.

Pothini, B. R., von Schonfeldt, H., 1978, Roof fall prediction at Island Creek Coal Company. *Stability in Coal Mines*. *Proceedings of the First International Symposium on Stability in Coal Mining*, Vancouver, British Columbia, Canada, pp 214 – 227.

Ramsey, J.M., and Chester F. M., 2004, Hybrid fracture and the transition from extension fracture to shear fracture, *Nature*, Vol. 428, pp 63 – 66.

Read, R. S., 2004, 20 years of excavation response studies at AECL's Underground Research Laboratory. *Int. J. Rock Mech. and Min. Sci*. Vol. 41, pp 1251 – 1275.

Roley, R. W., 1948, Pressure cutting: a phenomenon of coal mine roof failures. *Mechanisation*, Vol. 12, No. 12, pp 69 – 74.

Ryder, J. A., and Jager, A. J., 2000, *A Textbook on Rock Mechanics for Tabular Hard Rock Mines*. The Safety in Mines Research Advisory Committee (SIMRAC), Johannesburg.

Safety in Mines Research Advisory Committee (SIMRAC), 2002/2003 Annual Report.

Salamon, M. D. G. and Munro, A. H., 1967, A study of the strength of coal pillars. *J. S. Afr. Inst. Min. & Metall*. pp 55 – 67.

Song, I., Suh, M., Woo, Y. and Hao, T., 2002, Constitutive modelling of anisotropic rocks based on ultrasonic measurements. *Mining and Tunnelling Innovation and Opportunity*. *Proceedings of the 5th North American Rock Mechanics Symposium and the 17th Tunnelling Association of Canada Conference: NARMS-TAC 2002*. Hammah, R., Bawden, W., Curren, J., and Telesnicki, M. (eds), Vol. 1, University of Toronto. Pp 259 – 266.

Stacey, T. R., 1972, Three-dimensional finite element stress analysis applied to two problems in rock mechanics. *J. S. Afr. Inst. Min. & Metall.*, Vol. 72, No. 10, pp 251 – 256.

Stacey, T. R., 1981, A simple extension strain criterion for fracture of brittle rock, *Int. J. Rock. Mech. Min. Sci.,* Vol. 18, pp. 469 – 474.

Stacey, T. R., 1982, Contribution to the mechanism of core discing, *Jl S. Afr. Inst. Min. Metall.*, Vol. 82, no 9, September 1982, pp 269-274.

Stacey, T. R., 1989, Boring in massive rocks – rock fracture problems, *Proc. Seminar on Mechanised Underground Excavations,* S. Afr. Nat. Council on Tunnelling, pp. 87-90.

Stacey, T. R., 2006, *Personal Communication*.

Starfield, A. M. and Bleloch, A. L., 1986, *Building Models for Conservation and Wildlife Management,* MacMillan Publishing Co., New York.

Starfield, A. M. and Cundall, P. A., 1988, Towards a methodology for rock mechanics modelling, *Int. J. Rock. Mech. Min. Sci. & Geomech. Abstr.,* Vol. 25, No. 3. pp 99 – 106.

Thomas, E., 1950, Conventional timbering versus suspension supports. *Bureau of Mines Bulletin No. 489*, pp 175 - 181.

van der Merwe, N., 1993. Revised strength factor for coal in the Vaal Basin. *J. S. Afr. Inst. Min. & Metall.*, Vol. 93 pp 71 – 77.

van Der Merwe, J. N., 1995. *Practical Coal Mining Strata Control: A Guide for Managers and Supervisors at all Levels.* Jack Brillard Printing Services C. C., Johannesburg.

van der Merwe, J. N., 2000, Horizontal stress: The root of all evil? *Proceedings of the 19th International Conference on Ground Control in Mining*, Peng, S. S and Mark, C, (eds), pp 129 – 136.

van der Merwe, J. N. and Peng, S. S., 2000, Recent developments in rock engineering for coal mines – notes on the International Conference on Ground Control in Mines. *The Future, 12th International Conference on Coal Research*, The S. Afr. Inst. Min & Metall., Johannesburg.

van der Merwe, J. N., Madden, B. J., 2002, *Rock Engineering for Underground Coal Mining*, The S. A. Inst. Min. & Metall., Special Publications Series 7, Johannesburg.

van der Merwe, J. N., 2003, Predicting coal pillar life in South Africa. *J. S. Afr. Inst. Min. & Metall*, June 2003, pp 293 – 301.

van Heerden, W. L., 1970, Stress measurements in coal pillars. *Proc. 2nd Congr. Int. Soc. Rock. Mech.,* Belgrade, Vol. 2, Theme 4, Paper No. 16, 5pp.

van Heerden. W. L., 1983. Stress – strain relations applicable to overcoring techniques in transversely isotropic rocks. *Int. J. Rock Mech. Min. Sci. & Geomech. Abstr.* Vol. 20(6), pp 277-282.

Vervoort, A., 1998, Deformation and fracturing in underground mining. *Advances in Rock Mechanics,* Lin, Y (ed), World Scientific, pp 227 – 236.

Walker, G., and Altounyan, P., 2001, In situ stress measurement at Nooitgedacht, No. 5 Seam Section 50/51, *Rock Mechanics Technology (Pty) Ltd Report to Greenside Colliery*, AngloCoal, 14pp.

Wang, F. D., Ropchan, D. M. and Sun M. C., 1974, Proposed technique for improving coal mine roof stability by pillar softening. *Trans. Soc. Min. Eng. AIME*, Vol. 255, pp 59 – 63.

Wesseloo, J., 2000, Predicting the extent of fracturing around underground excavations in brittle rock. *Proceedings of the South African Young Geotechnical Engineers Conference. A joint venture between the S. Afr. I. Civil Engng & the S. Afr. I. for Engng and Environmental Geologists*, University of Stellenbosch, Western Cape, RSA, 12pp

World Coal Institute, 2005. INTERNET. www.worldcoal.org. Cited 10 January 2006.

York, G., Canbulat, I and Jack, B. J., 2000. Coal Pillar Design Procedures. *SIMRAC Final Project Report – COL337*, CSIR Division of Mining Technology.

Appendix A1: Laboratory Test Results

Table A1.1: Dynamic Young's modulus for loading along bedding for cylindrical samples

Sample no.	Length (mm)	Mass (g)	Diameter (mm)	Density (kg/m3)	Vp-time (µS)	Vs-time (µS)	Vp (m/s)	Vs (m/s)	Edyn (GPa)
A1	86.0	263.3	42.0	2209	26.1	50.9	3295	1690	16.7
A2	87.4	269.0	42.0	2221	26.4	51.3	3311	1704	17.0
A3	86.0	294.7	42.1	2461	26.1	50.0	3295	1720	19.1
A4	87.4	297.4	42.0	2455	26.3	51.6	3323	1694	18.7
A5	85.9	262.4	41.6	2247	26.5	48.4	3242	1775	18.2
A6	86.2	296.6	42.0	2483	25.9	52.0	3328	1658	18.2
A7	87.2	267.6	42.0	2214	26.6	49.2	3278	1772	18.0
A8	87.1	296.6	42.1	2445	26.4	50.8	3299	1715	18.9
A9	86.0	293.0	42.1	2446	25.6	51.8	3359	1660	18.1
A10	87.1	296.0	42.0	2452	25.0	50.1	3484	1739	19.8
A11	85.8	283.3	42.0	2382	26.1	48.6	3287	1765	19.3
Average	**86.6**	**283.6**	**42.0**	**2365.0**	**26.1**	**50.4**	**3318**	**1717**	**18.4**

Table A1.2: Dynamic Young's modulus for loading normal to bedding for cylindrical samples

Sample no.	Length (mm)	Mass (g)	Diameter (mm)	Density (kg/m3)	Vp-time (µS)	Vs-time (µS)	Vp (m/s)	Vs (m/s)	Edyn (GPa)
P1	86.6	270.3	42.1	2241	35.1	61.9	2467	1399	11.1
P2	87.0	271.8	42.1	2243	34.1	63.2	2551	1377	11.0
P3	81.6	255.6	42.1	2249	32.8	58.5	2488	1395	11.1
P4	81.6	255.7	42.1	2250	33.3	58.8	2450	1388	11.0
P5	86.6	271.9	42.1	2255	35.0	62.9	2474	1377	10.9
P6	81.6	255.5	42.1	2248	33.7	59.6	2421	1369	10.7
P7	86.6	271.6	42.0	2263	35.0	63.1	2474	1372	10.9
P8	86.9	273.7	42.2	2251	35.4	63.1	2455	1377	10.8
P9	81.8	256.2	42.1	2249	33.1	58.5	2471	1398	11.1
P10	86.7	272.4	42.1	2256	35.4	63.9	2449	1357	10.6
P11	81.6	257.3	42.2	2254	32.6	58.3	2503	1400	11.2
P12	81.6	257.8	42.1	2269	33.0	57.8	2473	1412	11.4
Average	**84.2**	**264.2**	**42.1**	**2252.3**	**34.0**	**60.8**	**2473**	**1385**	**11.0**

Table A1.3: UCS, Young's modulus and Poisson's ratio values (static) for cylindrical samples for loading normal to bedding

Sample No.	Load (kN) at failure	UCS (MPa)	Young's modulus (GPa)	Poisson's ratio
P1	56.6	40.66	1.8	0.18
P2	55.0	39.51	2.0	0.16
P4	54.4	39.08	1.9	0.16
P5	54.6	39.22	1.8	0.17
P7	52.0	37.53	1.6	0.10
P8	52.0	37.18	1.8	0.16
P9	57.0	40.95	1.6	0.15
P10	54.4	39.08	1.8	0.13
Average	**54.5**	**39.15**	**1.8**	**0.15**

Table A1.4: UCS, Young's modulus and Poisson's ratio values (static) for cylindrical samples for loading along bedding

Sample No.	Load (kN) at failure	UCS (MPa)	Young's modulus (GPa)	Poisson's ratio
A2	34.0	24.54	9.17	0.29
A3	32.8	23.56	13.01	0.23
A5	37.6	27.66	10.45	0.18
A8	34.0	24.42	10.83	0.17
A9	32.4	23.28	13.59	0.37
A10	35.4	25.55	11.48	0.37
A11	39.0	28.15	10.58	0.25
Average	**34.9**	**25.23**	**11.02**	**0.27**

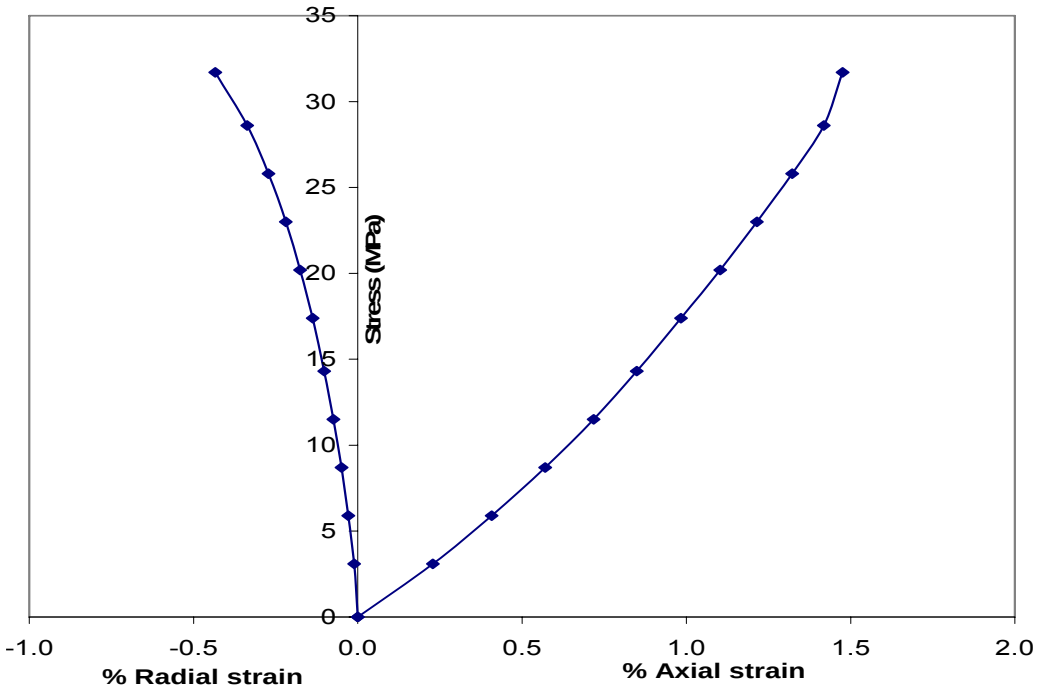

Figure A1.1: Typical stress – strain graph for a cylindrical sample for loading normal to bedding

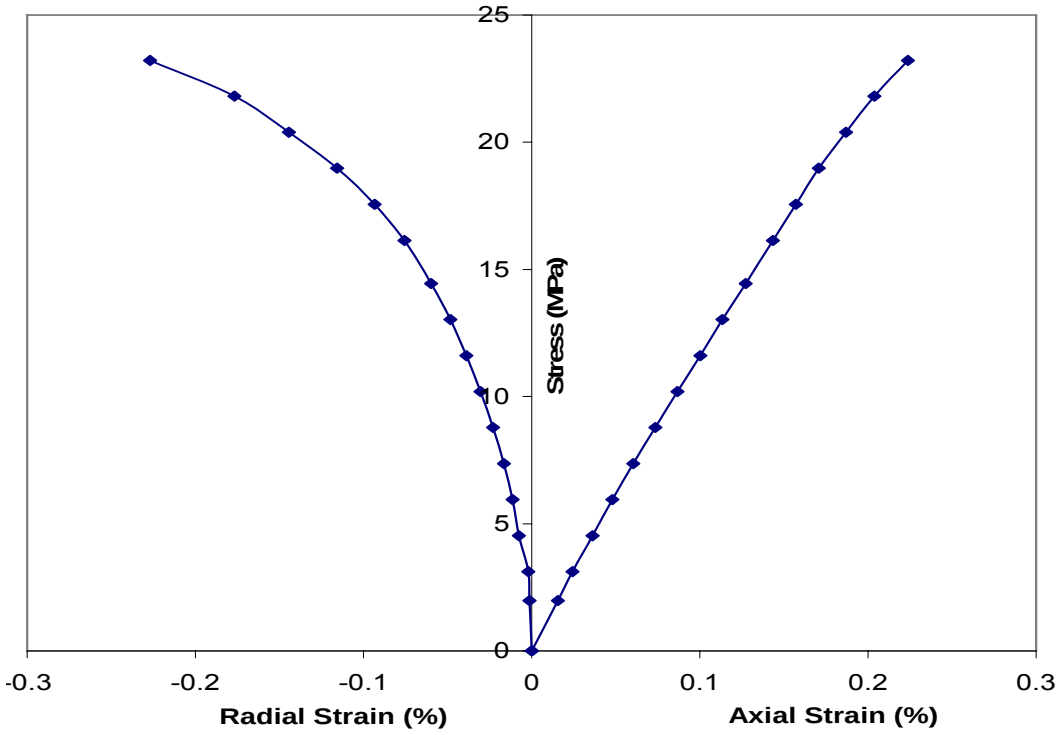

Figure A1.2: Typical stress – strain graph for a cylindrical sample for loading along bedding

Table A1.5: Tensile strength for loading along bedding

sample no.	diameter	thickness	load	tensile strength
A20	53.4	37.8	4.5	1.42
A21	53.5	37.7	3.4	1.07
A22	53.2	37.7	2.4	0.76
A23	52.9	37.8	3.4	1.08
A24	53.1	37.8	3.6	1.14
A25	53.2	37.7	4.2	1.33
A26	53.4	37.8	3.1	0.98
A27	53.2	37.9	2.6	0.82
A30	52.9	37.8	4.1	1.30
A31	52.9	37.8	4.2	1.34
A32	53.4	37.9	3.5	1.10
A33	53.1	37.8	3.1	0.98
A34	53.4	37.8	2.9	0.91
A35	53.5	37.8	3.8	1.20
A36	53.5	37.7	4.1	1.29
A37	53.2	37.8	3.1	0.98
A40	53.5	37.8	3.3	1.04
A41	53.1	37.9	3.6	1.14
A42	53.4	37.7	3.7	1.17
A43	53.3	37.9	2.9	0.91
A44	53.3	37.9	3.3	1.04
A45	53.1	37.8	2.5	0.79
A46	52.9	37.8	2.6	0.83
A47	53.1	37.8	3.4	1.08
Mean	**53.2**	**37.8**	**3.4**	**1.07**

Table A1.6: Tensile strength for loading normal to bedding

sample no.	diameter	thickness	load	tensile strength
P20	53.2	37.9	8.4	2.65
P21	53.2	37.8	9.4	2.97
P22	53.1	37.7	7.4	2.35
P23	53.3	37.6	9.6	3.05
P24	53.0	37.8	8.0	2.54
P25	53.2	37.7	9.8	3.11
P26	53.2	37.7	9.0	2.86
P27	53.0	37.8	9.2	2.92
P30	53.3	37.6	8.6	2.73
P31	53.1	37.6	8.8	2.80
P32	53.1	37.7	9.4	2.99
P33	53.2	37.8	9.2	2.91
P34	53.0	37.6	9.0	2.87
P35	53.0	37.6	8.6	2.75
P36	53.2	37.9	8.4	2.65
P37	53.3	37.6	9.6	3.05
P40	53.2	37.8	9.8	3.10
P41	53.2	37.6	7.8	2.48
P42	53.3	37.6	8.2	2.60
P43	53.2	37.8	7.8	2.47
P44	53.1	37.9	8.2	2.59
P45	53.2	37.7	9.6	3.05
P46	53.3	37.7	8.6	2.72
P47	53.3	37.7	9.8	3.10
Mean	**53.2**	**37.7**	**8.8**	**2.81**

Table A1.7: Calculated critical extension strain for loading parallel to bedding

Sample No.	Poisson ratio	Young's modulus (GPa)	UCS (MPa)	Factor, *f*	Critical extension strain
A3	0.23	13.01	23.56	0.25	0.000104
A5	0.18	10.45	27.66	0.25	0.000119
A8	0.17	10.83	24.42	0.25	0.000096
A9	0.37	13.59	23.28	0.25	0.000158
Average	**0.27**	**11.30**	**25.31**	**0.25**	**0.000119**

Appendix A2: Material Properties

Different constitutive behaviours require different material properties. These are discussed below.

1.1 Elastic properties

There are four material parameters for an elastic constitutive behaviour. These are the elastic modulus E, Poisson's ratio *v*, bulk modulus K and shear modulus G; and only two are required to fully specify the material. In FLAC3D, the bulk and shear moduli are used. The properties are different for the coal, shale and sandstone layers. Table A2.1 below summarises the material properties used in the analyses. The values in Table A2.1 are obtained from the following equations for an elastic material:

$$K = E / 3(1 - 2v) \quad \text{(1.1)}$$

$$G = E / 2(1 + v) \quad \text{(1.2)}$$

where K = bulk modulus

G = shear modulus

E = Young's modulus

v = Poisson's ratio

The values of Young's modulus and Poisson's ratio used in the calculation are those obtained from the laboratory tests for shale. For coal and sandstone the values used were supplied by the mine. These values are shown in Figure A2.2.

Table A2.1: Bulk and shear moduli values used in the elastic analysis

Material	Bulk modulus (GPa)	Shear modulus (GPa)
Coal	2.33	1.40
Shale	8.19	4.45
Sandstone	16.66	7.69

Table A2.2: Young's modulus and Poisson's ratio values used in the calculations

Material	Young's Modulus (GPa)	Poisson's ratio
Coal	3.5	0.25
Shale	11.0	0.27
Sandstone	20.0	0.3

1.2 Transversely isotropic properties

Laboratory results indicated that the shale layer is transversely isotropic. The following material properties are prescribed for this constitutive behaviour:

(i) E_1 = Young's modulus in the plane of isotropy

(ii) E_3 = Young's modulus in the direction normal to the plane of isotropy

(iii) v_{12} = Poisson's ratio characterizing lateral contraction in the plane of isotropy when tension is applied in this plane

(iv) v_{13} = Poisson's ratio characterizing lateral contraction in the plane of isotropy when tension is applied in the direction normal to it

(v) G_{13} = Shear modulus for any plane normal to the plane of isotropy

The shear modulus, G_{13}, for is determined from the following equation (Lekhnitskii, 1981):

$$G_{13} = E_1 E_3 / [(1 + 2v_{13}) + E_3]$$

Each parameters used in the equation is defined above. The different parameters making up the equation are obtained from laboratory tests. The values of the parameters used in the analyses for the shale layer are given below:

E_1 = 11 GPa, E_3 = 1.8 GPa, G_{13} = 1.23 GPa, v_{12} = 0.27 and v_{13} = 0.15

1.3 Mohr-Coulomb properties

In addition to the bulk and shear moduli the Mohr-Coulomb constitutive behaviour requires the peak values of tensile strength, cohesion, internal angle of friction and dilation angle. The values given in Table A2.3 are used in addition to those given in Table A2.1 for the Mohr-Coulomb analyses.

Table A2.3: Mohr-Coulomb material properties

Material Property	*Coal	Shale	Sandstone
Tensile strength (MPa)	-	1.0	1.5
Cohesion (MPa)	-	0.6	1.0
Friction angle (°)	-	35	40
Dilation angle (°)	-	15	18

*Coal – coal is modelled as an elastic material

1.4 Mohr-Coulomb strain softening material properties

In addition to the Mohr-Coulomb parameters, the Mohr-Coulomb strain softening constitutive behaviour requires the variation of cohesion, friction angle and dilation angle with plastic shear strain and variation of tensile strength with plastic tensile strain. The pillars are intact and the sandstone layers in the floor and roof did not indicate any failure. The shale layer is therefore assigned strain softening material properties. The coal layer is assigned linear elastic material properties while the sandstone layer is assigned Mohr-Coulomb material properties. Table A2.4 summarises the material properties used for the strain softening shale layer.

Table A2.4: Strain softening material properties for the shale layer

Plastic strain	Cohesion (MPa)	Friction (°)	Dilation (°)
0	0.6	35	15
$1x10^{-4}$	0.4	33	12
$2x10^{-4}$	0.1	31	7
$3x10^{-4}$	0.05	27	4
$4x10^{-4}$	0.05	27	4

The variation, with plastic strain, of cohesion, friction angle and dilation angle is an approximation obtained from the literature.

1.5 Extension strain properties

The elastic models are used for extension strain calculations. The input values used for the extension strain criterion are therefore the same as those used for the elastic models.

1.6 Other input parameters

Other input parameters required for all the models are the in situ stress conditions and the density of the rock mass. In situ stresses 52 m below the ground surface are as follows:

In situ maximum horizontal stress, σ_x:	6.24 MPa (North-South)
In situ minimum horizontal stress, σ_y:	4.55 MPa (East-West)
Vertical stress due to gravity, $\sigma_{z:}$	1.3 MPa (Vertical)

In situ stresses are assumed to vary with depth. Material density has been fixed at 2500kg/m^3 for the overburden material.

The interface was used to simulate the effect of a weak bonding at the coal-shale contact. The properties of the interface are as follows:

(i) Cohesion = 0.0 MPa
(ii) Friction angle = 30°
(iii) Shear stiffness = 42 GPa
(iv) Normal stiffness = 42 GPa